
Dépôt Institutionnel de l'Université libre de Bruxelles /
Université libre de Bruxelles Institutional Repository
Thèse de doctorat/ PhD Thesis

Citation APA:

Boereboom, T. (2012). *Greenhouse gases investigations in ice from periglacial environments* (Unpublished doctoral dissertation). Université libre de Bruxelles, Faculté des Sciences – Géographie, Bruxelles.

Disponible à / Available at permalink : <https://dipot.ulb.ac.be/dspace/bitstream/2013/209673/4/7d85d3f4-2871-468c-b919-3e4a504e4d00.txt>

(English version below)

Cette thèse de doctorat a été numérisée par l'Université libre de Bruxelles. L'auteur qui s'opposerait à sa mise en ligne dans DI-fusion est invité à prendre contact avec l'Université (di-fusion@ulb.be).

Dans le cas où une version électronique native de la thèse existe, l'Université ne peut garantir que la présente version numérisée soit identique à la version électronique native, ni qu'elle soit la version officielle définitive de la thèse.

DI-fusion, le Dépôt Institutionnel de l'Université libre de Bruxelles, recueille la production scientifique de l'Université, mise à disposition en libre accès autant que possible. Les œuvres accessibles dans DI-fusion sont protégées par la législation belge relative aux droits d'auteur et aux droits voisins. Toute personne peut, sans avoir à demander l'autorisation de l'auteur ou de l'ayant-droit, à des fins d'usage privé ou à des fins d'illustration de l'enseignement ou de recherche scientifique, dans la mesure justifiée par le but non lucratif poursuivi, lire, télécharger ou reproduire sur papier ou sur tout autre support, les articles ou des fragments d'autres œuvres, disponibles dans DI-fusion, pour autant que :

- Le nom des auteurs, le titre et la référence bibliographique complète soient cités;
- L'identifiant unique attribué aux métadonnées dans DI-fusion (permalink) soit indiqué;
- Le contenu ne soit pas modifié.

L'œuvre ne peut être stockée dans une autre base de données dans le but d'y donner accès ; l'identifiant unique (permalink) indiqué ci-dessus doit toujours être utilisé pour donner accès à l'œuvre. Toute autre utilisation non mentionnée ci-dessus nécessite l'autorisation de l'auteur de l'œuvre ou de l'ayant droit.

----- English Version -----

This Ph.D. thesis has been digitized by Université libre de Bruxelles. The author who would disagree on its online availability in DI-fusion is invited to contact the University (di-fusion@ulb.be).

If a native electronic version of the thesis exists, the University can guarantee neither that the present digitized version is identical to the native electronic version, nor that it is the definitive official version of the thesis.

DI-fusion is the Institutional Repository of Université libre de Bruxelles; it collects the research output of the University, available on open access as much as possible. The works included in DI-fusion are protected by the Belgian legislation relating to authors' rights and neighbouring rights. Any user may, without prior permission from the authors or copyright owners, for private usage or for educational or scientific research purposes, to the extent justified by the non-profit activity, read, download or reproduce on paper or on any other media, the articles or fragments of other works, available in DI-fusion, provided:

- The authors, title and full bibliographic details are credited in any copy;
- The unique identifier (permalink) for the original metadata page in DI-fusion is indicated;
- The content is not changed in any way.

It is not permitted to store the work in another database in order to provide access to it; the unique identifier (permalink) indicated above must always be used to provide access to the work. Any other use not mentioned above requires the authors' or copyright owners' permission.

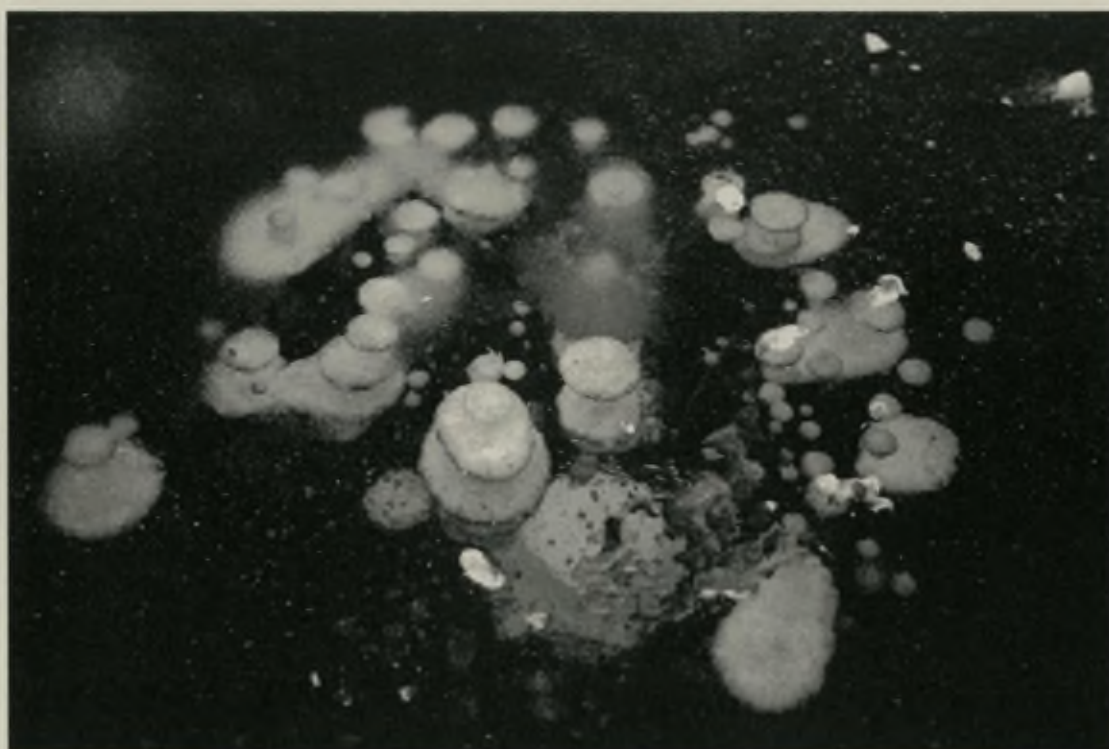
D 03889



Universite Libre de Bruxelles

PhD Thesis:

Greenhouse gases investigations in ice from periglacial environments



June 2012

Thierry BOEREBOOM

Supervisor: Prof. Jean-Louis TISON

Universite Libre de Bruxelles



003507924

Université Libre de Bruxelles

PhD Thesis:

**Greenhouse gases investigations in ice from
periglacial environments**



June 2012

Thierry BOEREBOOM

Supervisor: Prof. Jean-Louis TISON

Content

Content	1
Prologue	5
Chapter 1. Introduction	7
1.1 Climate change and the periglacial environment	7
1.2 Ice forms in the periglacial environment	12
1.3 Ice wedges overview	14
1.4 Lake ice overview	17
1.4.1 Lake ice formation	17
1.4.2 Impurities in lake ice	17
1.4.3 Bubbles in lake ice	18
1.5 This PhD thesis overview	21
Chapter 2. Stable isotope and gas properties of two ice wedges from Cape Mamontov Klyk, Laptev Sea, Northern Siberia	23
Abstract	23
2.1 Introduction	24
2.2 Study area and ice wedge description	25
2.3 Sampling and analytical methods	28
2.4.1 Stable ^{18}O and ^2H isotopes	29
2.4.2 Ice texture and fabrics	31
2.4.3 Gas properties	32
2.4.4 Sediments properties	34
2.5.1 Ice wedge infilling processes	35
2.5.2 Links to the regional paleoclimatic interpretation	42
2.6 Conclusions	47

Chapter 3. Gases properties of winter lake ice in Northern Sweden: implication for carbon gas release	49
Abstract.....	49
3.1 Introduction	50
3.2 Study area and sampling.....	52
3.3 Methods	53
3.4 Results	54
3.4.1 Ice characteristics	54
3.4.2 Gas composition	56
3.4.3 Total gas content.....	58
3.5 Discussion.....	58
3.5.1 A new lake ice type classification based on bubbles properties.....	58
3.5.2 Depth dependency of the gas composition	60
3.5.3 Ice type dependency of gas mixing ratios	67
3.5.4 Controls on bubble distribution in lake ice.....	68
3.5.5 Assessing a lower bound for lake ice melting contribution to the atmospheric methane budget.....	70
3.6 Conclusions	71
Chapter 4. Methane isotopic signature of bubbles in permafrost winter lake ice : a tool for quantifying variable oxidation levels	73
Abstract.....	73
4.1 Introduction	74
4.2 Study area : Lake characteristics and sampling procedure.....	75
4.3 Methods	76
4.4 Results	77
4.5 Discussion.....	78
4.6 Conclusions	85
Chapter 5. Conclusions	87
Annex A: Report: Gas properties of the EPICA Dronning Maud Land (EDML) basal refrozen water.....	91
Abstract.....	91
Introduction	92
Methods	93
Total gas volume	93

Gas composition	95
Results	96
Total gas volume	96
Gas composition	97
Discussion.....	98
Clathrate formation.....	98
Total gas content	99
Gas composition	102
Conclusion	103
Bibliography.....	105
Publications	119
Acknowledgements	121

Prologue

The work developed in this PhD thesis has been performed at the “Laboratoire de Glaciologie” of the “Université Libre de Bruxelles” between October 2005 and October 2011, while fulfilling my teaching assistant position at the same time. Over that period I have been working on different projects to find out the most relevant pathway to bring the most adequate contribution to this study dedicated to the relatively unexplored subject of gas properties of ice in the periglacial environment. Along these lines, the second chapter of this thesis, dealing with ice properties of Siberian ice wedges, relates to the first approach we made, in collaboration with Hanno Meyer from the Alfred Wegner Institute (AWI), whereas chapters 3 and 4 focus on lake ice properties in Northern Sweden. We have chosen to invest more time in the latter topic because we thought it might be more relevant in terms of the global carbon budget. These three chapters are the core of the thesis and the subject of scientific papers that have been submitted for publication in international journals with peer reviewing.

The Appendix at the end of this work is a report on the basal refrozen water from the Dronning Maud Land (DML) deep drilling of the European Project for Ice Coring in Antarctica (EPICA). We see this report as the core material for a first draft of a fourth manuscript worthy of publication in the near future. I led this study at the beginning of my PhD, before collecting the first samples from my field activity related to permafrost studies. Although the scientific questions in that study are not directly related to the thesis topic, we thought the work accomplished deserves to be included in the present document.

Wishing you a pleasant reading,

Thierry Boereboom

Chapter 1. Introduction

1.1 Climate change and the periglacial environment

The periglacial environment describes areas peripheral to ice sheets and glaciers and is characterized by cold or polar climatic conditions. Actually, it refers to a complex geomorphologic entity to which the main associated vegetations are the tundra and the taïga. This environment is typical of polar, subpolar or mountainous areas (French 2007).

Global climate change is responsible for recent variations in our environment (sea level rise, temperature increase, vegetal and animal migrations, ice melting, a.s.o.) and greenhouse gases (GHG), such as carbon dioxide and methane, are known to contribute to this perturbation (IPCC 2007). The global temperature rise observed from the 19th century (Figure 1.1) affects the earth system which reacts in many different ways, one of them being “permafrost degradation”.

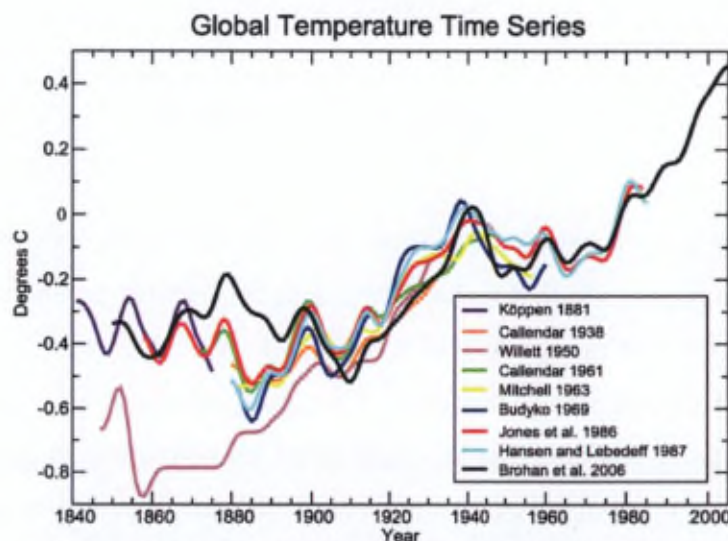


Figure 1.1: Global temperature evolution (IPCC 2007).

Permafrost is a periglacial environment characterized by ground or part of the ground which remain frozen year-round. It represents 24% of the present land surface of the Earth (French 2007) and the distinction is made, on the basis of surface coverage by frozen ground, between continuous (over 90% of exposed ground underlain by permafrost), discontinuous (50 to 90%), sporadic (10 to 50%), or isolated (below 10%) permafrost. Permafrost regions are mainly located in the Northern hemisphere (Scandinavia, Canada, Alaska, Greenland and Russia; Figure 1.2).

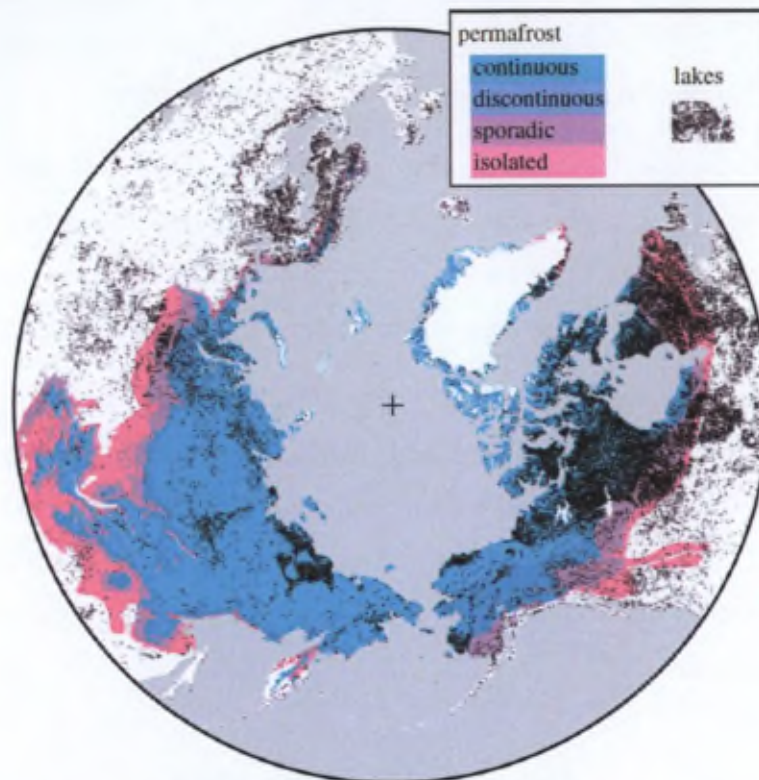


Figure 1.2: Permafrost and Pan-arctic distribution of lakes using the GLWD (Global Lakes and Wetlands Database) data northward of 45° (Walter *et al.* 2007).

Basically, a permafrost ground consists of two sections, the active layer which is the upper part of soil, sediment or rock that melts during summer and the perennially frozen ground which remains frozen for minimum two consecutive years. Figure 1.3 shows the thermal regime in this type of soil, the permafrost table corresponding to the upper surface of the perennially frozen part. The first sign of sensitivity of the permafrost to global warming is an increase of the active layer thickness. It further leads, if warming persists, to total permafrost degradation. This significant ice-rich soil melting begets land surface perturbation commonly

referred to as “thermokarst” (in reference to similitudes with the karst morphology, an erosional landform developed by water circulation in a limestone substrate) and favours the growth of wetlands and lakes. Thereafter, situations arise where the surface water is drained into the soil as unfrozen “pipes” develop. One issue of the wetland development is the synchrononeous increase of methane emissions. Methane is a greenhouse gas 23 times more efficient than carbon dioxide and it is produced in anaerobic environments such as wetlands and lake sediments by methanogenic bacteria, all of which belong to the archaeobacteria (Fenchel *et al.* 1998). There are two major microbiological pathways that produce methane in these conditions, the acetate fermentation (Equation 1.1) and the carbon dioxide reduction (Equation 1.2).

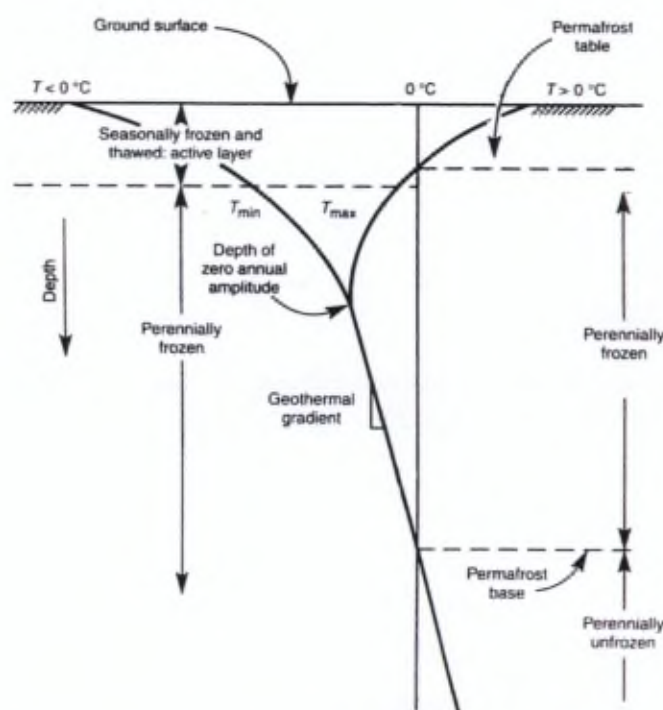


Figure 1.3: Thermal regime of permafrost ground (adapted from French 2007).

Recent studies (International Arctic Science Committee 2004; IPCC 2007) have shown that the Northern polar and subpolar regions are more affected by global warming, especially during the winter months. Figure 1.4 displays the surface temperature anomaly observed from

2000 to 2011 (in comparison with the 1951-1980 period) for the November to April period. One observes a temperature rise between 1 and 4°C in the Northern latitudes with clearly important consequences for the spatial distribution of ice and frozen soils melting (Figure 1.1). Along these lines, the degrading permafrost will continue to favour methane emissions and will probably increase its relative contribution to the global methane budget, as compared to the tropical sources.

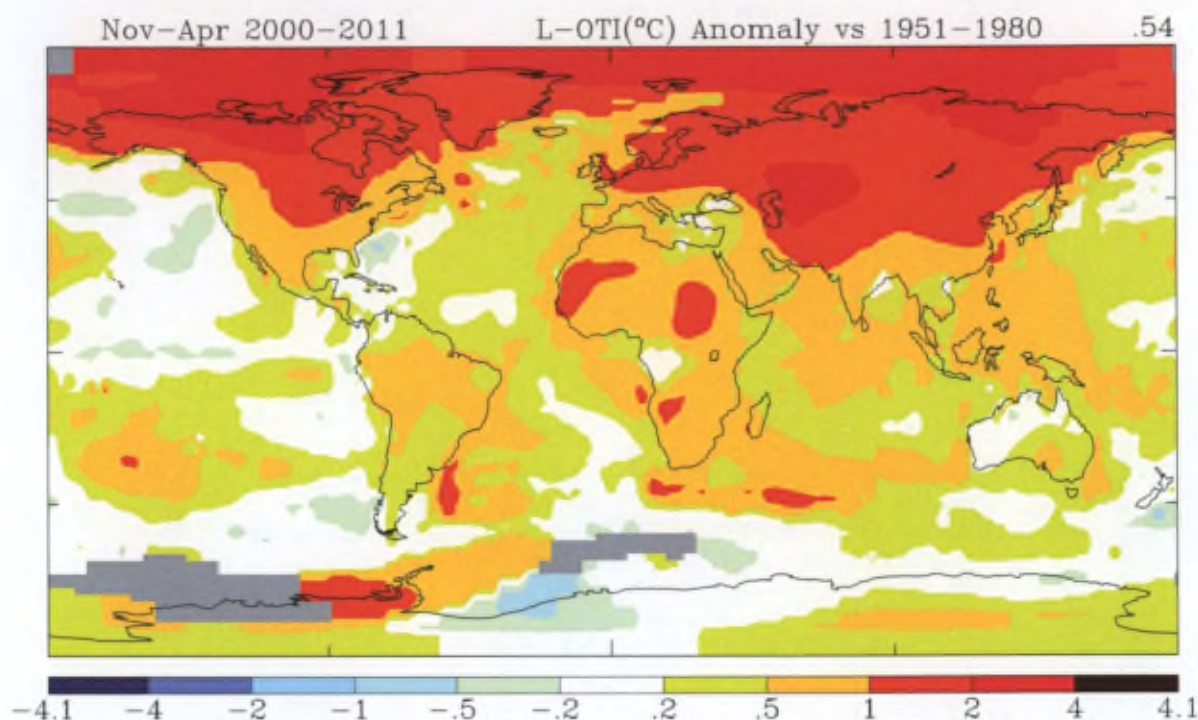


Figure 1.4: Northern winter surface temperature anomaly (*Data.GISS: GISS Surface Temperature Analysis from the National Aeronautics and Space Administration*)

Table 1.1 (adapted from IPCC 2007) shows a summary of methane budget estimates (expressed in $\text{Tg}(\text{CH}_4) \text{ yr}^{-1}$). Clearly, despite an important variability between the various authors (showing the degree of uncertainties in the budgets), wetlands are the main source of the natural methane released to the atmosphere.

References	Indicative ¹³ C, ‰	Hein <i>et al.</i> 1997	Houweling <i>et al.</i> 2000	Olivier <i>et al.</i> 2005	Wuebbles and Hayhoe, 2002	Scheehle <i>et al.</i> 2002	J. Wang <i>et al.</i> 2004	Mikaloff Fletcher <i>et al.</i> 2004a	Chen and Prinn, 2006	TAR	AR4
Base year		1983–1989		2000		1990	1994	1999	1996–2001	1998	2000–2004
Natural sources											
Wetlands	–58	231	163		100		176	231	145		
Termites	–70		20		20		20	29	23		
Ocean	–60		15		4						
Hydrates	–60				5		4				
Geological sources	–40		4		14						
Wild animals	–60		15								
Wildfires	–25		5		2						
Subtotal		231	222		145		200	260	168		
Anthropogenic sources											
Energy						74	77				
Coal mining	–37	32		34	46			30	48		
Gas, oil, industry	–44	68		64	60			52	36		
Landfills & waste	–55	43		66	61	69	49	35			
Ruminants	–60	92		80	81	76	83	91	189		
Rice agriculture	–63	83		39	60	31	57	54	112		
Biomass burning	–25	43			50	14	41	88	43		
C3 vegetation	–25			27							
C4 vegetation	–12			9							
Subtotal		361		320	358	264	307	350	428		
Total sources		592	222	320	503	264	507	610	596	598	582
Sinks											
Soils	–18	26			30		34	30		30	30
Tropospheric OH	–3.9	488			445		428	507		506	511
Stratospheric loss		45			40		30	40		40	40
Total sink		559			515		492	577		576	581
Imbalance											
		+33								+22	+1

Table 1.1 : Sources, sinks and atmospheric budgets of CH₄ (Tg(CH₄) yr^{–1}) (adapted from IPCC 2007).

Several studies are focusing on methane and carbon dioxide emissions from permafrost areas. These either look at degassing from peatland areas with automatic chamber measurements (e.g. Bäckstrand *et al.* 2010), or measure lakes and river (e.g. Semiletov 1999) emissions using specific technologies such as: bubble traps, floating chambers, headspace equilibration,

eddy flux tower, flux gradient technique (measuring CH₄ mixing ratio in air at different heights above water surface) or inverted funnels system (e.g. review table in Walter *et al.* 2010). The frozen ground itself is known to be a methane reservoir (Anderson *et al.* 2010; Walter Anthony *et al.* 2012).

that will liberate this GHG on future melting. Another very large methane reservoir is the clathrate pool where the gas is enclosed in the molecular structure of H₂O in peculiar temperature and pressure conditions, in deep permafrost soils or in oceans. Strangely enough, few studies have looked at gases entrapped in the ice, the latter being however a major component of the permafrost environment, as detailed in the next section.

Methane released to the atmosphere and into soils will take part in the global methane cycle. In the atmosphere ~90% of methane will react with hydroxyl (OH[•]) radical in the troposphere (Equation 1.3). OH[•] is formed by photodissociation of tropospheric ozone and water vapour. Remaining methane in the atmosphere is transported to the stratosphere (~5%) or oxidized by soils (~5%).



In soils, two forms of oxidation are recognized: 1) “high affinity oxidation” in dry soils where the CH₄ mixing ratio is close to the atmospheric value (<12 ppm) as upland and dry soils; 2) “low affinity oxidation” in wetland and submerged soils where CH₄ mixing ratio is higher than 40 ppm.

1.2 Ice forms in the periglacial environment

Regions affected by cold temperatures hold ice in various forms. Several classifications and terminologies exist and, in this work, following French (2007), we will distinguish 5 groups: pore ice, segregated ice, intrusive ice, vein ice and other types of ice. These different ice types have been extensively studied since the 1950's, mainly by a large number of Canadian and Russian authors. Generally, however, these studies focused on the ice genesis or the ice properties rather than on the impacts of the potential ice melting on atmospheric composition.

Pore ice is ice held in soils. It corresponds to the bonding cement that holds soil grains together. It is widespread in near-surface permafrost and in the active layer. The water content in soils containing this ice type is not supersaturated.

Segregated ice is a broad term for soil with a high ice content. The water content, in this case, being well above soil supersaturation. It consists of almost pure ice that often exists as an extensive horizontal layer (from a few millimeters thick to massive ice bodies up to tens of meters thick). The ice layer grows because of the active migration of water from the ground body surrounding feature.

Intrusive ice is formed by water intrusion, usually under pressure, into the seasonally- or perennially-frozen zone. Sill and pingo ice are two types of intrusive ice which are usually identified. Pingo ice, formed by pore-water expulsion, is a perennial frost mound consisting of a core of massive ice, produced primarily by water injection, and covered with soil and vegetation (Figure 1.5). Sill ice forms when water is intruded under pressure into a confining material and then freezes in a tabular mass.

Vein ice is formed by the water penetration into open fissures developed at the ground surface. The water origin prior to freezing is atmospheric, usually meltwater from snow. There are two types of vein ice. First, *single-vein* ice develops in small cracks, usually less than 0.2 cm thick and less than 70 cm deep. These form by thermal-contraction cracking at the ground surface. The second, forming an ice structure called *ice wedge*, is made from repeated-vein ice forms in a thermal-contraction crack that re-opens in approximately the same place for a number of years. It is a massive, generally wedge-shaped body with its apex pointing downward, composed of foliated or vertically banded, commonly white, ice. This ice type formation process is associated with a land surface characterized by polygonal nets, which result from ice-rich frozen soil thermal contractions (Figure 1.5). It is the dominant feature of permafrost areas.

Other ice types correspond to the presence of frozen water in response to specific situations within the permafrost area. Lake ice falls in this category. As discussed earlier on, lakes are a common feature in the poorly drained periglacial environment (the myriads of individual grey dots in Figure 1.2 shows the lakes distribution in the Northern subarctic area). These can be partially or completely frozen, during winter or year-round, depending on the annual thermal regime and the specific geometrical and hydrological conditions at the location. As we will show for the examples chosen in this thesis, lake ice can play an important role in the processes of gas exchange between the sediments, the liquid water and the atmosphere; with potential consequences for the earth radiative balance.



Figure 1.5 : A melting pingo and polygon wedge ice near Tuktoyaktuk, Northwest Territories, Canada (source : Wikipedia).

Since in this work, we mainly focus on ice wedges (Chapter 2) and on lake ice properties (Chapter 3 and 4), we will briefly summarize the current state of knowledge on these two ice types in the next sections.

1.3 Ice wedges overview

Ice wedges ice is the third most important ground-ice type (in terms of volume) behind pore and segregated ice (French 2007). They are formed below the active layer and they can reach several meters both in width and depth. Figure 1.6 is a sketch of the cycles of ice wedge formation processes. During winter the rapid cooling at low temperatures generates soil thermal-contraction cracking. In spring, the frost crack is filled with melt water and snow, which then refreezes deeper in the frozen ground. This leads to the formation of an initial ice vein which prevents the closure of the frost crack by volume addition. The following winter, the vertical ice-filled crack is reopened and the spring melt water and snow then percolates

into the crack, resulting in another ice vein as it freezes. Due to the thawing of the active layer, the uppermost part of the ice vein is destroyed in the summer.

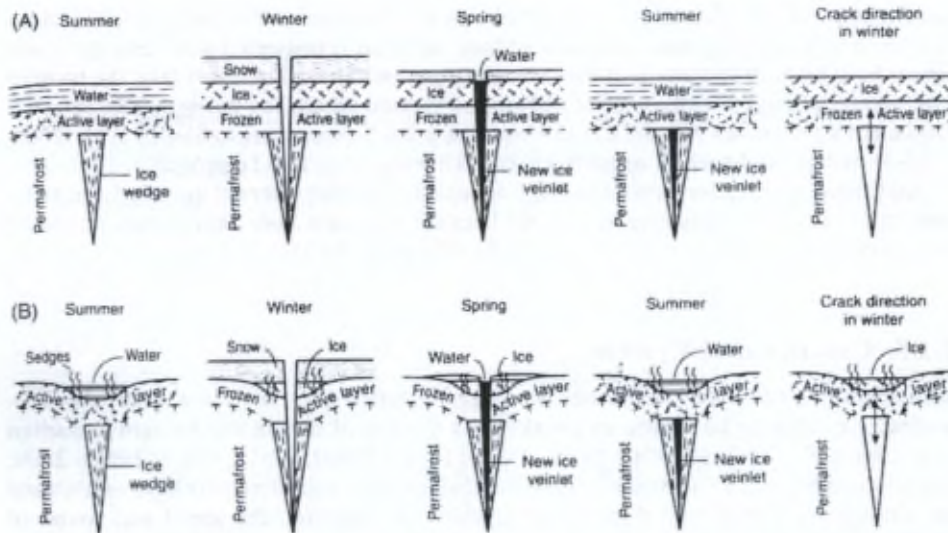


Figure 1.6: Diagram illustrating the growth of ice wedges beneath shallow pool of standing water (A) and beneath a water-filled ice-wedge trough (B) (French 2007).

Ice wedges crystallographic analyses have largely been discussed by several authors since the 1950's (e.g. Black 1954, 1963, 1976, 1978; Corte 1962; Shumskii 1964; Gell 1971, 1976, 1978; Raffi *et al.* 2004). C-axes orientation, grain growth and recrystallization seem to be governed by the temperature gradient and the lateral stress induced by the soil thermal contraction. C-axes are commonly oriented in the horizontal plane at the top and in the centre of the ice-wedge. This crystals reorganization is traditionally associated to the repeated lateral stress induced by the thermal contraction of the soil. As effect of this lateral stress, the crystals from the border are generally larger and characterized by elongated bubble into the crystal, suggesting ice deformation in this part of the ice wedge. C-axes can however also be vertically oriented especially along the ice wedge border where the crystals are older. In the central part of ice wedges, the crystals are smaller with small spherical bubbles at the grains boundary, which is typical of ice resulting from a snow/water mixture consolidation showing no indication of migration of a freezing front.

Isotopic studies ($\delta^{18}\text{O}$ and δD) on ice wedges ice revealed that this ice type can be, in adequate condition, a useful tool for paleo-climatic investigations, similar to what has been done for glacier ice in ice sheet. Since the ice veins forming the ice wedge generally record

the isotopic signature of each winter's precipitation, the horizontal profile from the centre to the border of the ice wedge enables to reconstruct past climatic conditions during ice wedge formation (Meyer *et al.* 2000, 2002a, 2002b, 2010a, 2010b; Dereviagin *et al.* 2002). Recent ice wedges in Northeast Siberia show $\delta^{18}\text{O}/\delta\text{D}$ values between -25‰/-190‰ and -20‰/-140‰ (Opel *et al.* 2011), while younger Holocene ice wedges values range between -26‰/-195‰ and -22‰/-175‰ and older Holocene ice wedges are -26‰/-202‰ to -24‰/-190‰ (Wetterich *et al.* 2008). The Pleistocene isotopic signature in the same area clearly differs by decreases of approximately 5‰ and 35‰ in the $\delta^{18}\text{O}$ and δD signatures, respectively (Popp *et al.* 2006) with $\delta^{18}\text{O}/\delta\text{D}$ values between -33‰/-250‰ and -31‰/-245‰ (Wetterich *et al.* 2008) with minima from the Last Glacial Maximum (-35‰/-290‰) as documented in a recent overview from Wetterich *et al.* (2011). Co-isotopic approaches use the deuterium excess (d) as a tracer for changes in the atmospheric source. For example, Meyer *et al.* (2010b), who identified the Younger Dryas cold event in Northern Alaskan ice wedges, also brought to the light a rapid reorganization of the Arctic atmospheric circulation following the opening of the Bering Strait, with d -transitions from about 6 ‰ to about 9 ‰, as also observed in the North GRIP deep ice core.

Gas properties in ice wedges are scarcely documented in the literature. Brouchkov and Fukuda (2002) studied methane and carbon dioxide in permafrost soils and in an ice wedge in central Yakutia. They observed CH_4 mixing ratio between 1 and 3118 ppm and CO_2 mixing ratio between 0 and 23,211 ppm in their ice wedge. They suggest that methane is produced in soils by bacteria under anaerobic conditions and is then trapped in the ice structure during the ice wedge formation. They also described an inverse relationship between methane and carbon dioxide, in both ice wedge and soils, suggesting potential CH_4 oxidation to CO_2 . They also showed that CO_2 concentration increases with the water content in permafrost soils. Yet, studies on bacterial communities performed on permafrost and ice wedge ice have detected specific biological processes in the ice such as respiration or methanogenesis (Gilichinsky *et al.* 2007; Katayama *et al.* 2007; Steven *et al.* 2008; Lacelle *et al.* 2011). Most recently, St-Jean *et al.* (2011) led a broad study on ice wedge properties and on the ice wedge infilling processes in which they demonstrate active respiration processes in bubbles and the influence of the water liquid content available during ice formation on the gas properties in the bubbles.

1.4 Lake ice overview

1.4.1 Lake ice formation

Lake ice is mainly characterized by vertically elongated crystals often called “candle ice”. The water starts to freeze at the lake surface with small crystals forming a primary ice layer. The next ice layer is constructed from the first layer, the crystals becoming progressively vertically elongated and larger because; a) the freezing front progresses from the lake surface into the water column; b) crystal growth is favoured along the basal plane, i.e. perpendicular to the optic axis and; c) the horizontal crystals growth is restrained by the presence of the other crystals. In a natural environment, the initial growth layer is often destructed by surface sublimation, since sampling generally occurs several months after ice formation. Figure 1.7 (a) illustrates the sequence described above with the crystallographic structure of the first layer at the top and the candle ice below. The c-axes of the elongated crystals are either concentrated in the horizontal plane or aligned on the vertical plane, the main orientation probably depending on the crystals characteristics in the primary layer (Weeks and Wettlaufer 1996; Petrenko and Whitworth 1999).

1.4.2 Impurities in lake ice

The dissolved compounds in the water, such as salts or gases, are mainly rejected at the ice-water interface during lake ice formation. However a fraction of some of these compounds will be incorporated into the ice structure, depending on several controlling factors. One of the main controls is the ice growth rate: at slow freezing, diffusion into the main reservoir, ahead of the freezing front will take over, while, at faster freezing, incorporation will be favoured, be it in the ice structure or at the crystals boundary. This process can be expressed by the following equation (Burton *et al.* 1953).

$$\alpha_{eff} = \frac{\alpha_{eq}}{\alpha_{eq} - (\alpha_{eq} - 1)e^{-\frac{z_{bl}v}{D}}} \quad (\text{Equation 1.4})$$

Where α_{eff} is the effective fractionation factor which depends on the equilibrium fractionation factor (α_{eq}), the boundary layer thickness (z_{bl}), the diffusion coefficient (D) and the growth rate (v). Many other factors will also play a role: the water turbulence, the water column depth, the water concentration, the type of impurity and its compatibility with solid water structure a.s.o. (Carte 1961; Bari and Hallett 1974; Adams *et al.* 1998; Petrenko and Whitworth 1999; Lorrain *et al.* 2002).

1.4.3 Bubbles in lake ice

Bubbles nucleation at the ice-water interface results from supersaturation of the dissolved gases in the water induced by the ice growth. A fast freezing rate favours a high bubbles concentration in the ice with bubbles of small radius, while bubbles will be larger at a lower freezing rate (Bari and Hallett 1974; Gow and Langston 1977; Adams *et al.* 1998; Lorrain *et al.* 2002). A constant freezing rate generally induces some “waves” of narrow vertical cylindrical bubbles in response to the supersaturation as illustrated in Figure 1.7 (b). This bubble formation results in decreasing the dissolved gases concentration at the ice-water interface, which then results in bubble-free ice growth phases.

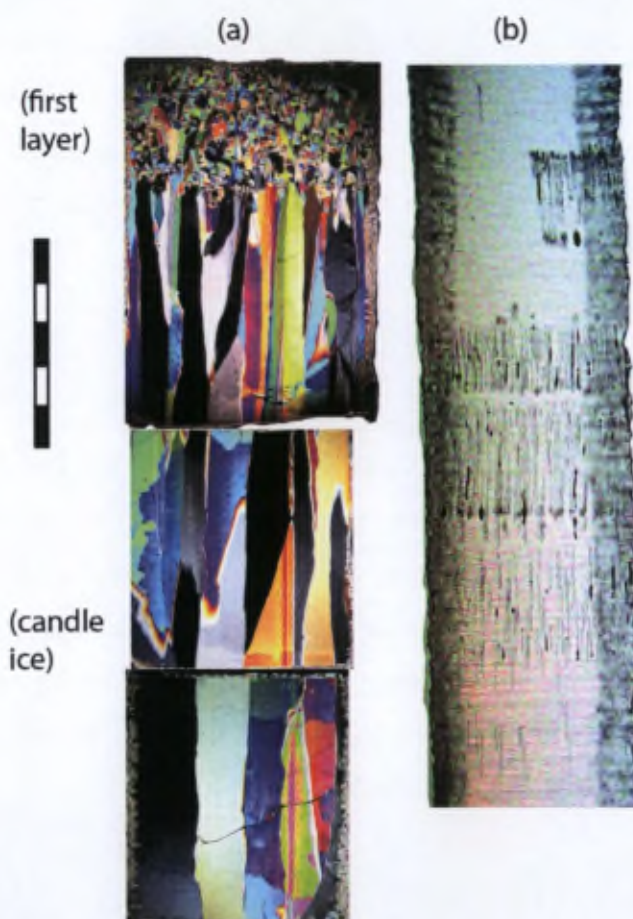


Figure 1.7 : Thin section illustrating the crystallographical structure of the ice (a) and waves of narrow elongated bubbles, typical of constant freezing front growth (b). (a) and (b) are not from the same core. Units on the left side scale is centimeters.

Several descriptions of bubble shapes in lake ice exist in the literature: vertical cylindrical bubble as described above (e.g. Nedell *et al.* 1987; Squyres *et al.* 1991; Wharton *et al.* 1993;

Adams *et al.* 1998; Lorrain *et al.* 2002), tear shaped bubbles or plume-like bubble patterns as seen in the vicinity of a sediment (Adams *et al.* 1998) and “tabular” bubbles with ± 1 cm height and several cm width (e.g. Squyres *et al.* 1991). The latter generally originate from a “bubbling event” initiated in from the sediment below.

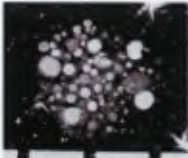


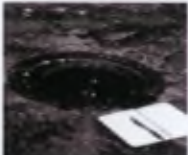
Seep	Description	CH ₄ (%)	Ebullition (mg CH ₄ d ⁻¹)		
			Summer	Winter	Annual
	A Isolated bubbles in multiple ice layers	73 ± 11, n = 6	28 ± 19, n = 3	8 ± 5, n = 8	16 ± 10
	B Merged bubbles in multiple ice layers	75 ± 3, n = 35	210 ± 8, n = 2	81 ± 29, n = 4	131 ± 30
	C Single gas pockets stacked in ice	76 ± 3, n = 41	1042 ± 210, n = 6	925 ± 98, n = 9	971 ± 142
	Hotspot Relatively open hole in winter lake ice	78 ± 2, n = 52	3130 ± 244, n = 4	3240 ± 412, n = 10	3197 ± 484

Table 1.2 : Classification of ebullition seeps by CH₄ bubble-clusters patterns in lake ice; CH₄ mixing ratios in bubble gas (% by volume); and summer, winter, and annual ebullition determined by long-term flux measurements. Error estimates (standard error of *n* seeps) represent differences in CH₄ mixing ratios and ebullition between individual seeps in each category. The lines on the meter sticks in the photos of type A and B mark 10 cm wide intervals (Walter *et al.* 2010).

The size of this type of bubbles can be much larger (up to 1 m in diameter) in lakes from permafrost areas, due to sustained methane degassing from the sediment, in this changing environment. Walter *et al.* (2006, 2007a, 2007b, 2008a, 2008b, 2010) studied methane properties of these bubbles showing variable methane mixing ratios (Table 1.2) and isotopic signatures (Figure 1.8). Different bubble types are defined from the different sources (Figure 1.8): a) background ebullition, is typically a low-magnitude flux that covers the majority of the lake surface area, it is characterized by lower CH₄ content and younger radiocarbon age (Holocene), and is often produced in surface sediments; b) point source, is characterized by higher CH₄ mixing ratios and older radiocarbon ages, it is supposed to be emitted through

deeper sediments; c) hotspot, emits bubbles with a high CH_4 mixing ratio (up to 90%) and ancient radiocarbon age (up to 43 000 years), suggesting that CH_4 is produced at great depth in the lake's thaw bulb from an ancient organic matter source (Pleistocene-aged), sometimes extremely high ebullition rates are sufficient to maintain open holes in lake ice throughout the winter.

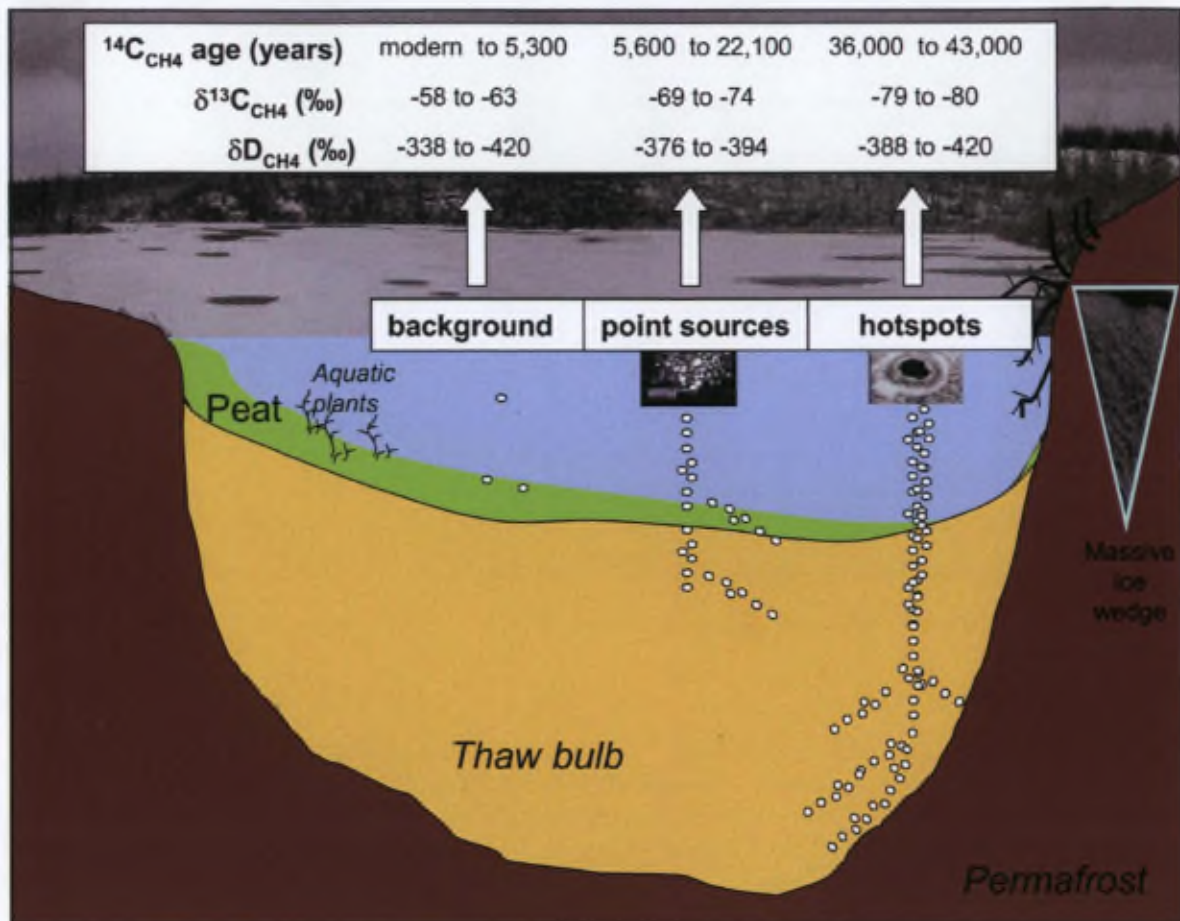


Figure 1.8: Cross-section of a North Siberian thermokarst lake showing dynamics of background, point-source and hotspot ebullition with respective CH_4 isotopic signature and emission (Walter *et al.* 2008a).

These studies mainly focused on thermokarst lakes because this environment is currently very “dynamic” since the lakes (and the lakes surfaces) are growing due to permafrost degradation, providing recently unfrozen soils, rich in organic matters.

1.5 This PhD thesis overview

Quantifying methane release from permafrost ice to the atmosphere is a major objective of this work, in order to reduce uncertainties when taking into account this powerful greenhouse gas in climate change modelling. There are already a large number of studies on methane emissions from several environments such as soils, oceans, lakes or agriculture. Permafrost areas are changing quickly and they contain a large amount of ice which can potentially contribute to the global methane budget. However very few studies focus on gas entrapped in ice and further released to the atmosphere when the ice is melting.

In this thesis, we contribute new data on gas properties and methane release of two permafrost ice types. Indeed, we use our glaciological background and our expertise on gas measurements in ice to study two Siberian ice wedges (Chapter 2) and winter ice of four lakes from Northern Sweden (Chapter 3 and 4). These two studies led us to demonstrate that ice properties can be a useful tool to understand ice formation processes and to characterize physical and biological processes at work in this environment.

The multiparametric study on ice wedges discussed in Chapter 2 reaches two goals: a) it provides new data on gas properties of ice wedge ice allowing us to refine our understanding of ice veins formation processes and b) it uses contrasted co-isotopic signatures of the ice wedges to open new perspectives on major atmospheric circulation changes in the Arctic, both between the Holocene and the Pleistocene and within the Pleistocene.

Chapter 3, discusses gas properties in permafrost lake ice and shows, *inter alia*, that the presence of an annual ice cover influences atmosphere – water exchanges and induces a methane release on lake ice cover melting which is sensibly different from the emissions for the rest of the year. A new physico-chemical bubbles classification in lake ice is also proposed in this chapter.

Chapter 4 is a logical follow up of chapter 3 since we analyse in this chapter the stable methane isotopic composition from gas bubbles, to investigate and characterize the biogeochemical processes occurring in lakes during the length of the ice cover period.

Finally, as underlined in the Prologue, the Appendix at the end of this thesis, is a report on the basal refrozen water from the Dronning Maud Land (DML) deep drilling of the European Project for Ice Coring in Antarctica (EPICA). This report will be used as the core material for a fourth manuscript synthetizing the data we acquired in the early stages of our research activity at the Université Libre de Bruxelles.

Chapter 2. Stable isotope and gas properties of two ice wedges from Cape Mamontov Klyk, Laptev Sea, Northern Siberia

This paper has been published as : « Stable isotope and gas properties of two ice wedges from Cape Mamontov Klyk, Laptev Sea, Northern Siberia », Boereboom T., Samyn D., Meyer H. and Tison J-L. in The Cryosphere Discussions (December 2011) and accepted for publication with revisions in The Cryosphere (final decision pending).

Abstract

This paper presents and discusses the texture, fabric, water stable isotopes ($\delta^{18}\text{O}$, δD) and gas properties (total gas content, O_2 , N_2 , Ar, CO_2 , and CH_4 mixing ratios) of two climatically contrasted (Holocene vs. Pleistocene) ice wedges (IW-26 and IW-28) from Cape Mamontov Klyk, Laptev Sea, in Northern Siberia. The two ice wedges display contrasting structures: one being of relatively “clean” ice and the other showing clean ice at its centre as well as debris-rich ice on both sides (referred to as “ice-sand wedge”). Our multiparametric approach allows discriminating between three different ice facies with specific signatures, suggesting different climatic and environmental conditions of formation and various intensities and nature of biological activity. More specifically, crystallography, total gas content and gas composition reveal variable levels of meltwater infiltration and contrasting contributions from anaerobic and aerobic conditions to the biological signatures. Stable isotope data are shown to be valid for discussing changes in paleoenvironmental conditions and in the temporal variation of the different moisture sources for the snow feeding into the ice wedges infillings. Our data set

also give further support to the previous assumption that the ice wedge IW-28 was formed in Pleistocene and the ice wedge IW-26 in Holocene times. This study sheds more light on the conditions of ice wedge growth under changing environmental conditions.

2.1 Introduction

Ice wedges are a common geomorphological feature of permafrost areas in the Northern Hemisphere and widespread in Alaska, Canada and Siberia. The analysis of ice wedges properties is therefore commonly used to provide proxy-data for paleoclimatic and paleoenvironmental reconstructions. First, the isotopic signature ($\delta^{18}\text{O}$ or δD) of the ice is thought to reflect the isotopic characteristics of the winter precipitation which are a function of the temperature at the site (Vaikmäe 1989; Lauriol *et al.* 1995; Vasil'chuk and Vasil'chuk 1998; Dereviagin *et al.* 2002; Meyer *et al.* 2002a, 2002b; Raffi *et al.* 2004). As an example, recent ice wedges in Northeast Siberia show $\delta^{18}\text{O}/\delta\text{D}$ values between -25‰/-190‰ and -20‰/-140‰ (Opel *et al.* 2011), while younger Holocene ice wedges values range between -26‰/-195‰ and -22‰/-175‰ and older Holocene ice wedges are -26‰/-202‰ to -24‰/-190‰ (Wetterich *et al.* 2008). The Pleistocene isotopic signature in the same area clearly differs by decreases of approximately 5‰ and 35‰ in $\delta^{18}\text{O}$ and δD , respectively (Popp *et al.* 2006) showing $\delta^{18}\text{O}/\delta\text{D}$ values between -33‰/-250‰ and -31‰/-245‰ (Wetterich *et al.* 2008) with minima from the Last Glacial Maximum (-35‰/-290‰) as documented in a recent overview from Wetterich *et al.* (2011).

Co-isotopic approaches, use the deuterium excess (d) as a tracer for changes in the atmospheric source. For example, Meyer *et al.* (2010b), who identified the Younger Dryas cold event in Northern Alaskan ice wedges, also brought to the light a rapid reorganization of the Arctic atmospheric circulation following the opening of the Bering Strait, with d -transitions from about 6 ‰ to about 9 ‰, as also observed in the North GRIP deep ice core.

Other ice wedge properties can be useful to understand and reconstruct the environmental condition prevailing during ice wedge genesis. St-Jean *et al.* (2011) recently used ice crystallography, bubble content, gas composition and stable O-H isotopes of ground ice to identify contrasting genetic processes between ice wedges formed during the Late Pleistocene period under cold and dry climatic conditions and ice wedges formed during the Holocene in warmer and wetter conditions. Ice wedges formation primarily results from cyclic frost-cracking and crack infilling by ice (e.g. Mackay 1974). The cracking results from

the thermal contraction of the soil the winter (Lachenbruch 1962) and the origin of the ice infilling can be attributed to several sources (or mixture of sources) such as: a) unmodified winter snow, b) hoarfrost accretion during winter and c) snow melt infiltration in spring, subsequently refreezing in the crack to form “ice veins” (e.g. Lauriol *et al.* 1995; Opel *et al.* 2011; St-Jean *et al.* 2011). In their work, St-Jean *et al.* (2011) contrast a Pleistocene ice wedge in which the ice filling rather results from dry snow compaction or hoarfrost accretion and an Holocene ice wedge in which liquid water infiltration and refreezing dominates.

Ice wedges incorporate variable amounts of sediment depending on the sediment, snow and/or water availability at a given time. Frost cracks can be completely filled by blown sediments in very dry conditions forming a “sand wedge” (e.g. Berg and Black 1966) or can be filled-in by successive ice veins and sediments layers as described in Meyer *et al.* (2002a) or in Romanovsky (1976). This latter type of structure will be here referred to as an “ice-sand wedge” (also termed “composite wedge”).

In this paper, we propose a multi-parametric approach including stable isotope composition, total gas content, gas composition, as well as textures and fabrics to study two specific ice wedges from the Laptev Sea region. These two ice wedges were sampled from a cliff in the framework of the project “Process studies of permafrost dynamics in the Laptev Sea”, which aimed to address the paleoenvironmental history of the Cape Mamontov Klyk area (Schirrmeister *et al.* 2008; Bobrov *et al.* 2009; Müller *et al.* 2009). These specific ice wedges were chosen for this study due to their contrasting ages (Holocene vs. Pleistocene) as indicated by their stable isotope signature and stratigraphic position in a dated regional sequence. The aim of the study is two-fold: a) to improve our understanding of the imprint of the contrasted Holocene/Pleistocene climatic and environmental conditions on the ice wedge properties and infilling processes and b) to interpret the specific deuterium excess signature of the two ice wedges in terms of potential changes in atmospheric moisture sources.

2.2 Study area and ice wedge description

The two studied ice wedges are part of a coastal bluff on the Laptev Sea coast, about 300 km west from the Lena Delta (73°36' N; 117°10' E, Figure 2.1). This area belongs to the subarctic tundra in a region of continuous permafrost, with a thickness of 400-600 m (Yershov 1989). The active layer shows a maximum thaw depth of 0.2-0.5 m in July. The area is dominated by a continental arctic climate with long severe winters and short cold summers.

The cliff from which the ice wedges originate is subdivided into four different sedimentological units (A to D, from old to young; Figure 2.2a) and described in detail by Schirrmeister *et al.* (2008). From the bottom of the cliff to its top, we distinguish a lower sand unit (unit A) that consists of yellowish-grey, irregularly-laminated fine-grained sand, lacking visible plant remains. Grass roots in the uppermost horizon of this unit were dated to 44.5 ky (Schirrmeister *et al.* 2008). Above, unit B consists of an alternation of four cryoturbated peat-rich horizons and irregularly-laminated, dark-grey silty to fine-grained sandy interbeds. Unit C is known as “Ice Complex”, a type of ice-rich permafrost deposit of Late Pleistocene age widespread in Arctic Siberia attributed at this site to the Sartan period (Schirrmeister *et al.* 2008). The Ice Complex deposits are composed of alternating mineral-rich (greyish) and organic-rich (brownish) sediment layers. The upper unit (unit D) consist of peat soils of Holocene age originating from fillings of small thermokarst or polygonal ponds developed on top of the Ice Complex or from Holocene thermoerosional or fluvial deposits.



Figure 2.1 : Location of the Cape Mamontov Klyk sampling site in Arctic Siberia. The studied ice wedges were exposed on a coastal cliff on the Laptev Sea coast.

Ice wedge 26 (IW-26, Figure 2.2b) was sampled within unit C in the upper part of the cliff, at 18.6 m above sea level, and is therefore embedded within late Pleistocene Ice Complex sediments (Schirrmeister *et al.* 2008). IW-26 is about 1.6 m in width and about 2.5 m in height are visible on Figure 2.2. Sampling was performed across the full ice wedge width, approximately 1.2 m below the surface. The ice samples consisted of foliated grey to white, and in parts yellowish, ice with small (millimetric) gas bubbles. The wedge ice shows a low

content of mineral particles and organic matter (fine-disperse individual particles or thin layers following the foliation).

The second ice wedge studied in this paper, IW-28 (Figure 2.2c), has been attributed to unit A in the lower part of the cliff and was sampled at 1 m above sea level. It developed in sandy sediments. IW-28 is up to 5 m wide in its upper part at the top of the cliff. The ice wedge is laterally associated with an ice-sand wedge (ISW-28), a portion of which was also sampled (Figure 2.2c, left of sampling box). In the central section, the wedge ice has a white and milky appearance, and small millimetric gas bubbles are frequent (Figure 2.3d). The mineral content and the organic matter contents are both low, with particles dispersion similar to that in IW-26 and foliation layers that are 1-3 mm wide. For the ice-sand wedge portion, the ice is mixed with a significant amount of fine-grained sediments alternating with clean ice layers.

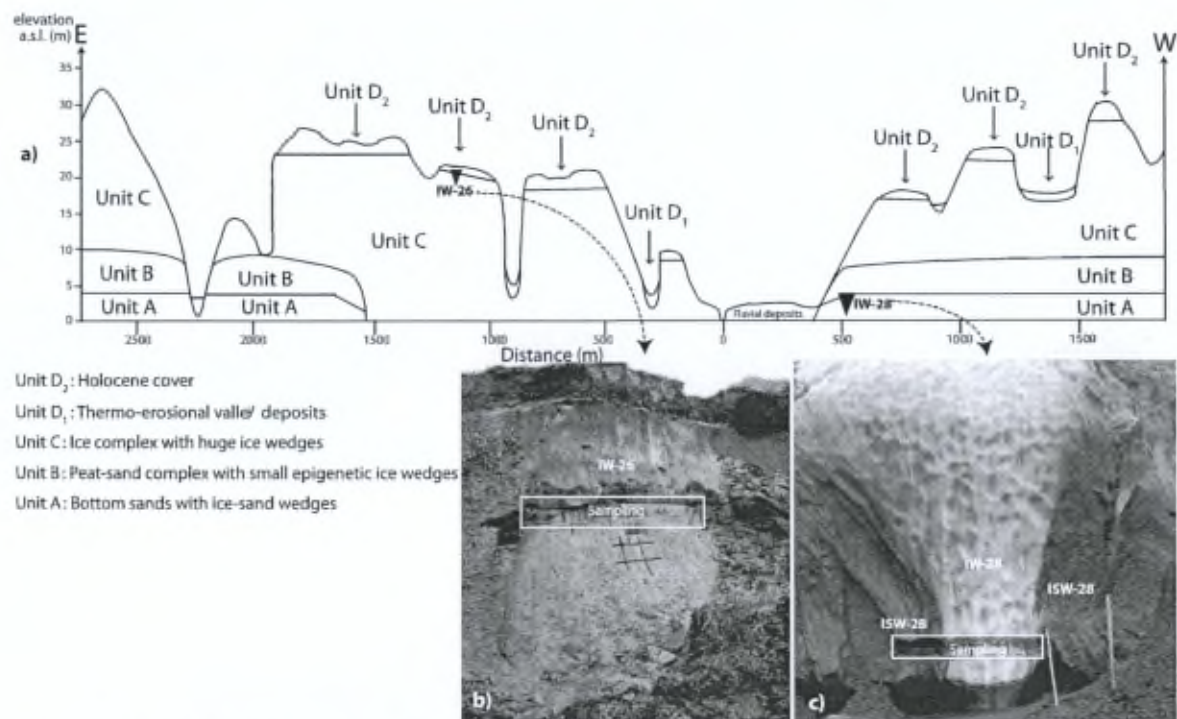


Figure 2.2 : a) General stratigraphic scheme of the main section of Mamontov Klyk (adapted from Schirrmeister *et al.* 2008) with positions and general settings b) and c) of ice wedges 26 (IW-26) and 28 (IW-28) respectively. The sampling areas are outlined with white boxes, on approximately 160 cm and 190 cm for respectively IW-26 and IW-28. Rectangular parallelepipeds have been removed from the cliff with chain-saw of which the upper part (1.5 cm thickness) has been used in this work. Note that IW-28 was sampled in both the ice-sand wedge (ISW-28, left of box) and in the ice wedge itself (IW-28, right of box).



Figure 2.3 : Thin section photographs of the textural properties of the ice wedges. a) IW-26, b) ISW-28 (ice-sand wedge), the left part of ice wedge 28 with debris sub vertical layers (note the crystal elongation along the foliation), c) IW-28, clean ice in the central part of ice wedge 28 and d) thick section photograph of ice from IW-28 in transmitted light allowing bubble content observation.

2.3 Sampling and analytical methods

The ice wedges were sampled as ice blocks using a chain saw, in horizontal transects covering the entire ice-wedge width and partly including the ice-sand wedge section from now on referred to as ISW-28 (Figure 2.2c). Samples used in this paper for fabric, texture, gas and stable isotope analyses are derived from horizontal sections (± 1.5 cm thickness) in the top part of the blocks extracted from the ice wedge.

Horizontal thin sections were prepared using a traditional biological microtome (Leitz 1400) for the clean ice and a diamond-wire saw (Well 6234) for the debris-laden ice, following the standard procedures from Langway (1958) and Tison (1994), respectively.

Crystal-size determination was performed using two different techniques. The first was the mean linear intercept method developed by Pickering (1976). The number of grain boundaries (\bar{N}) crossed by a random linear traverse of length (\bar{L}) across the thin section was averaged over many traverses. The mean grain diameter (\bar{d}) was estimated using the following equation: $\bar{d} = \bar{N}/\bar{L}$. The second method, proposed by Jacka (1984), estimates the mean diameter by counting the number of entire crystals in a known area and assuming a circular cross-section following the equation $\bar{d} = \sqrt{4A/\pi N}$, where A is the area of thin section studied and N is the crystal count.

Stable water isotopes were measured at high resolution (approximately every centimeter) with a Finnigan MAT Delta-S mass spectrometer at the Alfred Wegener Institute, Research Unit Potsdam using equilibration techniques. Hydrogen and oxygen isotope ratios are presented as per mil difference relative to V-SMOW (‰, Vienna Standard Mean Ocean

Water), with internal 1σ errors better than 0.8‰ and 0.1‰ for δD and $\delta^{18}O$, respectively (Meyer *et al.* 2000).

Gas inclusions entrapped in the ice were analysed for their total gas volume (27 samples) and gas composition (CO_2 , O_2 , N_2 , Ar, and CH_4). Gas composition (CH_4 = 24 samples, Ar = 7 samples, other gases = 30 samples) was measured by gas chromatography (Interscience Trace GC) using an FID detector for CO_2 and CH_4 and a TCD detector for O_2 , Ar and N_2 . Between 20 to 35 grams of sample were used for each measurement. For CO_2 , O_2 , Ar and N_2 , we used the dry-extraction technique described in Raynaud *et al.* (1982) and Barnola *et al.* (1983). For CH_4 , we used the melting-refreezing procedure described in Raynaud *et al.* (1988) and Blunier *et al.* (1993). The levels of precision of the measurements are 2.5% for CO_2 , 0.4% for O_2 and N_2 , 2% for Ar and 3% for CH_4 . The total gas content (27 samples) was determined using a Toepler pump and a melting-refreezing extraction technique described in Martinerie *et al.* (1994). The precision of the measurements is $\leq 5\%$.

The limited amounts of ice provided for the gases and fabrics analyses did not yield enough material to perform a full granulometric analysis of the sediment inclusions, which is nevertheless beyond the scope of this paper. At a later stage of the interpretation, however, the residual sediments collected after the gas analyses have been treated by HCl (1 mol.l⁻¹) and H_2O_2 (30%) for qualitative detection of calcium carbonate or organic matter, respectively.

2.4 Results

2.4.1 Stable ^{18}O and 2H isotopes

Ice wedge IW-26 shows $\delta^{18}O$ values ranging between -22.6‰ and -25.8‰ and δD values between -170‰ and -191‰, respectively (Figure 2.4a). The IW-26 samples plot on a slope of 6.63 in the D- ^{18}O diagram (Figure 2.4c, grey squares). The isotopic composition of ice wedge IW-28 is also shown in Figure 2.4a and a clear distinction has to be made between the two different facies of the ice wedge: the ice-sand wedge (ISW-28) and the ice wedge itself (IW-28). These differ both in terms of deuterium-excess (Figure 2.4b) and co-isotopic relationship (Figure 2.4c). The ice-sand wedge ISW-28 displays $\delta^{18}O$ values between -29‰ and -30.9‰ and δD values between -230‰ and -246‰. The samples show a low variability in d ($1\sigma = \pm 0.6\%$) with a mean value of 1.4‰, and they are aligned on a slope of 8.03 in the co-isotopic plot.

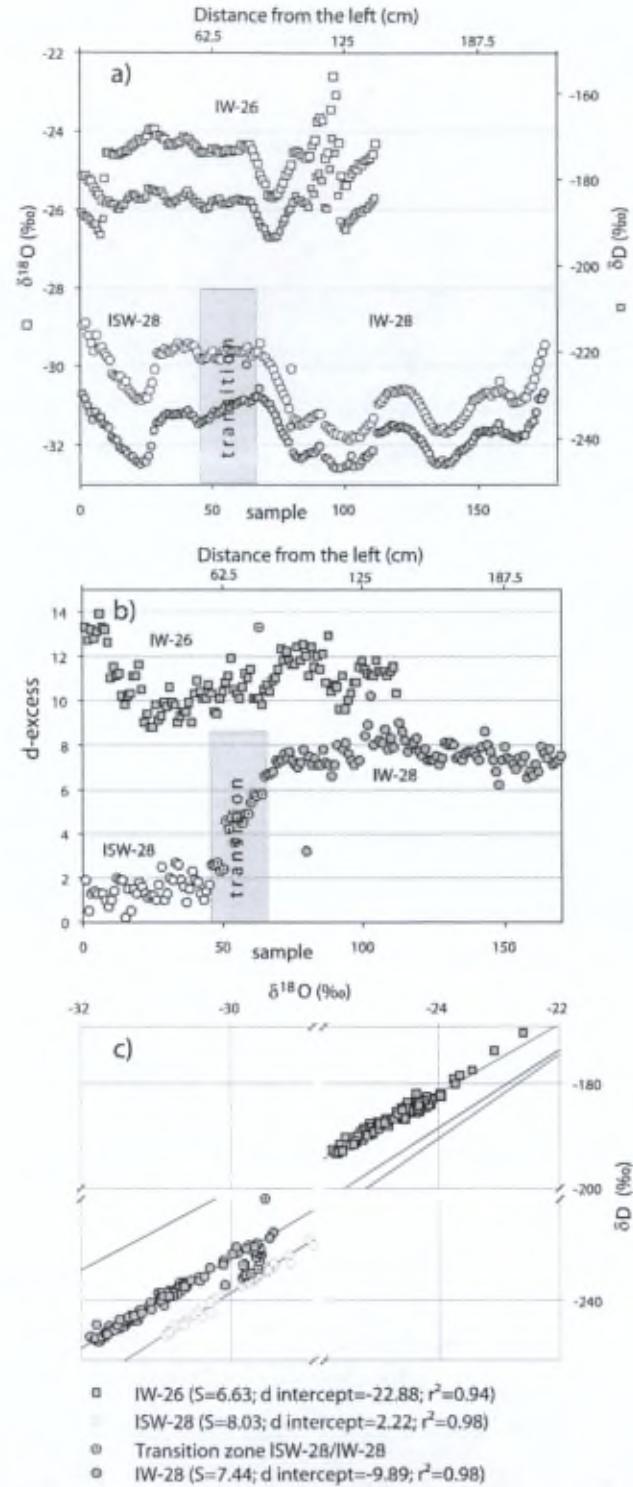


Figure 2.4 : Isotopic data for the two ice wedges: a) $\delta^{18}\text{O}$ and δD profiles, b) d-excess (d) and c) $\delta^{18}\text{O}$ - δD relationship. Numbers on the bottom x-axis of a) and b) refer to ice sample ordering, increasing from left to right, in the outcrop. The equivalent horizontal distance from extreme left is shown on the upper x-axis.

For the ice wedge part IW-28, $\delta^{18}\text{O}$ and δD range between -29.4‰ and -31.9‰, and between -229‰ and -247‰, respectively. The d also shows a low variability ($1\sigma = \pm 0.7\text{‰}$) with a mean value of 7.5‰ and a slope of 7.44 is measured in the co-isotopic diagram. The transition has $\delta^{18}\text{O}$ values between -29.5‰ and -29.9‰, a δD between -223‰ and -237‰, and shows variable d values intermediate between the other two parts (Figure 2.4c).

2.4.2 Ice texture and fabrics

Figure 2.3 shows thin section photographs that are typical of the three main facies encountered in the two studied ice wedges. In IW-26, the texture is homogeneous, lacking any significant elongation (Figure 2.3a). The crystal diameter is ranging between 0.40 and 0.60 cm (10 to 30 mm², Figure 2.5) and c-axis orientations are concentrated in the horizontal plane with preferred orientation perpendicular to the foliation azimuth (Figure 2.6a).

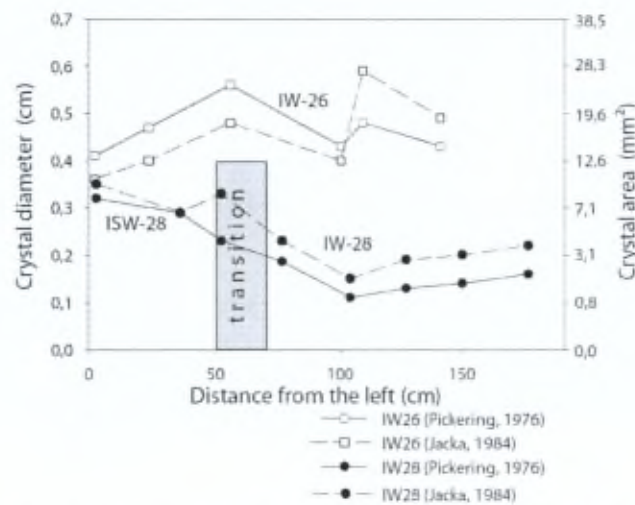


Figure 2.5 : Crystals size measurements using the two techniques described in the “sampling and analytical methods” section.

The ISW-28 texture shows, within a matrix of relatively large equigranular grains, several monocrystalline layers of elongated crystals with a well-developed “ribbon structure”, and crystal growth being geometrically associated to the fine debris layers that surround them, oriented parallel to the (subvertical) foliation plane (Figure 2.3b). On Figure 2.5, crystal diameter is ranging between 0.2 and 0.4 cm (3 to 10 mm²). In IW-28, the central part of the ice wedge shows an equigranular texture (Figure 2.3c), with crystals smaller than in ISW-28

(0.1 to 0.2 cm - 1-3 mm², Figure 2.5). Both ISW-28 (Figure 2.6b) and IW-28 (Figure 2.6c) show c-axes orientation patterns similar to IW-26, although the preferred orientation perpendicular to the foliation azimuth is less obvious for ISW-28 given the limited number of observations (due to larger grains).

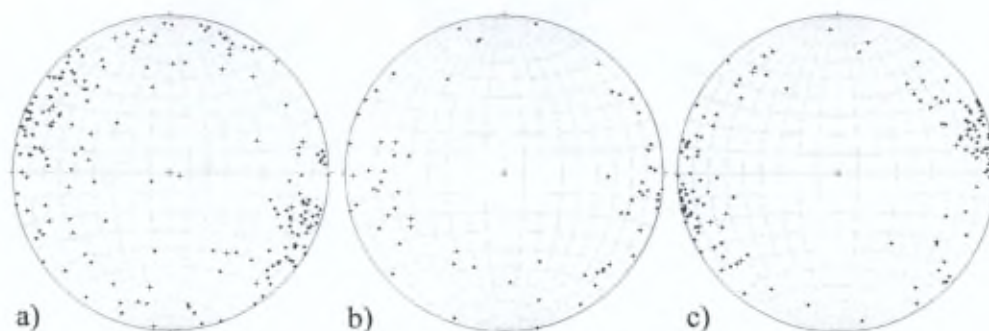


Figure 2.6 : Schmidt equal-area diagrams for the c-axes of horizontal thin sections. a) a total of six thin sections from IW-26 ($n = 199$) showing horizontal girdle with 1 maximum, b) a total of two thin sections from ISW-28 ($n = 70$) showing horizontal girdle, c) a total of five thin sections from IW-28 ($n = 150$) showing horizontal girdle with 1 maximum.

2.4.3 Gas properties

The contrast between the three facies (IW-26, ISW-28 and IW-28) is also evident from their gas properties (Figure 2.7). Table 2.1 summarizes minimum, mean and maximum values observed for the three facies. Total gas contents in our ice wedges are lower than in ice resulting from simple snow compaction as in ice sheets (see ranges in Table 2.1) and the total gas content of IW-28 is higher than those of ISW-28 and IW-26. For CO₂, all ice wedge mixing ratios are clearly higher than the atmospheric values, the highest values being observed in IW-26 (mean = 62 000 ppm) and ISW-28 showing lower values (mean = 3 000 ppm) than IW-28 (mean = 25 000 ppm). On the contrary, CH₄ mixing ratios show their lowest values in IW-26 with values in the range of atmospheric mixing ratio (mean = 1 ppm), intermediate values for IW-28 (mean = 8 ppm) and the highest values in ISW-28 (mean = 55 ppm). Oxygen shows consistently lower values than the atmosphere (of the order of 10%) and nitrogen is slightly higher, balancing other constituents.

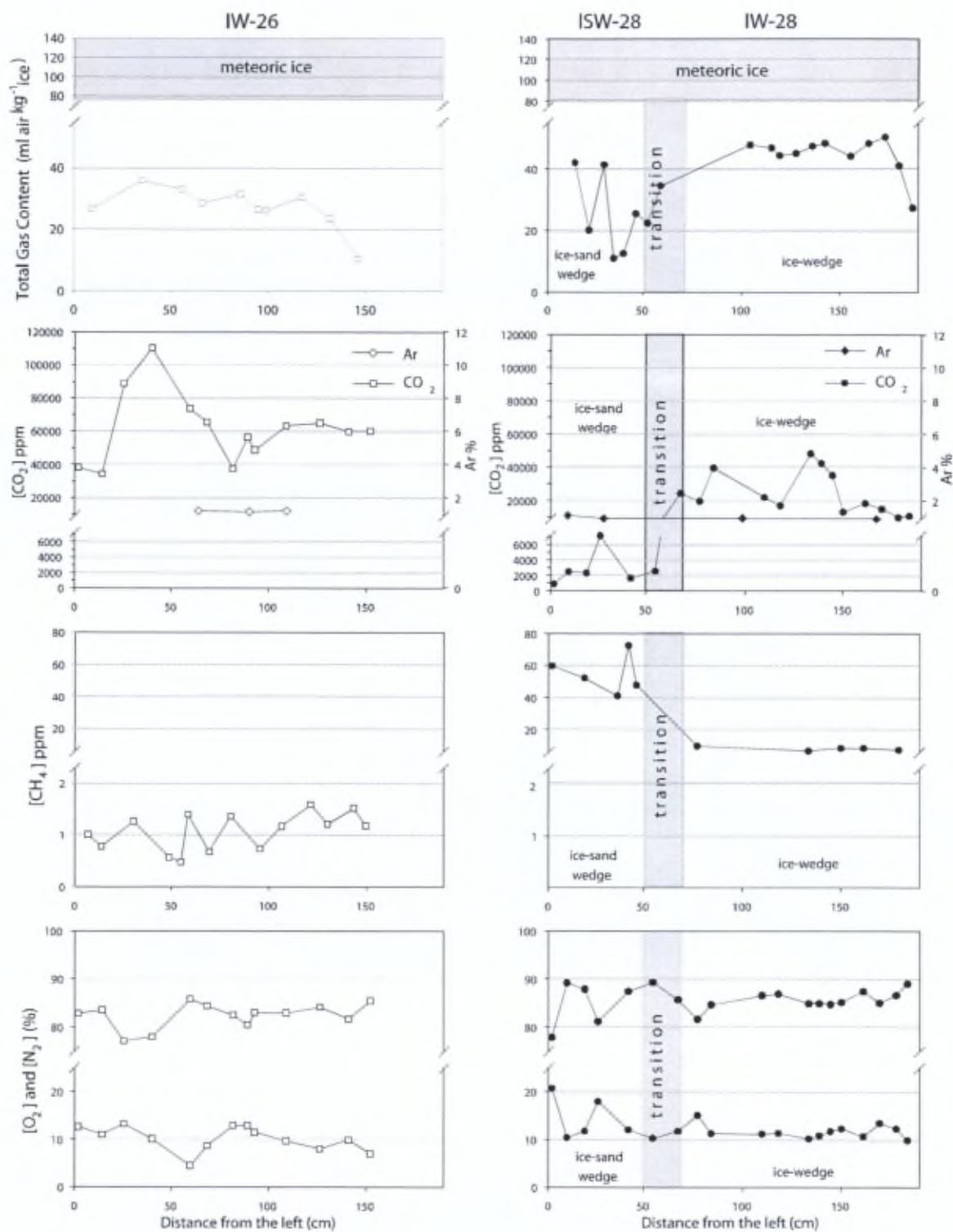


Figure 2.7 : Gas properties of ice wedges IW-26 (left) and ISW-28/IW-28 (right).

2.4.4 Sediments properties

Residual sediments collected from four ice samples have been treated with HCl and H₂O₂ (2 samples from ISW-28 and 2 samples from IW-28). The ISW-28 samples have strongly reacted with H₂O₂ while the IW-28 samples only showed a very limited reaction. We therefore argue that there is organic matter in the ISW-28 sediment inclusions, but only limited amounts in IW-28. On the other hand, the HCl treatment did not show detectable bubbling activity under the binocular for any of the 4 sediment samples treated, supporting that carbonate contents are negligible within the sediment enclosed in our ice wedges.

	IW-26	ISW-28	IW-28
Crystal area range (mm ²)	10.18 – 27.34	4.15 – 9.62	0.95 – 4.15
Crystal shape	equigranular	granular/rectangular elongated vertically sediments at grain boundary	equigranular
c-axes	1 max in horizontal girdle	horizontal girdle	1 max in horizontal girdle
Bubble size	~1mm	~1mm	~1mm
Bubble shape	spherical	spherical	spherical
Total gas content (ml/kg) (Meteoric ice =75-140*)	10/36 (homogeneous) (27)	11/42 (heterogeneous) (25)	27/50 (homogeneous) (45)
N ₂ (%)	77/86 (82)	78/89 (85)	82/89 (86)
O ₂ (%)	5/13 (10)	10/21 (15)	10/13 (12)
Ar (%)	(1.16)	(1.03)	(0.93)
CO ₂ (ppm)	35 000/110 000 (62 000)	860/7000 (3000)	10 000/48 000 (25 000)
CH ₄ (ppm)	0.5/1.6 (1)	41/72 (55)	7/10 (8)
δ ¹⁸ O (‰)	-25.8/-22.6 (-24.9)	-30.9/-28.9 (-29.9)	-31.9/-29.4 (-31)
δD (‰)	-191/-170 (-188)	-246/-230 (-237)	-247/-229 (-240)
δ ¹⁸ O/δD slope (‰)	6.63 (r ² =0.94)	8.03 (r ² =0.98)	7.44 (r ² =0.98)

*Martinerie *et al.* (1992)

Table 2.1 : Summary of results and comparison between IW-26, ISW-28 and IW-28. Values separated with / are the minimum and the maximum, (number) corresponds to mean values.

2.5 Discussion

In this section, we will first summarize and interpret ice texture and fabrics, co-isotopic signature and gas properties in terms of the infilling process of the studied ice wedges (see also Table 2.1). We will then attempt to link these processes to the regional paleo-climatic and paleo-environmental setting of the study area.

2.5.1 Ice wedge infilling processes

IW-26

IW-26 is characterized by relatively large grains (Table 2.1), suggesting either older crystals or conditions favouring recrystallization at higher temperature. The equigranular texture implies no preferred direction of growth (as would be the case for the freezing of a water reservoir) and no significant deformation process. The horizontal girdle of the c-axes with a localized maximum could be explained in several ways: a) gravity settling of individual snow grain in a narrow vertical crack; b) preferential growth along c-axis (better conduction) in a horizontal temperature gradient (perpendicular to crack sides); c) effect of the deformation in wedge during cyclic contractions or d) a combined version between these processes. The spherical bubbles (as opposed to tubular shapes expected in the case of water freezing) also imply no directional freezing, comforting a snow-water mixture hypothesis rather than water infilling for the ice wedge genesis. The total gas content is low in comparison with a dry firn densification process (between one tenth and one third of the value of a dry firnification process) suggesting a liquid water contribution to the ice formation or a process expelling the gases, eventually along the frost crack if the latter is only partially filled or if the infilling is still permeable.

CO₂ mixing ratios in IW-26 are well above the present-day values (Figure 2.7, row 2, left and Table 2.1). This indicates that the ice did not form through simple low temperature pressure-driven dry firnification process of snow enclosing the atmospheric gas composition. Previous studies of ice forming close to a bedrock environment have shown that this is very often the case, mainly because of either the presence of liquid water and/or significant biological activity within the enclosed organic matter fraction (Souchez *et al.* 1995a). Theoretically, the high CO₂ solubility in water could raise the CO₂ mixing ratio in the dissolved phase up to about 20 000 ppm (at 0°C and 1 atmosphere, with limited effect of pressure and impurities). Freezing of a CO₂ saturated freshwater reservoir in a closed system

could therefore display such high CO₂ values. There are however a number of other potential ways to further increase the CO₂ mixing ratio in our ice wedge ice such as diffusion-driven gas fractionation at the freezing front, CO₂ degassing on calcium carbonate precipitation, thermal trapping or biological respiration. Rejection of impurities at the interface by ice growing in a water reservoir will set up a strong diffusion gradient in the adjacent liquid boundary layer. This could lead to a further increase of the mixing ratio of the least diffusive gas in the solution, as for instance CO₂ (Killawee *et al.* 1998). However, theoretically, this effect cannot increase the CO₂ concentration by a factor higher than the ratio of the CO₂ diffusion coefficient (D_{CO₂}) to the air diffusion coefficient (D_{air}) in water; i.e. by a factor of about 1.6 (using typical values for D_{CO₂}, D_{N₂}, D_{O₂}). This would increase the CO₂ mixing ratio to about 30 000 ppm, provided that the freezing process can be assimilated in this case to ice growing in a liquid interface. Killawee *et al.* (1998) have shown that unidirectional freezing of a supersaturated CaCO₃ solution leads to a strong CO₂ enrichment of the refrozen water due to the CO₂ degassing resulting from the carbonate precipitation. The lack of reaction of our ice wedge sediments to an HCl "attack" however does not support the existence of significant amounts of CaCO₃. Finally, biological respiration is the most likely active process since bacteria and microbial communities have been identified in permafrost ice and in ice wedges (Gilichinsky *et al.* 2007; Katayama *et al.* 2007; Steven *et al.* 2008).

The considerations above suggest that the CO₂ mixing ratios of IW-26 result from a combination of purely physical processes (solubility) and biological respiration processes. Isotopic measurements of the ¹³C of CO₂ or of the ¹⁸O of the O₂ in our samples would further support this assessment (Souchez *et al.* 2006; Cardyn *et al.* 2007), but these data are currently not available. Interestingly though, the range of CO₂ values in the IW-26 ice wedge is similar to that observed in the basal ice of the GRIP ice core (up to 130 000 ppm), where δ¹⁸O_{air} values as low as -39‰ clearly indicate the occurrence of bacterial respiration processes (Souchez *et al.* 2006). Tison *et al.* (1998) and Souchez *et al.* (1995b), among others, demonstrated that the GRIP basal ice developed under climatically mild pre-ice sheet periglacial conditions. The latter are thus potentially similar to those conditions existing during the formation of our ice wedges. Another approach would be to test for the conservation of the sum of O₂ and CO₂ concentration, given the stoichiometry of the respiration reaction, as suggested by Souchez *et al.* (1995a). However this approach is not valid in our case since a liquid water phase is present allowing most of the carbon dioxide

produced by the respiration process to dissolve as HCO_3^- into the solution, at least at normal pH levels (Zeebe and Wolf-Gladrow 2001).

CH_4 mixing ratios are rather low (Figure 2.7, row 3, left - Table 2.1), in the range of Pleistocene – present day atmospheric values and we therefore assume no significant contribution from a substrate source or bacterial production.

The $\delta^{18}\text{O}/\delta\text{D}$ values in IW-26 are in the range of Late glacial to Holocene ice wedges (Figure 6b in Wetterich *et al.* 2011). The slope (6.63) of the linear regression line in the co-isotopic diagram of Figure 2.3c is however quite different from the known values of the Local Meteoric Water line in the region (slope of 7.6 at Tiksi Station, H. Meyer, unpublished data). Paleoclimatic interpretation of the stable isotopes signature in ice wedges is usually challenged by the possibility that water phase changes during evaporation/sublimation or melting/refreezing may affect the isotopic composition through fractionation, and therefore potentially alter the original paleoclimatic signature of the ice wedge. Refreezing processes will shift the δ values towards less negative values (e.g., max. +3‰ for $\delta^{18}\text{O}$ and +21‰ for δD in a single refreezing process) and will also decrease the slope of the $\delta^{18}\text{O}$ - δD co-isotopic relation (Souchez and Lorrain 1991). This is described by the “freezing slope”, which is expressed in the more general case of open systems as:

$$S = \frac{\alpha-1}{\beta-1} * \frac{1000+\delta_i\text{D}}{1000+\delta_i^{18}\text{O}} \quad (\text{Equation 2.1})$$

where $\alpha = 1.0208$ for deuterium

$\beta = 1.003$ for ^{18}O

δ_i = isotopic composition of the initial liquid

This concept has been used by St. Jean *et al.* (2011) to associate lower co-isotopic slopes to melting-refreezing processes in Holocene ice wedges. It is however important to underline that a “freezing slope” as such will only develop if the scale of the freezing process (size of the water reservoir) is considerably larger than the resolution of the isotopic sampling. In the case of ice wedges, typical crack-widths are of the order of a few centimeters, and annual “ice veins” are generally observed to be between 1 mm and 1 cm in width. It is therefore quite unlikely to develop a “freezing slope” from a several meters wide ice wedge, using a stable isotopes data set at a resolution of a few centimeters (about 1 cm in our case). This is probably also one of the reasons why $\delta^{18}\text{O}/\delta\text{D}$ signatures of ice wedges might have paleoclimatic significance. Small-scale refreezing or evaporation/sublimation processes, if

present, are however likely candidates to induce localized small-scale variability towards lower slopes, which might explain the observed lower co-isotopic slope and the lowering of the correlation coefficient ($r^2 = 0.94$) observed in the case of IW-26.

To summarize, our IW-26 analyses enable us to conclude that ice-vein formation in this ice wedge results from refreezing of a water-snow mix, with a large proportion of snow, no directional freezing, although a slight influence of the horizontal temperature gradient on the depositional c-axes orientations might exist. The co-isotopic slope is probably affected by small scale freezing dispersion of the samples. Relatively low gas content and a mixed signature of solubility and respiration processes are also demonstrated for CO₂. These properties are consistent with an ice wedge developing under warm and wet Holocene conditions.

ISW-28

ISW-28 shows medium grains size suggesting less recrystallization and/or younger age than IW-26 (which is actually precluded by the relative stratigraphical position of the two ice wedges, as discussed before). The alternation of equigranular and rectangular crystals (ribbon layer) elongated parallel to the crack side is the main characteristic of the ice-sand wedge part. This type of structure has, to our best knowledge, never been described in ice wedge and resembles the "stratified facies" found in basal glacier ice (e.g. Tsijiore Nouve, Switzerland) or ice resulting from film water refreezing on subglacial cavity floors. In our case we assume interface freezing on the cold surface of the frost crack walls of a thin running water film originating from summer melting of the surface lips of the partially open (unfilled) crack (as opposed to a "top-down" or "side-center" refreezing of an "in situ" bulk water reservoir). Sediments at layer boundaries suggest entrainment with the melt water from the surface, rejection from the growing ice and, finally, freeze-in during "shut-down" phases of the water supply. The horizontal girdle drawn by the c-axes distribution does not show a localized maximum, but, as mentioned before, the number of sample is relatively low. The observed high small-scale variability of total gas content is probably due to the alternation of layer with bubbles (episodes of wet snow metamorphism) and layers without (ribbon layer formed through water film freezing). CO₂ is higher than atmospheric values (solubility effect) but well below solubility limit of 20 000 ppm, therefore suggesting an "open system" freezing with gas rejection to atmosphere. CH₄ mixing ratios are much higher than the atmospheric

value, suggesting methane production in bubbles or in soil, in close vicinity to the bubbles before their occlusion in the ice vein. Note that the sediments in the ice-sand wedge part are rich in organic matter and provide an adequate substrate for methanogenic bacteria.

Methane production implies an anaerobic environment for the methanogenic archaea to work efficiently (e.g. Wagner and Liebner 2009). Although ice wedges can be a source of methane (e.g. Meyer *et al.* 2010a), the range of observed methane mixing ratios seems to be negligible compared to other methane sources studied for the carbon budgets in permafrost area (IPCC 2007). Apart from a few values close to atmospheric in ISW-28, the O₂ mixing ratio fluctuates around 10% (Figure 2.7, row 4), being only half the atmospheric O₂ value. It is hard to tell if this value is the gaseous composition of the local environment (in the crack into the frozen soil) before the bubbles “close-off” or if this value is a result of biogeochemical post-occlusion processes. Whichever way, it does not imply a fully anaerobic environment. However, for O₂ measurements only ± 35 g of samples were taken, each containing a large number of millimetric bubbles. As already suggested for the GRIP basal ice (where both high CO₂ and high CH₄ values were measured in the same samples) and in other environments like soils and marine sediments (Souchez *et al.* 1995b), the mean O₂ mixing ratio might well reflect a situation where some bubbles are depleted in oxygen and others have mixing ratios close to atmospheric levels. The bubbles can therefore provide contrasted closed system micro-environments in some cases favourable to aerobic respiration (high CO₂, low CH₄) and in others to bacterially mediated methanogenesis (high CH₄, low CO₂).

The $\delta^{18}\text{O}$ and δD values match well with Pleistocene stadial signature in the studied area (Figure 6c in Wetterich *et al.* 2011). The slope in the co-isotopic diagram (8.03) could be indicative for the variability of the autumn – winter snow input to the crack during the integrated period of the ice-sand wedge history. Snow samples in this region do not receive additional secondary moisture (because open water bodies are frozen in winter) and therefore are generally situated close to the GMWL (Meyer *et al.* 2002a, 2002b) with slopes in the co-isotopic diagram close to 8.

ISW-28 ice veins properties suggest a mixed origin altering episodes of consolidation of a “water-snow” mix (granular) and of events of running water film refreezing at the sides of the open frost crack. The fact that the crack is not always filled with snow might indicate periods favouring debris incorporation either through an increased input of particulate contribution from the surface or because of a thinner snow cover (lower precipitations). It is worth noting that a globally colder-drier period (as suggested by the low precipitation) does

not necessarily mean less melting in the period when frost cracks are open, if debris availability allows strong summer albedo effects. The biological activity in ISW-28 is characterized by low to moderate aerobic respiration but high methanogenic activity related to availability of organic matter and lower than atmospheric oxygen levels. These conditions obviously existed during the early stages of IW-28 development (ISW-28).

IW-28

IW-28 shows the smallest grain size. This is potentially the combined result of a lower Arrhenius growth rate at lower temperature and less liquid water availability (which would otherwise enhance crystal growth rate). Clearly these factors took over the "time factor" (older ice) in the recrystallization process. The equigranular ice does not show preferred direction of freezing and the horizontal girdle shows one localized maximum sub-perpendicular to the foliation, as for the IW-26. As in IW-26 also, the spherical bubbles indicate no directional freezing and favour a consolidation process of a snow-water mixture for the origin of the ice veins. However, the highest total gas content with values reaching about 50% of those observed in dry firnification), suggest less liquid water contribution than in IW-26. This might be linked to the small-scale hydrodynamical processes at play as the meltwater percolates into the snow infilling. Colder temperatures in the surface permafrost from the previous winter would favour rapid freezing in the surface layer and limit water percolation further down-crack. Detailed vertical gas content profiles would certainly be useful in documenting these processes further.

CO₂ mixing ratios contrast with those observed in the ISW-28 section and are closer to those observed in ice wedge IW-26, showing the potential combination of pure physical solubility processes with biological respiration, although the latter is less developed than in IW-26. CH₄ mixing ratio, largely higher than the atmospheric values, are also intermediate between those of IW-26 and ISW-28. $\delta^{18}\text{O}$ and δD values are similarly low as compared to ISW-28 and might suggest a slightly colder period for IW-28.

IW-28 should therefore be formed from a water-snow mix, at relatively low temperature than IW-26, with a large proportion of snow, no directional freezing and less sediments input than in ISW-28. The latter results in moderate CH₄ mixing ratios, although these are higher than those measured in the Holocene ice wedge IW-26. Fabrics are still dominated by horizontal c-axes including a single maximum roughly perpendicular to the

crack sides, suggesting gravity settling control or contraction deformation effects rather than recrystallization growth, given the isotropy of the bubbles and crystal shapes.

Our interpretation of ice wedge filling process and ice vein formation contrasts with St-Jean *et al.* (2011) which suggest that the Holocene ice wedges result from the freezing of liquid water and that the Pleistocene ice wedges result rather from snow densification and/or hoarfrost accretion. Our study suggests variable water-snow mix as source of the ice with higher water contribution during the Holocene period. Coherently with Lacelle *et al.* (2011) and St-Jean *et al.* (2011) data, however, our $\delta(N_2/Ar)$ and $\delta(O_2/Ar)$ results (Figure 2.8) indicate an increasing influence of biological processes with the increasing amount of water in the water-snow mix. Interestingly, the proximity of the debris source could result in a larger proportion of melting as compared to the snow matrix, and enhanced methanogenesis even though the climate is colder. The latter is supported by a study of Meyer *et al.* (2010a) in Northern Alaska, where an ice wedge component formed during the colder Younger Dryas displays higher methane mixing ratios as compared to an ice wedge section formed during the warmer Allerød. Clearly, environmental, physical and biological controls need to be considered when discussing ice wedge properties.

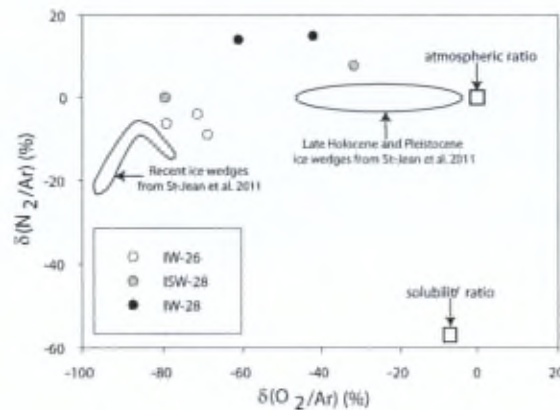


Figure 2.8 : $\delta(N_2/Ar)$ and $\delta(O_2/Ar)$ of ice wedges IW-26, ISW-28 and IW-28 using the following equation: $\delta(N_2/Ar) = \left(\frac{R(N_2/Ar)_{sa}}{R(N_2/Ar)_{st}} - 1 \right) * 100$ where *sa* refers to the sample and *st* to the standard value (standards used are 22.43 and 83.60 for O_2/Ar and N_2/Ar , respectively). An equivalent formula is used for determining $\delta(O_2/Ar)$.

2.5.2 Links to the regional paleoclimatic interpretation

Results from texture, fabric and gas analyses allow to differentiate between three facies within the two studied ice wedges (IW-26, ISW-28 and IW-28), which can also be discussed in terms of the regional paleoclimatic interpretation from available stable isotopes data.

The IW-26 displays least negative δD and $\delta^{18}O$ values, largest crystal sizes, lowest total gas contents and is embedded in the Ice Complex structure of Pleistocene age. However, its isotopic composition is coherent with Holocene age ice wedges ($\delta^{18}O$ around -24 to -25‰; Meyer *et al.* 2000, 2002a, 2002b, 2010b; Dereviagin *et al.* 2002; Schirrmeister *et al.* 2002; Popp *et al.* 2006). A period of mild temperatures would also increase the rate of biological respiration processes and the availability of organic matter.

The lower isotopic composition of IW-28 suggests a Pleistocene origin (compare Figure 6b of the recent regional overview in Wetterich *et al.* (2011)). The situation is however certainly more complex for the ISW-28/IW-28 case as suggested by the strong contrast in their d values, while showing in both cases low internal variability (mean d = 1.4‰ for ISW-28 and mean d =7.5‰ for IW-28) for similar δD ranges (Figure 2.4). Also worth noting is the sharp monotonic transition in d values at the interface between ISW-28 and IW-28.

There is a number of ways to explain low d in precipitations (and in the ice that evolves from it), that either belong to the “water cycle processes” or to the “*in-situ* post-deposition processes”. Extensive work has been done dealing with the concept and use of d in co-isotopic studies, especially in the field of deep ice-core interpretation and the relation to temperature changes at precipitation sites and oceanic sources (Craig 1961; Dansgaard 1964; Merlivat and Jouzel 1979; Yurtsever and Gat 1981; Jouzel *et al.* 1982, 2005a, 2005b; Jouzel and Merlivat 1984; Johnsen *et al.* 1989; Vimeux *et al.* 1999, 2002; Stenni *et al.* 2004, 2001; Masson-Delmotte *et al.* 2005). It is commonly admitted that, although humidity and wind speed at the source also play a role, in most cases, the $\delta^{18}O_{ice}$ and δD_{ice} primarily depends on the temperature at the site (T_{site}) and to a lesser extent on the temperature at the source (T_{source}). The reverse is true for the d in the ice. The latter is indeed mainly driven by kinetic isotopic effects during evaporation at the oceanic source, and these will be enhanced for higher temperatures and lower relative humidity, increasing the d value (Merlivat and Jouzel 1979; Masson-Delmotte *et al.* 2005). It should however be kept in mind that at equivalent source temperatures, lower winds would also increase the relative humidity at the source and therefore decrease the d -excess. As shown in the deep ice core records from Greenland, large

topographic and atmospheric circulation changes during the last glacial period (the presence of ice sheets of variable size, larger but fluctuating extension of the sea ice) are responsible for an antiphase relationship between δ values (T_{site}) and d values (T_{source}). Indeed, during mild events, when Greenland was warmer (less negative δ 's) and sea ice less extent, the moisture source was closer (colder) and therefore the d lower than during more severe phases. This results in the samples from these milder periods (less negative δD and $\delta^{18}O$) aligning, in a δD - $\delta^{18}O$ diagram, on a line with slope close to 8, but with the d -intercept at +4‰ instead of +8‰ (e.g. Figure 7 in Johnsen *et al.* 1989).

Today, the main source of the winter precipitation in our study area (west of ~140°E) is probably located in the Northern Atlantic (Kuznetsova 1998; Rinke *et al.* 1999). However, as discussed by Meyer *et al.* (2002b) and Wetterich *et al.* (2011), Pleistocene moisture sources for the same area less straightforward to locate. Two hypotheses were discussed (Table 2.2): (1) refers to a permanent Atlantic source, with a latitudinal variation similar to that suggested by Johnsen *et al.* (1989), as described above for Greenland. In that scenario, a contrasting d signature would represent a temporal shift (within the Pleistocene, e.g. interstadial/stadial) from a milder (Table 2.2, col. 2) glacial period (higher T_{site}) with a higher relative humidity (i.e. lower T_{source} and/or lower winds, and therefore lower d values in ISW-28) to a colder glacial period (lower T_{site}) with a lower relative humidity (i.e. higher T_{source} , and/or higher winds, and therefore higher d value in IW-28). The amount of precipitation, however, should be lower during cold stadial periods and higher during interstadials (as for the difference between glacials and interglacials in deep ice cores and in permafrost). Alternatively, (2) the combination of the full development of the Eurasian Ice Sheet (the easternmost extent of which reached the western part of Taymyr Peninsula) and of an extended sea ice cover in the Barents and Kara seas and the Northern Atlantic (stadial, Table 2.2, col. 5), might have considerably reduced (deflected or even blocked; Meyer *et al.* 2002a) the penetration of Atlantic air masses to the Laptev Sea region. In that case, a stronger influence of the North Pacific winter moisture source, with low d values and low precipitation (e.g. Clark and Fritz 1997), could have existed. Note however that the occurrence of this specific North Pacific moisture low d isotopic signature east of our study site is still somewhat controversial in ground ice (Schwamborn *et al.* 2006). During interstadials (Table 2.2, col. 4), on the contrary, a distinct Northern Atlantic source could have been re-established, with potentially higher d values (more “southerly” sources) and higher

precipitation (Lacelle *et al.* 2011). We will discuss below these two alternatives, in the light of the other ice properties.

(1) variables	(2) <u>Hyp. 1: Atlantic source</u> low sea ice Interstadial	(3) high sea ice Stadial	(4) <u>Hyp. 2: Atlantic vs. North Pacific</u> Interstadial	(5) Stadial	(6) ISW-28	(7) IW-28
δ -values (T° site)	high	low	high	low	low	lower
d -values (T° source)	low	high	high	low	low	high
Precipitation (distance controlled)	high	low	high	low	low	high

Table 2.2 : Comparison of relative values of δ , d and precipitation amount for the two sections of ice wedge ISW-28/IW-28 with expected values for the two atmospheric moisture sources hypotheses discussed in the text.

Climatic seasonal variations (temperature, precipitation, etc.) are also able to disturb d (Johnsen *et al.* 1989; Meyer *et al.* 2002b) but ice wedges are known to be built from the winter snow precipitation mainly and the spring meltwater derived from it. Post-depositional “*in situ*” phase changes could also be responsible for lowering the d values of the samples (Meyer *et al.* 2002b). Isotopic fractionation during ice wedge consolidation was discounted by Michel (1982) based upon the argument that freezing is generally too fast to allow for it. However, conditions might be different for the formation of the “ribbon facies” in the ice-sand wedge for example. Figure 2.9 shows the effect of equilibrium fractionation during hypothetical 10% refreezing (grey squares) of water resulting from the melting of each of the samples from IW-28 (black dots). The mean isotopic composition of the 10% refrozen fraction was computed using the formulation in Souchez and Lorrain (1991) as in Equation (2.2), with a frozen fraction (K)=0.10.

$$\bar{\delta}_s = 10 * (1000 + \delta_0) * [(1.1 - K)^\alpha - (1 - K)^\alpha] - 1000 \quad (\text{Equation 2.2})$$

where $\bar{\delta}_s$ = δ value of refrozen samples

δ_0 = δ value of water (melted IW-28 ice sample, no fractionation on melting (Moser and Stichler 1980; Souchez and Lorrain 1991))

K = frozen fraction

α = fractionation coefficient (1.0208 for deuterium and 1.003 for ^{18}O)

The refrozen IW-28 samples indeed reproduce the d of the ISW-28 samples and lie on the same co-isotopic line. They are however clearly offset towards less negative δ values, and more negative δ values than observed in IW-28 would be required to explain the observed ISW-28 δ -range. This is not precluded, given the existence of some more negative values from the Sartan period reported by e.g. Wetterich *et al.* (2011; Figure 6) in other ice wedges of the area. Experimental sublimation/evaporation processes of a snow pack have also been shown to shift the remaining reservoir towards less negative isotopic values with a slope that is less than 8 (Souchez and Lorrain 1991 and references within). However, although they could reproduce the observed d values in ISW-28, both of these post-depositional processes would need to be occurring at a rigorous equivalent rate (e.g., 10% refreezing, fixed evaporation percentage) for all samples to plot on a co-isotopic line as well defined as the one observed for the ISW-28 samples, with a slope close to 8. In fact, the very good alignment of all the ISW-28 samples on a line with a slope of 8.03 ($r^2=0.98$, with a fairly low range of the δ values) is an argument to favour a “classical” Rayleigh-type “source to sink” fractionation history.

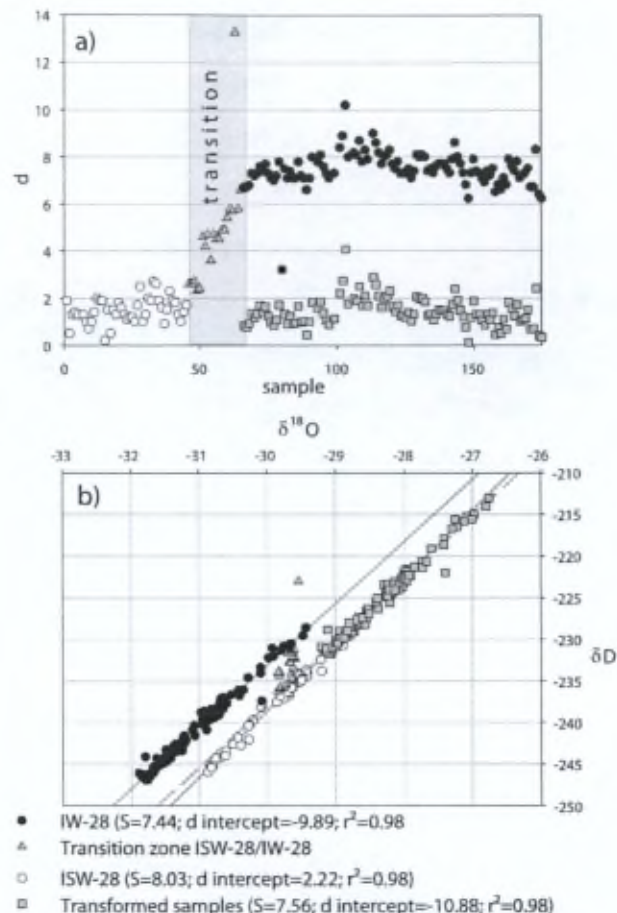


Figure 2.9 : d (a) and co-isotopic plots (b) of observed data for ISW-28 (open circles) and IW-28 (black dots) compared to a simulation (grey squares) on the effect of hypothetical equilibrium refreezing of 10% of melted fraction in IW-28 sample, using Equation 2.1. The refrozen theoretical IW-28 samples reproduce the d of the ISW-28 samples and lie on the same co-isotopic line. They are however clearly offset towards less negative δ values.

This leaves us therefore with the first hypothesis of a major shift in the moisture source (higher d), as the ice wedge growth switches from ISW-28 to IW-28, across the transition. Do the other ice properties allow us to decipher between the two alternative moisture source changes, with opposite conclusions in terms of the d signature? The answer is not straightforward. Indeed, ISW-28 has very low d -values (Table 2.2, col. 6 and Figure 2.4) which would either correspond to an interstadial period in hypothesis 1 (Atlantic source, little sea ice cover - Table 2.2, col. 2) or to a stadial in hypothesis 2 (North Pacific source - Table 2.2, col. 5). The latter option is coherent with the deduced lower relative precipitation amounts from the observation of the ice-vein properties at ISW-28. However, in that case, the “in-situ” temperature should be lower at ISW-28 than at IW-28 (which would then be typical of re-establishment of an Atlantic source with higher d -values and higher precipitation).

Alternatively, higher T_{site} for ISW-28 fit to an interstadial in hypothesis 1 (change in position of Atlantic source), but then higher precipitation amounts should be expected (Table 2.2, col. 2). Note however that the δ -contrast is low between ISW-28 and IW-28, and that it should also be strong if hypothesis 1 was valid, with much higher values for ISW-28, provided that the mechanism is similar to the one presented for the Greenland Ice Sheet “stadial-interstadial” alternation by Johnsen *et al.* (1989). The latter assumption is hypothetical. Indeed, precipitation and temperature regimes on the downwind side of major ice-sheets might have been quite different to those existing in its centre parts (e.g. foehn effects which would locally increase temperatures and lower precipitations). One could also argue that the “switch” from North Pacific to Atlantic sources in hypothesis 2 could also be primarily linked to changes in the Greenland and Eurasian Ice Sheets geometries, which might in turn not be directly linked to contrasted global temperature regimes but to other mechanisms such as ice-ocean interactions.

In the ISW-28 ice-sand wedge the dominance of debris input over snow filling, suggests a period of limited precipitation in accordance with the North Pacific winter moisture source with a low d value. However, the thin sections suggest the presence of meltwater and of melting-refreezing processes in an open-system, sandwiched with refrozen snow layers of limited extension (also supported by the total gas content measurements). Intuitively, these would be preferably associated to warmer periods, but they could also simply result from albedo effects in this debris-rich environment.

2.6 Conclusions

Detailed crystallographic, gas content and composition, and water isotope analyses of the IW-26 and IW-28 ice wedges allowed us to shed more light on the processes involved in ice wedge growth. Ice wedge IW-26 has developed in a mild Holocene environment. Higher temperatures and higher meltwater infiltration resulted in enhanced recrystallization, larger crystal sizes, lower total gas content and favourable conditions for biological respiration, inducing relatively high CO_2 levels. Ice wedge ISW-28/IW-28 developed in a relatively mild Pleistocene environment, during which a large change in atmospheric sources occurred, as documented by a sharp monotonous transition in deuterium excess from stable values at ca. 1.4‰ in ISW-28 (early growth) to stable values at ca. 7.5‰ in IW-28, that cannot be explained through post-depositional processes. This transition occurred without significant

changes in the site temperature as indicated by constantly low $\delta^{18}\text{O}$ and δD values. It is however difficult to select potential mechanisms behind the changes in atmospheric sources. The transition is however concurrent with major changes in the ice wedge morphology. The ice-sand wedge ISW-28 properties show a smaller contribution of refrozen "snow-water mix" in the ice veins, with regular episodes of film water open-system refreezing on the crack walls, associated with important losses of total gas content and abundance of surface-derived debris inclusions forming the "ribbon facies". This heterogeneous medium, rich in organic matter, might have favoured the anaerobic micro-environmental conditions necessary to explain the maximum CH_4 levels in that unit. Ice veins texture in IW-28 resemble more the refrozen "snow-water mix" of IW-26, but with smaller crystal sizes and larger total gas content, as would be expected from colder conditions.

The changes in d between ISW-28 and IW-28 are most likely linked with changes in the moisture source region from Atlantic to Pacific or changes within an Atlantic source region. The combined observed low d values and limited snow contribution to the ice vein matrix, suggesting low precipitation, in ISW-28 is consistent with a North Pacific atmospheric source for the local precipitation at the time of ISW-28 formation. The length and persistence of this low d event is however unknown since it has not been observed at any other ice wedge study site west of 130°E . The significant contrast in ice veins metamorphic processes between ISW-28 and IW-28, suggesting a larger contribution of melting-refreezing processes in the former, could result from slightly milder conditions at ISW-28. However, the close proximity of the soil-sediment source has certainly fostered melting through albedo feedbacks.

Finally, comparing our methane mixing ratios in IW-26 and IW-28 reveals that substrate availability is as important as the temperature regime in controlling production rates in the permafrost environment.

Chapter 3. Gas properties of winter lake ice in Northern Sweden: implication for carbon gas release

This paper has been published as : "Gases properties of winter lake ice in Northern Sweden: implication for carbon gas release", Boereboom T., Depoorter M., Coppens S. and Tison J-L., " in Biogeosciences, 9, 827-838, 2012.

Abstract

This paper describes gas composition, total gas content and bubbles characteristics in winter lake ice for four adjacent lakes in a discontinuous permafrost area. Our gas mixing ratios for O₂, N₂, CO₂, and CH₄ suggest that gas exchange occurs between the bubbles and the water before entrapment in the ice. Comparison between lakes enabled us to identify 2 major "bubbling events" shown to be related to a regional drop of atmospheric pressure. Further comparison demonstrates that winter lake gas content is strongly dependent on hydrological connections: according to their closed/open status with regards to water exchange, lakes build up more or less greenhouse gases (GHG) in their water and ice cover during the winter, and release it during spring melt. These discrepancies between lakes need to be taken into account when establishing a budget for permafrost regions. Our analysis allows us to present a new classification of bubbles, according to their gas properties. Our methane emission budgets (from $6.52 \cdot 10^{-5}$ to $12.7 \text{ mg CH}_4 \text{ m}^{-2} \text{ d}^{-1}$ at 4 different lakes) for the three months of winter ice cover is complementary to other budget estimates, as our approach encompasses inter- and intra-lake variability.

Most available studies on boreal lakes have focused on quantifying GHG emissions from sediment by means of various systems collecting gases at the lake surface, and this mainly during the summer "open water" period. Only few of these have looked at the gas enclosed in the winter ice-cover itself. Our approach enables us to integrate, for the first time, the history of winter gas emission for this type of lakes.

3.1 Introduction

Lakes in subarctic environments are affected by and contribute to the current global warming. In permafrost areas, lakes are net emitters of methane and carbon dioxide, two greenhouse gases (GHG). Lakes areas in these regions represent up to 30% of land surface (e.g. Walter *et al.* 2008a) and this ratio could increase in the coming years, as permafrost degradation supports lakes development. These lakes, embedded in recently unfrozen sediments, sustain anaerobic condition favouring methane emissions. The latter have been largely studied in recent years (e.g. review Table in Walter *et al.* 2010), since they are recognized as an important contributor to the greenhouse effect. Nevertheless, CH₄ emissions are still not included in Global Climate Models (GCMs) because of large uncertainties (IPCC 2007a; Koven *et al.* 2011).

Methane is produced within lake sediments as a result of acetate fermentation or CO₂ reduction in anaerobic conditions. Methane reaches the atmosphere through the plants system, by bubbling or by diffusion through the water column. Bubbling is easily identified at lake surface and has been mainly studied during ice free periods using various techniques (e.g. floating chambers, bubble traps, inverted funnel systems). During winter periods, bubbles are enclosed in the ice, indicating that methane emission from sediment is still an active process. In peculiar situations, the emissions are so intense that they inhibit the ice formation (hotspot). The transit in the water column can induce several biochemical reactions. Methane can be oxidized to CO₂ in an oxic medium, via methanotrophic bacteria, and lakes can supply such an environment depending on their geometry and hydrology. Due to the temperature of the maximum of density of fresh water (+4°C), lakes in periglacial areas are known as dimictic i.e. presenting two periods of stratification and two overturn events. The first overturning events happen at springtime, soon after ice cover melting, and the second one when the winter starts, before freeze in (Casper *et al.* 2000; Bastviken *et al.* 2004). Stratification favours the development of an anoxic layer whereas overturning causes oxygenation in the water column. Lakes are therefore mainly stratified during the winter and the ice cover will further limit

atmosphere – water interactions. This closed system will result in the buildup of CO_2 and CH_4 concentrations in the water and mixing ratios in the ice. At spring melt, these gases will be released to the atmosphere within a few days (Michmerhuizen *et al.* 1996). Methane will resituate mainly from ice melting and bubbles emissions while carbon dioxide will release rather from gas diffusion as water overturns and equilibrates with the atmosphere (Michmerhuizen *et al.* 1996; Phelps *et al.* 1998; Casper *et al.* 2000). Indeed, the solubility of these two gases is very different: in fresh water at 20°C pure CH_4 saturation is about 1.6 mol m^{-3} whilst the CO_2 saturation is reached at about 39 mol m^{-3} . Moreover, lakes characteristics (size, depth, water circulation, hydrological system) should also influence gas emissions, a process which has only been scarcely described.

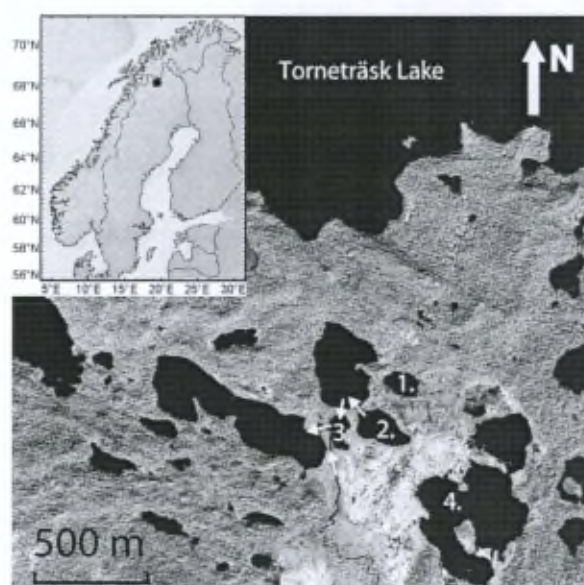


Figure 3.1 : Location map and lakes configuration (the arrows show water connections). The lakes are all embedded in a mire. Lake 1, small and closed; Lake 2, small and connected to another lake; Lake 3, small, receiving water from a river to the South, connected to another lake to the North and draining into another lake to the West; Lake 4, bigger and closed.

Most studies have performed measurements on open water and only a few have focused on the gas properties of the lake ice cover. Here we present, to our knowledge, the first high resolution profiles of the total gas content and gas composition of lake ice from 4 lakes in Northern Sweden. This approach enables us to discuss gas enclosure in lake ice during the 3 months period of ice growth prior to ice cores collection. In this pilot study, interactions between the water column and the ice cover as well as the intra- and inter-lake variability in

hydrodynamic regimes are also shown to control bubbles composition, although a larger number of study cases is clearly required to quantitatively assess these relationships.

3.2 Study area and sampling

The four investigated lakes are embedded in the Stordalen Mire peat bog area (68°21' N, 19°02' E), near the Torneträsk lake (Figure 3.1). It is a sporadic or discontinuous permafrost area (Johansson *et al.* 2006a, 2006b; Åkerman and Johansson 2008) with low vegetation (Sonesson *et al.* 1980; Svensson *et al.* 1999).

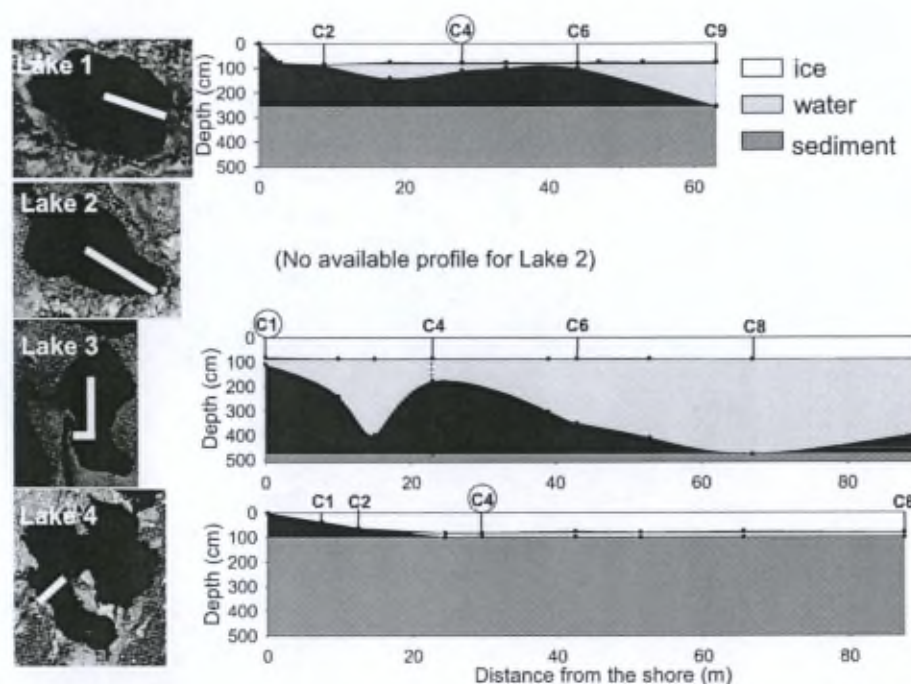


Figure 3.2 : Lakes geometry along the profiles and ice core sampling locations. The white line on lakes shows the transect direction, letters and numbers correspond to the cores studied for the bubbles morphology and circles indicate cores analyzed for their gas properties. The dotted line in the Lake 3 profile shows the change of azimuth of the transect.

Transects from the center to the bank have been performed for each lake, in order to study the intra-lake variability. Ice cores were extracted along these transects. Several of these were analyzed for their gas properties. In this paper, we present 3 cores from Lake 2, and 4 cores from the other lakes. Figure 3.2 shows the ice cores locations, ice thickness and the depth profiles at times of core retrieval. We also collected about fifteen individual “ice embedded large flat bubbles”. These were ranging from 2 to 5 cm in diameter and were outcropping near

the surface, but not especially along the studied transects. While Lake 1 and Lake 4 appear disconnected from any obvious water circulation pattern, Lake 2 and Lake 3 are not. We will refer to this contrast by using the “closed” vs. “open” lake terminology, respectively. Lake 1, Lake 2 and Lake 3 display a small surface area of 0.01 to 0.02 km². Lake 4 is quite larger (0.19 km²). According to water connections in the winter, Lake 1 is closed. Lake 2 has a semi-open character because of its connection to another lake downstream (see Figure 3.1). Its profile hasn't been documented in details here, but its maximum depth is known to be 5 meters (Kokfelt *et al.* 2009). Lake 3 is relatively deep (5m) for its size. It is an open system as it benefits from water fluxes throughout the winter. Incoming water originates from the river (see Figure 3.1), and flows into the lake to the West (pers. com. David Olefelt 2008). Lake 4 consists of three interconnected areas and seems to behave as a closed system. Only the southern area has been studied in this paper. There, the lake is shallow with a maximum depth of 105 cm.

The lake ice was drilled at the end of the winter in the last days of March 2008, near to maximum ice thickness.

3.3 Methods

The drilling was performed using a SIPRE-type ice auger (7.5 cm in diameter), the samples were cut with a band saw in a -20°C cold room. Horizontal thick sections (± 8 cm x 7 cm x 0.5 cm) were processed continuously along the ice cores using a Leitz 1400 microtome following the standard procedures from Langway (1958).

Gases entrapped in the ice were analysed every 5 cm (30g – 50g) for their total volume and composition (CO₂, O₂, N₂ and CH₄). Gas composition was measured by gas chromatography (Interscience Trace GC) using a FID detector for CO₂ and CH₄ and a TCD detector for O₂ and N₂. The gases were collected using the dry-extraction technique (extraction by crushing under vacuum (10⁻³ Torr) and at low (-50°C) temperature) described in Raynaud *et al.* (1982) and Barnola *et al.* (1983). Precision of the measurements is 2.5% for CO₂, 0.4% for O₂ and N₂, and 3% for CH₄.

Total gas content was determined using a Toepler pump, applying the melting-refreezing extraction technique described in Martinerie *et al.* (1994). This system consists in placing a cubic ice sample with length of about 4 cm into an hermetic vessel thoroughly evacuated (10⁻³ Torr). The Toepler pump extracts, collects and measures the volume of all

gases present in the vessel after the ice had been melted (hot water bath) and slowly refrozen from the bottom, in order to reject all gases during the new ice formation. The associated total gas volume error is $\leq 5\%$ for ice containing small spherical bubbles as in glacier ice. This error can be largely increased for cylindrical bubbles (as observed in lake ice) since part of them can be open by cross-cutting during the sample preparation. The amount of gas lost can be estimated using calculation developed in Martinerie *et al.* (1990) and is depending of the length, width and spacing of the cylindrical bubbles. In our case, the proportion of loss from the cylindrical bubbles varies between 20% and 90% for bubbles lengths of 0.6 cm and 3.2 cm respectively.

Ice thickness and depth measurements were performed with an ice thickness gauge designed (precision: ± 1 cm) by Kovacs, an American company specialized in ice drilling and coring equipment.

3.4 Results

3.4.1 Ice characteristics

Figure 3.3 summarizes the ice and bubbles morphology from the 15 studied ice cores, as seen in transmitted light through the 0.5 cm thick sections. Visually, bubble shapes show a large variability. However, 6 major ice types have been identified from bubble characteristics. Type 1 is peculiar and scarce, we call it "snow ice", because this ice type results from liquid water infiltration and refreezing in the snow cover at the lake surface. We observed this ice type at the very top of core 1 on Lake 3. Type 2 corresponds to ice without visible bubbles. We will refer to it as "clear ice", and it has been found in most part of the Lake 3 ice cover but also in small sections of Lake 1 and Lake 2 cores. Ice with elongated cylindrical bubbles (ice type 3) is predominant in Lake 4 (e.g. around 40 cm depth) but also in some sections of Lake 1 and Lake 2. Ice with spherical or nut shape bubbles is found at the bottom of all the shallow depths cores of Lake 1. Note that this ice type 4 is quite rich in bubbles.

Some core sections clearly display a mixture of cylindrical, spherical, and nut shaped bubbles as for example, section 47-65 cm depth in core 6 of Lake 1. This fifth ice type is called "mixed ice". Finally, as described earlier in the paper, we can sometimes observe a sixth ice type which contains bigger isolated large flat bubbles (see, top of core 2 in Lake 1). These bubbles can be very large with a diameter of up to a meter and are generally filled up by small hexagonal ice crystals, giving a whitish appearance to the bubble. These crystals,

resulting probably from the inverse sublimation process after bubbles formation, reduce the gas volume in the latter. In this work, the maximum bubble size analyzed was obviously constrained by the corer diameter.

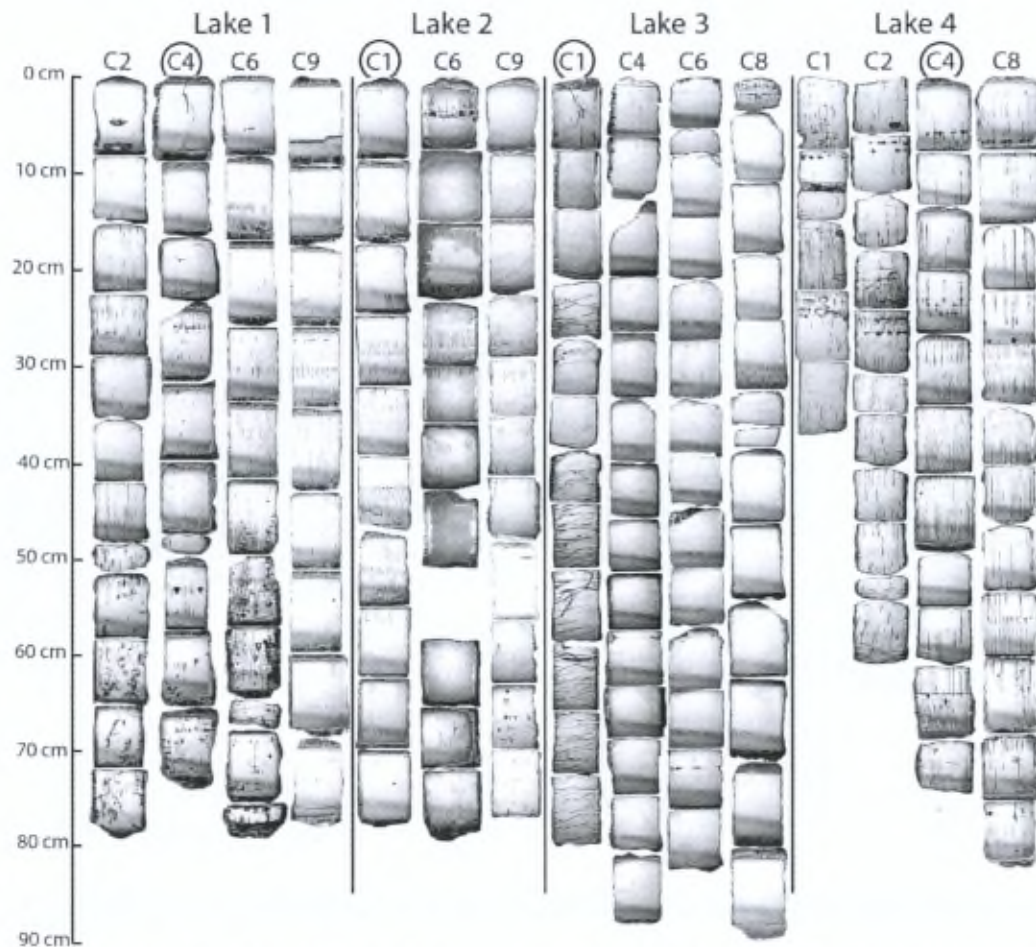


Figure 3.3 : Ice characteristics, bubbles shapes and distribution in the 15 studied ice cores (see Figure 3.2 for location). Circles denote the cores analyzed at high resolution for their gas properties.

The genesis of the various ice types described above will be discussed further in this paper, but we would like to emphasize at this stage how the spatial distribution of these ice types varies within each lake as well as in between them. In Lake 1, the bubble content drastically increases between 50 cm depth and the bottom of cores 2, 4 and 6 where we find ice type 4 and 5. This feature does not exist in core 9, sampled above deeper water (Figure 3.2), where the bottom part is made of “clear ice” (ice type 2). Of all lakes studied, Lake 3 shows the lowest bubble density. It predominantly consists of ice type 2 (clear ice) except for two discrete zones with cylindrical elongated bubbles (around 30 cm depth and at the top of

core 8) (Figure 3.3). The sub horizontal lines in core 1 from the same lake are not bubble but natural fractures. Lake 4, which is nearly frozen to bottom along the whole profile (Figure 3.2), on the contrary, shows a large density of bubbles for all cores at all depths, dominated by ice type 3 (elongated bubbles) and mixed ice (ice type 5). Finally, in all of the 15 ice cores for which thick sections have been made, we can identify a common zone of higher bubble density at about 30 cm depth (Figure 3.3).

3.4.2 Gas composition

Spatially continuous gas composition measurements have been performed at high resolution (5cm) in a selected core of each lake (cores 4, 1, 1 and 4 for respectively lakes 1, 2, 3 and 4). We also measured the gas composition within the individual large flat bubbles of ice type 6. Results are presented in Figure 3.4.

Methane mixing ratios (Figure 3.4a) vary largely between 3 ppm and 47%. Large flat bubbles show the maximum mixing ratios whereas profiles values are at the level of tens to hundreds of ppm with a few peaks around 10 to 20%. We observe an increase for all lakes (except for Lake 3) around 25 cm depth. Methane mixing ratios for lakes 1 and 4 increase with depth whereas the mixing ratios of lakes 2 and 3 remain low.

Unlike methane, the range of CO₂ mixing ratios (Figure 3.4b) is the same for the large flat bubbles (ice type 6) as for the cores profiles (between 200 and 4000 ppm). One exception is snow ice at the very top of lake 3 (9%). For all lakes, however, the CO₂ mixing ratio increases with depth with a maximum value of 46 600 ppm.

Oxygen mixing ratio (Figure 3.4c left) is about 20% near the surface of all lakes, to the exception of some large flat bubbles with lower values at 10 %. In Lake 1, 2 and 4, there is also a relative minimum at 10-15% around 25 cm depth and a clear decrease again between 40 cm depth and the bottom of the cores to mixing ratios of 5 to 15%. Lake 3, on the contrary, is remarkably stable at a value of 21%, close to the atmospheric value, although with very low total gas content (see Figure 3.4e and section 4.3.).

Nitrogen mixing ratios (Figure 3.4c right) are around 78% near the lakes surface and, in most cases, logically evolve as mirror-image of the O₂ mixing ratio (since these two species are dominant in the mix).

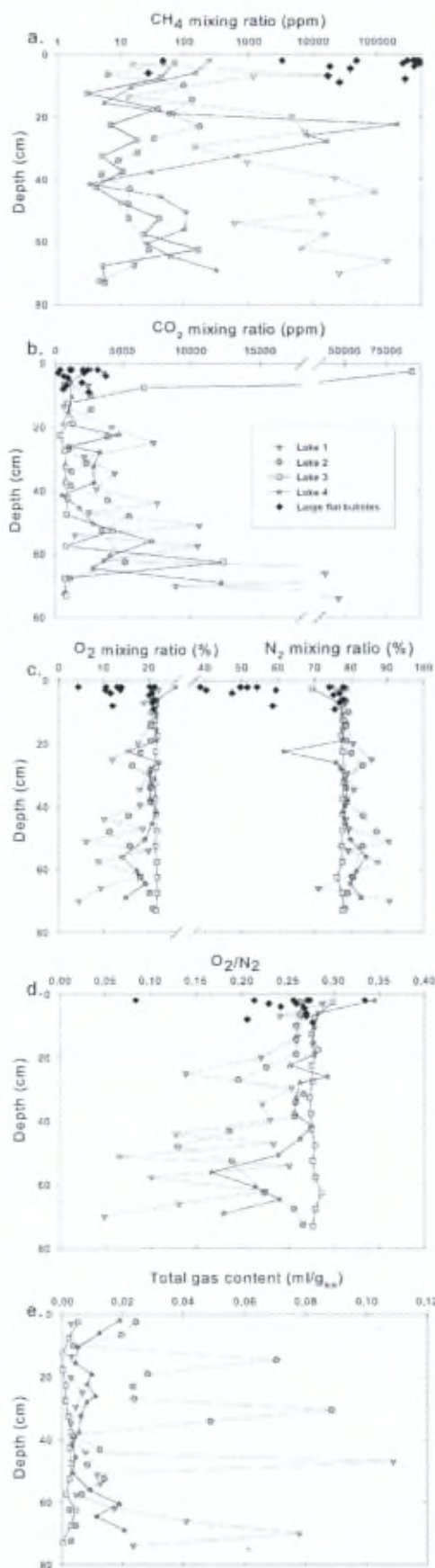


Figure 3.4 : Gas composition and total gas content versus depth for one core of each of the four studied lakes and for fifteen isolated bubbles sampled near the ice surface. A logarithmic scale has been chosen for CH₄. Note that the total gas content is not presented for the isolated bubbles (see text for details).

The O_2/N_2 ratio (Figure 3.4d) varies between 0.084 and 0.33 for ice type 6 and between 0.26 and 0.34 for the cores profiles near the lakes surface. The ratio decreases with depth to a minimum value of 0.05 for Lakes 1, 2 and 4 whereas it remains constant for Lake 3 with a value of 0.28. The decrease of the ratio actually always reflects a decrease in the oxygen, which is confirmed by a comparison of O_2 and N_2 concentrations in the water (not shown).

For Lake 1, 2 and 4 repeated changes of the ratio are seen throughout the depth, superimposed to the general trend.

3.4.3 Total gas content

The total gas content results of Figure 3.4e should generally be considered as minimum values. As discussed in the method section, the extraction process indeed underestimates the total gas content from the samples, by cutting through bubbles on sampling and therefore losing part of their gas content. This error becomes significant for ice with cylindrical elongated bubbles (between 20% and 90% for bubbles length about 0.6 cm and 3.2 cm respectively) and it is difficult to determine the ratio of each bubble length for a given sample.

This being said, our values are in the same range or slightly higher than other studies previously performed on lake ice (e.g. Lorrain *et al.* 1999, 2002). Note also that values above the maximum equilibrium dissolved gas content of fresh water (about $0.023 \text{ ml g}^{-1}_{\text{ice}}$) are also observed in lakes 1 and 2.

We do not show values for ice type 6 since this has no meaning (single isolated bubbles).

3.5 Discussion

3.5.1 A new lake ice type classification based on bubbles properties

Bubble formation processes and shapes in lake ice have already been discussed at length by several authors (Carte 1961; Bari and Hallett 1974; Gow and Langston 1977; Adams *et al.* 1998). These authors suggest that bubble shapes and density result from a balance between ice growth rate and diffusion of rejected gases in the liquid reservoir ahead. As the ice grows, most of the gases remain dissolved in the water since gas solubility in ice is at least 2 orders of magnitude smaller than in water (Killawee *et al.* 1998). With a faster freezing front, bubbles will form and be rather elongated and perpendicular to the ice front. They can sometimes be accompanied by “nut shape” bubbles. At low freezing rates, the ice can be

devoid of bubbles if the expelled gases are able to diffuse and dissolve in the water reservoir. Finally another type of bubbles is commonly encountered in lake ice covers of permafrost areas. It originates from sediment degassing (Walter *et al.* 2006) and consists of large flat bubbles trapped within the ice as it grows around.

The data collected in this paper enable us to propose a new “process-driven” lake ice type classification based on bubbles characteristics and associated gas composition. This classification, summarized in Figure 3.5, combines the influence of dissolved gases in the water, sediment degassing and gas-water interactions within the water column. It differs from the one established by Walter *et al.* (2006), mostly by the bubble size range that we address. Indeed, in this work, we are limited by the sampling method to bubbles that are smaller than 5 cm in diameter. Each of the 6 ice types described in section 4 and Figure 3.5 can then be associated to a specific genetic process for the bubble inclusions. Type 1 (snow ice) is formed by liquid water infiltration in blown snow at the surface of the lake and subsequent refreezing. Type 2 (clear ice) is typical of lake ice formed in conditions of slower freezing (favouring diffusion ahead of the freezing front) of a water reservoir which is undersaturated or not supersaturated enough for bubble nucleation to take place. Type 3 (elongated bubbles) and 4 (spherical and nuts shape bubbles) is typical lake ice where bubbles solely result from the capture of exsolved gases as the boundary layer at the ice-water interface gets strongly supersaturated from impurity rejection by the ice (higher freezing rates, closed system freezing). Type 6 ice (large flat bubbles) is the signature of an ebullition process from the sediment on the lake floor, captured at the base of the ice cover. Finally, type 5 is the expected mixed facies when both exsolution and ebullition contribute to the bubble content at the same location.

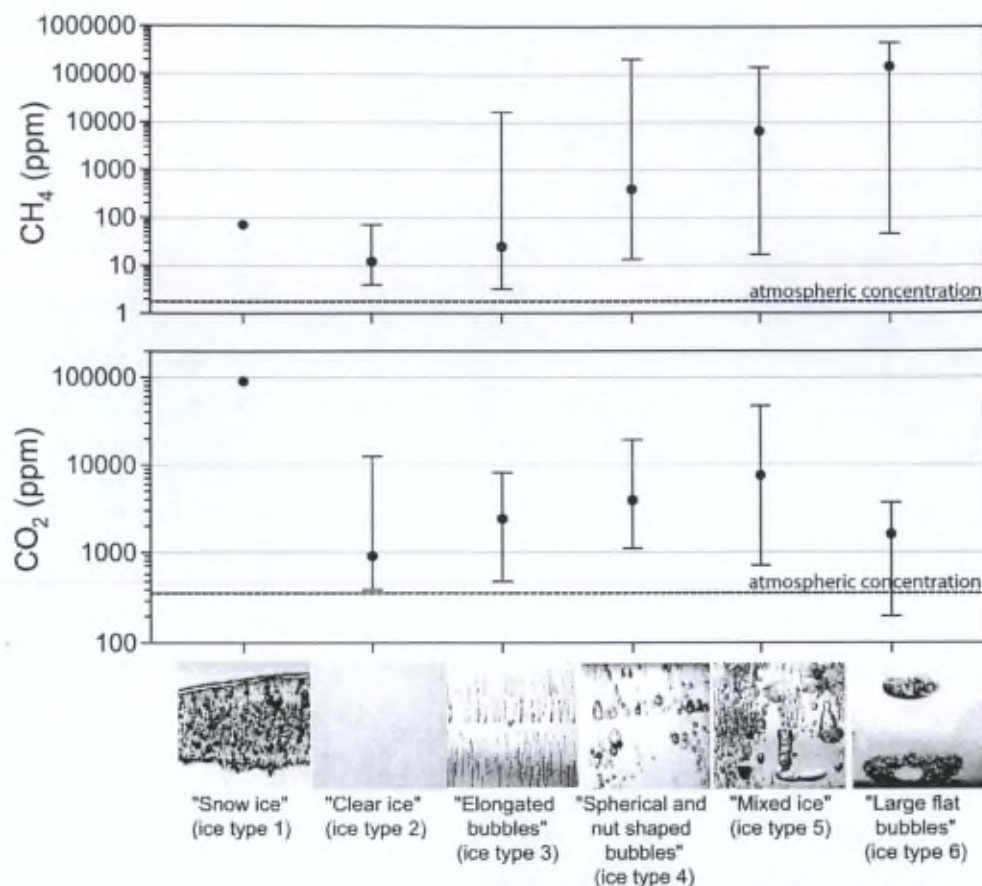


Figure 3.5 : Ice types classification from bubble shapes and density, with associated ranges of CO₂ and CH₄ mixing ratios. Note the logarithmic mixing ratio scale. Black dots are median values and vertical bars represents the variability in the observations.

3.5.2 Depth dependency of the gas composition

In parallel with the different bubble characteristics of the various ice types, the composition of these gaseous inclusions varies with depth in most cases. Figure 3.4c, for example, shows a clear decrease of the oxygen mixing ratio from 20% near the surface to about 5 to 10% at 70 cm depth. Simultaneously, the CO₂ mixing ratio increases from 500-1500 ppm up to a maximum value of 40 000 ppm. Oxygen depletion with depth is a known phenomenon in stratified lakes (e.g. Casper *et al.* 2000) and generally attributed to respiration processes.

In order to decipher the impact of biogeochemical processes from the mere physical evolution of gas properties under the specific hydrodynamic conditions of a freezing lake, we have estimated the evolution of gas concentration in water (mol l⁻¹) and of gas mixing ratios (ppm, %) in water and ice, using the simple following approach. We hypothesize that the initial gas composition of the lake water is in equilibrium with the atmosphere for O₂, N₂ and

CH₄ and showing a pCO₂ of 600 ppm as measured by Jonsson *et al.* (2007) in early autumn for lakes in our study area. We further assume, that the reservoir evolves as a closed system and that no supersaturation persist for a significant period of time before bubbles nucleation takes place. We then compute, using Henry's law (Equation 3.1) and the total gas content measured in the ice (Figure 3.4e), the theoretical evolution of gas concentrations (mol l⁻¹) in the water reservoir with depth at all times applying a simple mass balance between ice and water (Figure 3.6). This is shown as white diamonds for oxygen, carbon dioxide and methane in Figure 3.7 (nitrogen not shown).

$$c = k_h \cdot p \quad (\text{Equation 3.1})$$

Where c = dissolved gas concentration (mol l⁻¹)

k_h = Henry's constant (mol l⁻¹ atm⁻¹)

p = gas partial pressure (atm)

k_h values and temperature corrections were applied as recommended in Sander's review (1999). Further, theoretical mixing ratios in water and ice (using Henry's law again) can be reconstructed (Figure 3.6), as shown for all gases in Figure 3.8.

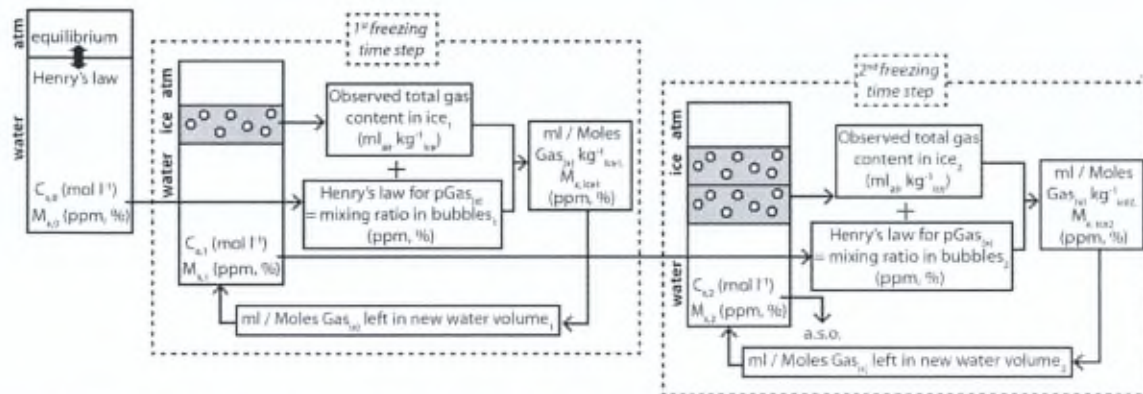


Figure 3.6 : Conceptual diagram for the calculations performed to reconstruct theoretical gas concentrations and mixing ratios in ice and water in the case of a closed system reservoir in which gases are considered as passive tracers (no biogeochemical transformations). C= concentration in water, M = mixing ratio in the water, 0 = initial water, 1 = 1st freezing step, 2 = 2nd freezing step, a.s.o = repetition of the process. Specific calculation in the case of carbon dioxide, taking into account the carbonate system equilibria, are detailed in the text.

A specific approach has been adopted in the case of carbon dioxide to take into account the evolution of the carbonate system as freezing occurs. Observed autumnal ranges (Jonsson *et*

al. 2007) of $p\text{CO}_2$ (around 600 ppm) and of total dissolved inorganic carbon (DIC - around $100 \mu\text{moles kg}^{-1}$) have been used in the USGS version of the CO2Calc program (Robbins *et al.* 2010) to assess the initial alkalinity (TA) of the water reservoir before freezing. CO2Calc was then used iteratively to recalculate equilibrium $p\text{CO}_2$ (and therefore mixing ratio in the newly formed bubbles) from updated TA and DIC at each freezing step, taking into account the amount of DIC stored as CO_2 bubbles in the newly formed ice. Used settings for the CO2Calc program were: salinity = 0‰, temperature = 0°C , Pressure = 1 atm, K1 and K2 from Millero 1979, KHSO_4 = Dickson, pH scale = NBS scale.

This theoretical model is clearly a simple theoretical reference scenario treating gases as passive tracers in that: a) no water mass advection from other lakes is allowed, b) bubbles nucleation is occurring as soon as maximum solubility is reached, c) selective diffusion ahead of the freezing front is neglected (which might affect the mixing ratios by a maximum factor of 2 to 3 in the early stages of freezing (high freezing rates, top layers) and d) surmised homogenization of the gas rejected in the reservoir will be potentially partly hampered due to the temperature-driven density stability of the water column (increasing the potential supersaturation at the ice-water interface). Note however that the latter should not affect our results since we use the observed total gas contents in the ice (as opposed to a parametrization of ex-soluted gases from the level of supersaturation) and since the potential absence of physical mixing should affect all gases in the same way (therefore not altering the mixing ratios deduced from gas concentrations in the new water volume - Figure 3.6). Despite these limitations, our theoretical curves of Figure 3.7 and Figure 3.8 allow us to put forward potential discrepancies due to either open system conditions or biogeochemical processes.

As expected from the limited amount of gas enclosed as bubbles in the ice, theoretical concentrations in water regularly increase with depth (Figure 3.7, N_2 not shown). Also, following relative solubilities, mixing ratio increase for all gases but nitrogen, as nitrogen is the dominant and least soluble species (Figure 3.8a).

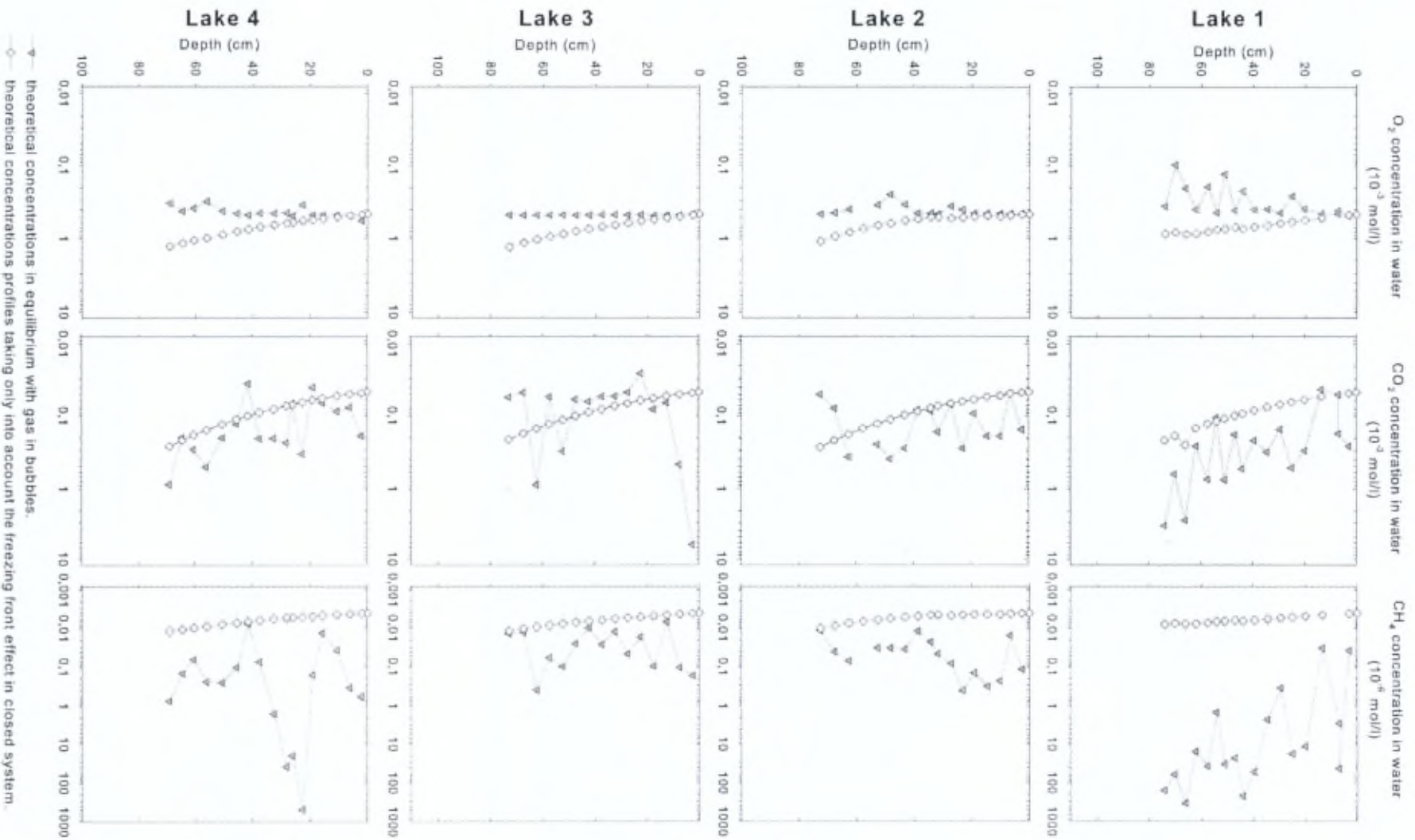


Figure 3.7 : Theoretical O_2 , CO_2 and CH_4 concentrations in water as a function of depth for each lake: triangles represent values in equilibrium with measured gas mixing ratios in bubbles (calculated using Henry's law); diamonds show theoretical values calculated by only taking into account the "reservoir effect" in a closed system (see text for details).

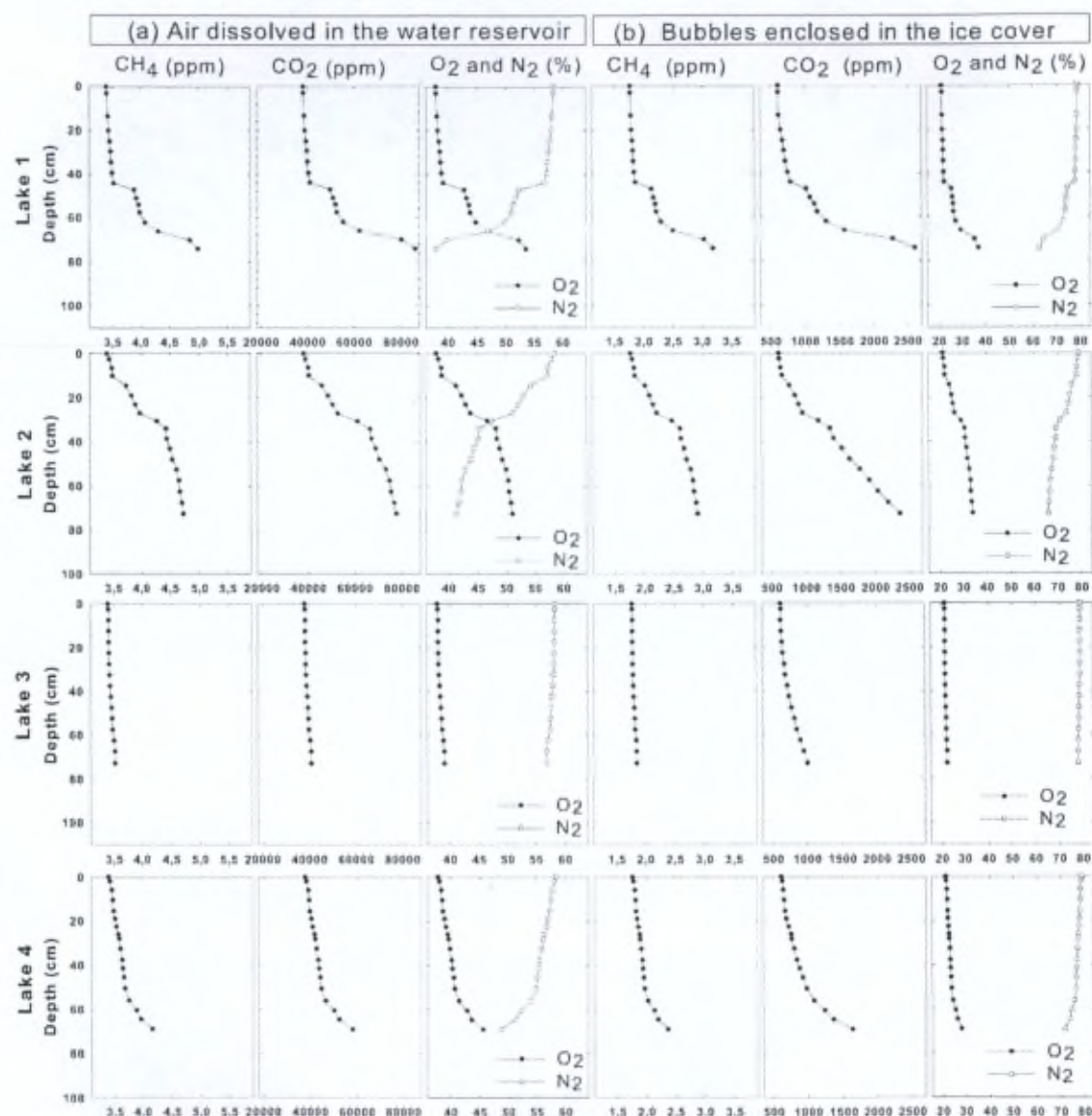


Figure 3.8 : Theoretical evolution of mixing ratios for (a) air dissolved in water and (b) bubbles in ice, assuming lakes are closed reservoir, using observed total gas contents and equilibrium mixing in water from Henry's law for mass balance in the ice and assuming no gas fractionation occurs at the ice water interface (see text for details).

Maximum theoretical water concentrations are reached at the bottom of Lake 1 with value of 5.0 ppm in CH_4 , 86 000 ppm in CO_2 and 54% for O_2 , resulting in ice bubbles mixing ratios of

3.2 ppm, 2600 ppm and 36.9%, respectively. Another salient feature of Figure 3.8 is the behavior of Lake 3 showing only little changes with depth, as expected from its deeper waters (Figure 3.2).

Real gas concentrations in the water can also be reconstructed using the measured gas mixing ratios in the ice and applying Henry's law. This is shown for O_2 , CO_2 and CH_4 as grey triangles in Figure 3.7.

Are the observed ice gas mixing ratio profiles of Figure 3.4 then coherent with the closed system theoretical evolution shown in Figure 3.8b? Methane shows a wide range of values (from a few ppm to 100 000) and no systematic increasing trend with depth. Only exceptionally is the maximum "closed system" value of a few ppm observed (here as a minimum in the profiles), and not necessary at the bottom of the ice cover. This clearly suggests that exsolution is not the dominant process in controlling methane mixing ratios in the ice, but rather the varying contribution of ebullition process.

Comparing observed to theoretical profiles for carbon dioxide in lakes 1, 2 and 4 shows a similar trend of increasing mixing ratio in ice (Figure 3.8b) and concentrations in water (Figure 3.7, middle panel). However, again, in both cases, observed values can be higher than theoretical ones by up to an order of magnitude, with considerable superimposed variability. An additional source of carbon dioxide is therefore required, and this from the very beginning of the growth season as shown by the lake water supersaturation level of the reconstructed water concentrations from bubbles in the ice (Figure 7, central panel). Could this be the result of respiration processes in the reservoir? The behavior of dissolved oxygen is worth considering in that respect. Indeed, instead of showing the expected increase of mixing ratio (Figure 3.8a) and concentration in water (Figure 3.7, left panel, white diamonds) with depth, reconstructed water concentrations actually slightly decrease in lakes 1, 2 and 4. This could be interpreted as the signature of respiration. Looking at relative increase of CO_2 and decrease of O_2 in Figure 3.7 reveals important contrasts between lakes and between depths in a given lake. In the lower half of lakes 2 and 4 oxygen loss and CO_2 gain are in relative balance, which does not preclude a respiration control in the water column during ice growth. On the contrary, in the upper half of the ice cover from the same lakes, negligible amounts of oxygen are lost, whilst excess carbon dioxide is present. For Lake 1, CO_2 gain is at all times in excess of the O_2 loss, also suggesting an alternative source to respiration for CO_2 , from the very beginning of the lake ice growth. Finally, Lake 3, which has been described as a relatively open system, shows three distinct sections; a lower one coherent with

episodic respiration processes and returns to a fully open system regime, a top section where the CO₂ gain overwhelms the (negligible) O₂ loss (as in all other lakes), and a middle section where CO₂ concentrations are again what would be expected from open system conditions.

To summarize, dissolved CO₂ concentrations in the waters of lakes 2, 3 and 4 could be explained by "in situ" respiration processes for waters generating the lower part of the lake ice cover (late growth), whilst an extra source (as compared to simple equilibrium with atmosphere) is needed for the waters generating the upper part of the lake ice cover (early growth). For Lake 1, this extra source is needed at all times. Although reservoir closure is unable to explain the observed levels of water concentration, it could be partly responsible for the general trend of CO₂ concentrations in lakes 1, 2 and 4.

Several mechanisms, other than respiration, could be responsible for the high levels of observed dissolved CO₂ in our lake waters. Gas ebullition from the sediment can certainly contribute to the CO₂ increase. Sulfate-reduction, which is often associated to the methanogenesis process (Fenchel *et al.* 1998), is also a provider of carbon dioxide. The particular smell of H₂S, another by product of the reaction, has been detected in the course of sampling. Denitrification, methane oxidation or acetate fermentation can also contribute to the CO₂ content (Stumm and Morgan 1996). In our case, the similarity of the reconstructed CH₄ and CO₂ concentration profiles in water in most lakes (Figure 3.7, middle and right panels) suggest that acetate fermentation might be the dominant extra CO₂ source at work, as opposed to methane oxidation. This also puts forward acetate fermentation as the source for methane. $\delta^{13}\text{C}$ and δD isotopic analysis of the CH₄ would of course help in deciphering the sources, but these unfortunately are not available at this time. The generalized CO₂ excess in the surface layer of all lakes could reflect the dynamical instability of the lake waters in the autumn, bringing bottom enriched waters to the lake surface just before the onset of freezing.

The O₂/N₂ ratio (Figure 3.4d) reflects the changes in the oxygen mixing ratio and can therefore be used as an indicator of the stratification process in the lake during the winter. However, it can also be a measure of the hydrological regime in the lake (open vs. closed system). For example, Lake 3 shows a constant O₂/N₂ ratio throughout the depth because the input of atmosphere equilibrated waters from the river upstream (Figure 3.1) inhibits the changes in oxygen mixing ratios due to the ice cover freeze on (closure) or biological processes as discussed above. It is interesting to note that local CO₂ mixing ratio increases occur at about 50 and 60 cm depth, despite the water circulation. This suggests that these excursions correspond to local ebullition events, as confirmed in the CH₄ profile.

3.5.3 Ice type dependency of gas mixing ratios

Figure 3.5 shows contrasted CH_4 and CO_2 signatures for the various ice types described in section 5.1. Only one measurement is available for the “snow ice” (type 1), and it shows the highest CO_2 value of the whole study at 90 000 ppm. This is hard to explain by physical processes only. Figure 3.8a shows that CO_2 values up to 86 000 ppm can be reached for gas dissolved in water during closed system freezing of lake reservoir (at about 70% freezing). Bulk freezing of residual water from the final stages of closed system freezing of a lake, expelled at the surface through the moat and bathing the snow cover, could therefore lead to such high CO_2 values. This is however quite unlikely, since our “snow ice” was measured at the surface of Lake 3, which was the least “closed”. Bacterial respiration of organic matter blown with the snow at the lake ice surface is another plausible explanation. Strangely enough, oxygen does not show the expected concentration decrease if aerobic respiration had been active. Ice types 2 to 4 should span the range of theoretical CO_2 mixing ratios shown in Figure 3.8b (600 to 2600 ppm) if the water was initially with a pCO_2 about 600 ppm. We know from the discussion above that this is not true, and the observed range of 3000 to 4000 ppm is in accordance with ex-solution from a lake water displaying the observed excess- CO_2 concentration. The “mixed ice” (type 5), with apparent contribution from both exsolution bubbles and small bubbles resulting from sediment ebullition, shows higher CO_2 and CH_4 mixing ratios as compared to ice type 3 and 4. This suggests that the small bubbles coming from the sediment contribute to increase both the carbon dioxide and the methane content as surmised from the discussion in the previous section. The large flat bubbles (type 6), also derived from sediment ebullition are globally richer in methane but poorer in carbon dioxide. This however does not mean that the amount of carbon dioxide in these bubbles is lower as compared to ice type 5, since the data are shown as mixing ratio (i.e. relative concentration). It is nevertheless disturbing, if ice type 5 is a mixture between ice types 3/4 and 6, that the CO_2 mixing ratio is not at an intermediate value (as does CH_4 in Figure 3.5). This suggests that a small fraction of methane (not detectable in Figure 3.7) might have been oxidized to CO_2 in the lake environment. Finally, it is striking that, although they show an increasing mean/median methane concentration value, ice types 4, 5 and 6 display similar (large) concentration ranges. This probably reflects the combination of increased supersaturation of the ex-soluted waters in the nearly closing reservoir (ice type 4) and direct ebullition from the sediment nearby (ice type 6).

Our results globally underline that the lake ice cover signature is far from being governed by pure ebullition only. As illustrated by the contrast between ice type 5 and 6, the least soluble methane dominates ebullition, while carbon dioxide mixing ratio is higher in the lake ice storage. Clearly, our data indicate that exsolution dominates the lake ice cover signature. Further, the fact that methane mixing ratios observed in bubble type 6, the closest to pure ebullition, are still largely lower than those observed in studies of pure ebullition fluxes, indicates that substantial exchanges with dissolved gases occurred for those ice entrapped ebullition products. This however needs to be weighed, in terms of budget, by the overwhelming amount of gas liberated through ebullition, as compared to the one stored in the lake ice.

3.5.4 Controls on bubble distribution in lake ice

Intra-lake and inter-lake comparison in our dataset shows that there is a control of geometry on the bubble distribution in the ice, which is of potential interest in the perspective of upscaling regional dataset to global carbon budgets. For instance, the proximity of the bottom of the lake increases the amount of bubbles in the ice. Figure 3.2 and Figure 3.3 indeed show that the lower part of cores C2, C4 and C6 of Lake 1 (in shallow areas) is rich in bubbles while core C9 (located above deeper waters) is not. Lake 4 is shallow and nearly frozen to the bottom and its ice cores are bubble rich. This suggests that shallow lakes will enclose more gas in the ice cover. Other factors such as the amount of organic matter locally available or the sedimentation rate would of course further affect the gas fluxes from the sediment, but these were not documented in the present data set.

The hydrological regime of the lake system can also directly impact the gas content in the lake ice. Our study shows that if a lake is part of an open drainage system, the ice can be nearly devoid of gas. Lake 3, which is fed by a river (Figure 3.1), and where the water drains into another lake, is a good example (Figure 3.3). The three other lakes, on the contrary, are closed or open to another lake without significant water circulation and all show a significative bubble content. In the first case it would be adequate to investigate if the lack of bubbles in the ice is counterbalanced by a supplementary provision in the connected lakes, and to understand how they will affect the quantity (fluxes) and the quality (CH_4 vs. CO_2) of the gases released to the atmosphere.

The proximity of the lake banks does not seem, in our data set, to affect the bubble distribution despite the fact that lakes can be more methane productive along lakes margins (e.g. Walter *et al.* 2007b). However, all lakes are relatively small, and the situation might be different for larger lakes.

Local events of atmospheric pressure drop has also been claimed to trigger bubble production in lake ice (Mattson and Likens 1990; Semiletov 1999). In this study, we observed two simultaneous bubbling events for the 4 lakes, the first one around 30 cm depth (well documented in Figure 3.3) and the second around 60 cm (clearly seen during cores handling). To investigate a potential relationship of these events to marked atmospheric pressure changes, we first need to reconstruct a time line for the buildup of the lake ice cover. A simple (neglecting geothermal heat flux) thermodynamic model for freezing (Hinkel 1983) has been run, based on Equation 3.2:

$$\rho_i \lambda \frac{\partial Z_i}{\partial t} = \frac{(T_0 - T_s)}{\left(\frac{Z_i}{K_i} + \frac{Z_s}{K_s}\right)} \quad (\text{Equation 3.2})$$

Where ρ_i = density of ice (kg m^{-3})

λ = latent heat of fusion (J kg^{-1})

Z_i = ice thickness (m)

Z_s = snow thickness (m)

K_i = thermal conductivity of ice ($\text{W m}^{-1} \text{ } ^\circ\text{C}^{-1}$)

K_s = thermal conductivity of snow ($\text{W m}^{-1} \text{ } ^\circ\text{C}^{-1}$)

T_0 = temperature at ice/water interface ($^\circ\text{C}$)

T_s = surface temperature ($^\circ\text{C}$)

t = duration of constant T_s (s)

The model reconstructs the ice thickness Z_i as a function of temperature from the first day of freezing. It has been run both with and without a snow cover to obtain a reasonable prediction of the evolution of the ice cover. The snow cover data set from the nearby weather station doesn't account for snow redistribution at the surface of the lakes. Therefore the model has been run both with and without a snow cover to obtain a reasonable prediction of the evolution of the ice cover. From those runs, we have correlated in Figure 3.9 (hatched area) the observed major bubbling events at around 30 and 60 cm depth with major occurrences of

atmospheric pressure drops. This confirms that attention should be drawn to major atmospheric pressure events in assessing methane release efficiency from boreal lakes.

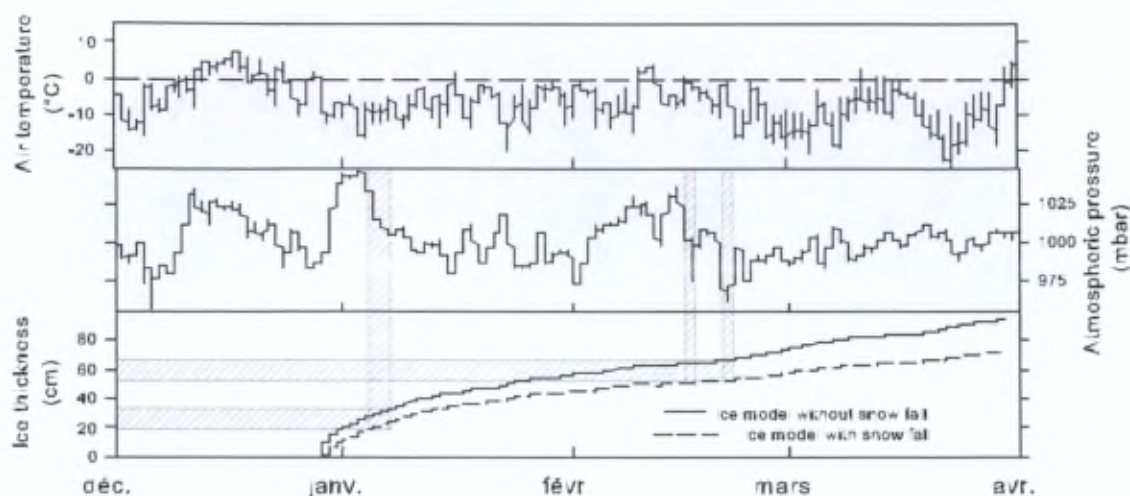


Figure 3.9 : Air temperature and atmospheric pressure versus modelled ice thickness from Equation 3.2 (see text). The dotted line takes snow falls into account. Shadow hatchings show depth fitting with the air pressure drop events. The two highlighted drops correspond with the depth of the two synchronous bubbling events described in the text.

3.5.5 Assessing a lower bound for lake ice melting contribution to the atmospheric methane budget

In this section we present a “back of the envelope” calculation for a minimum winter contribution of periglacial lakes to methane fluxes to the atmosphere. We rely on our ice type/bubbles classification to perform a budget for methane accumulation in lake ice during the winter. We first calculate the proportion of each ice type in each core considering it as representative for the whole lake ice cover. We then multiply this proportion by the minimum, mean (median) and maximum CH_4 mixing ratio for this type of ice and by the observed mean total gas content of the given ice type. This provides an ice-type weighed concentration of methane in ml CH_4 per gram of ice for each lake. This value is then integrated over the lake ice mass and divided by the lake area and by the number of days the ice cover existed. Results are presented in Table 3.1. Although these values do not represent the actual flux of methane to the atmosphere during the relatively short melting period, they provide a mean winter daily flux, that can be more easily compared to spring-summer flux estimates available in the literature.

We consider these values as minimal for two reasons: a) because the total gas volume measurements were probably biased towards gas losses (see subsection 4.3), and b) because we cannot include the contribution of bubbles above 5 to 6 cm in diameter, which are most likely the larger contributors to the methane budget (Walter *et al.* 2010). We however consider our results as a measure of the “background contribution” of permafrost lake ice; without the big bubbles events. This work is therefore complementary to other studies focusing on large methane emission observed in spring, due to the ice cover melting and water turnover which releases the excess dissolved gases stored in the water column (Michmerhuizen *et al.* 1996; Phelps *et al.* 1998). It is also complementary to studies focusing on larger bubbles in winter lake ice (e.g. Walter *et al.* 2006, 2007b, 2008a, 2010).

Methane fluxes (mg CH ₄ m ⁻² d ⁻¹)	Minimum	Mean or median	Maximum
Lake 1	1.34 10 ⁻³	3.01	12.7
Lake 2	3.91 10 ⁻⁴	4.32 10 ⁻²	4.4
Lake 3	6.52 10 ⁻⁵	4.35 10 ⁻⁴	1.14 10 ⁻²
Lake 4	3.59 10 ⁻⁴	3.21 10 ⁻²	4.22

Table 3.1: Bounds for methane fluxes released by the winter lake ice cover. The median value is used if the mean value is higher than the standard deviation.

Our results present a large variability between each lake. Lake 1 shows values (1.34 10⁻³ – 12.7 mg CH₄ m⁻² d⁻¹) comparable to other studies (Kling *et al.* 1992; Rudd *et al.* 1993; Zimov *et al.* 2001; Bastviken *et al.* 2004; Repo *et al.* 2007) reporting values from 0.3 to 77 mg CH₄ m⁻² d⁻¹. Lakes 2, 3 and 4, on the contrary, show values from 6.52 10⁻⁵ to 4.4 mg CH₄ m⁻² d⁻¹ which are in the lowest range of those reported in most studies on methane fluxes from lakes (values observed from 0 to 3240 mg CH₄ m⁻² d⁻¹; Walter *et al.* 2010). We did expect to find moderate contribution from lake ice in the winter, but we show here that these are not negligible and worth considering in global budget estimations.

3.6 Conclusions

This work contributes to the study of methane released from lakes in periglacial environments. It provides new results on the winter gas storage associated to the lake ice cover buildup. A new genetic lake ice types classification is proposed, based on bubbles

shapes, density and gas composition. It is used to provide a first minimal estimate of methane fluxes associated to winter storage in the lake ice cover, which are complementary to previous studies focusing on spring and summer fluxes from open water sources and studies focusing on large bubbles in lake ice. It is shown that although moderate, as expected, these fluxes are not negligible with respect to other sources.

Gas composition study of the bubbles reveals strong supersaturation of the lake water both in methane and carbon dioxide, especially in the lakes that evolve in near closed system. These high concentrations are thought to mainly result from interaction with biological processes in the sediment, of which acetate fermentation would be a likely candidate, given the observed synergy between CO_2 and CH_4 in the profiles. Part of the excess CO_2 could also result from respiration processes, as indicated by oxygen losses, especially during the second half of the ice growth period. Mere closure of the lake reservoir cannot explain the observed concentration excess, but could be partly responsible for the global trend of increasing concentrations with depth in the water and in the ice.

We also demonstrated that lakes geometry and hydrological regime affect the amount and characteristics of gases enclosed in the ice, although this pilot study obviously does not have yet the statistical power to derive quantitative relationships. Finally, we confirm that atmospheric pressure regimes can trigger bubble nucleation and sediment ebullition events and therefore should be considered as a factor in methane release efficiency.

Future work will focus on the stable isotope composition of the bubbles in the different ice types, in order to decipher the relative importance of physico-chemical and biologically mediated processes in controlling the gas properties in permafrost lake ice.

Chapter 4. Methane isotopic signature of bubbles in permafrost winter lake ice : a tool for quantifying variable oxidation levels

This paper has been submitted as: "Methane isotopic signature of gas bubbles permafrost winter lake ice: a tool for quantifying variable oxidation levels", Boereboom T., Sapart C., Röckmann T. and Tison J-L. to JGR-Biogeosciences.

Abstract

The current atmospheric methane (CH_4) increase is known to induce possible feedbacks of natural sources of CH_4 . In particular, thawing of permafrost areas in the Arctic is considered as an important feedback, since the Arctic experiences the fastest climate change and hosts large carbon stocks. Subarctic lakes can be considered "hotspots" of CH_4 emissions, but they are also for a large part of the year frozen and CH_4 is then trapped in gas bubbles in the ice. Here, we present measurements of CH_4 mixing ratio and $\delta^{13}\text{C}\text{-CH}_4$ in 4 types of bubbles identified in subarctic lake ice covers located in a sporadic or discontinuous permafrost area. Our analysis reveals that different bubble types contain CH_4 with different, specific isotopic signatures. The evolution of mixing ratio and $\delta^{13}\text{C}\text{-CH}_4$ suggest that oxidation of dissolved CH_4 is the most important process determining the isotopic composition of CH_4 in bubbles resulting from gas exsolution occurring during the ice growth process. A first estimate of the CH_4 oxidation budget (mean = $0.12 \text{ mg CH}_4 \text{ m}^{-2} \text{ d}^{-1}$), highlights the impact of the ice cover on CH_4 emissions from subarctic lakes. The increased exchange time between gases coming from the sediments and the water column, due to the capping effect of the lake ice cover, reduces

the amount of CH₄ released “as is” and favours its oxidation into carbon dioxide; the latter being further added to the HCO₃⁻ pool through the carbonate equilibration reactions.

4.1 Introduction

Subarctic lakes in permafrost areas are net CH₄ emitters contributing to the greenhouse effect (IPCC 2007). Studying this contribution is complex because of the high spatial and temporal variability of CH₄ emissions from lakes and of the complexity of the biochemical processes taking place in aquatic environments. CH₄ is produced in unfrozen lake sediments by acetate fermentation and/or CO₂ reduction. It reaches the atmosphere mainly by bubbling but also by diffusion through the water column and by transport through plants. Most studies on CH₄ lake emissions focus on the ice-free period, but only a few of them are studying the winter period contribution (e.g. review Table in Walter *et al.* 2010) and the potential influence of the lake ice cover (see Chapter 3). Nevertheless, degassing from lakes and the CH₄ mixing ratio in bubbles are known to be lower during the winter compared to the summer (Chapter 3; Phelps *et al.* 1998; Walter *et al.* 2006, 2007b, 2008a, 2010).

When ice covers subarctic lakes, the underlying water is isolated from the atmosphere and can be stratified. These peculiar closed system conditions increase the exchange time between the gases degassing from the sediments and the water column. Such conditions are favourable for CH₄ oxidation into carbon dioxide and gas equilibration. Chapter 3 have investigated the behaviour of gas bubbles that are trapped in lake ice. They revealed lower CH₄ mixing ratios (from 3 ppm to 46%) than those reported in studies performed during the ice-free period showing CH₄ mixing ratios up to 80% (Walter *et al.* 2010). Walter *et al.* (2008a) also describe lower methane mixing ratios in bubbles enclosed in the winter ice cover and tribute it to oxidation process without discussing the controlling factors. Furthermore in Chapter 3, a new “process-driven” bubble classification in lake ice revealed that the gas composition depends on, inter alia, the bubble type, the lake depth and the hydrological status of the lakes.

Analyzing stable isotope ratios is an efficient tool to identify the mechanisms involved in the release and transport of CH₄ in permafrost lakes. In this paper we present, for the first time, the $\delta^{13}\text{C}$ -CH₄ signatures of four specific types of lake ice bubbles in order to better understand the processes that control their gas composition in the winter and to better constrain the potential influence of lake characteristics.

4.2 Study area : Lake characteristics and sampling procedure

The ice samples analyzed were collected in 4 lakes in the Stordalen Mire peat bog area (68°21'N, 19°02'E) near the Torneträsk Lake, in Northern Sweden (Figure 4.1). This area presents a sporadic or discontinuous permafrost cover, which has already previously been investigated for CH₄ emissions (e.g. Chapter 3; Johansson *et al.* 2006a; Bäckstrand *et al.* 2010). The lakes were chosen according to their different characteristics in order to study the potential influence of size, depth and hydrological system on the properties of the bubbles trapped in the lake ice cover. Lakes 1, 2 and 3 have a relatively small surface area of 0.01 to 0.02 km² with variable depth (from 1 to 5 m) whereas Lake 4 is larger (0.19 km²) with a maximum observed depth of 1 m. Lake 1 and 4 are disconnected from other water circulation patterns, Lake 2 is connected to Lake 3 and the latter is affected by water circulation with incoming water originating from a river and flowing into the NW lakes (Figure 4.1). For each lake shallow ice coring was performed at the end of the winter, more precisely during the last days of March 2008, along a transect from the lake center towards its banks. Next to the transects, supplementary samples with distinguishable individual large flat bubbles were collected.

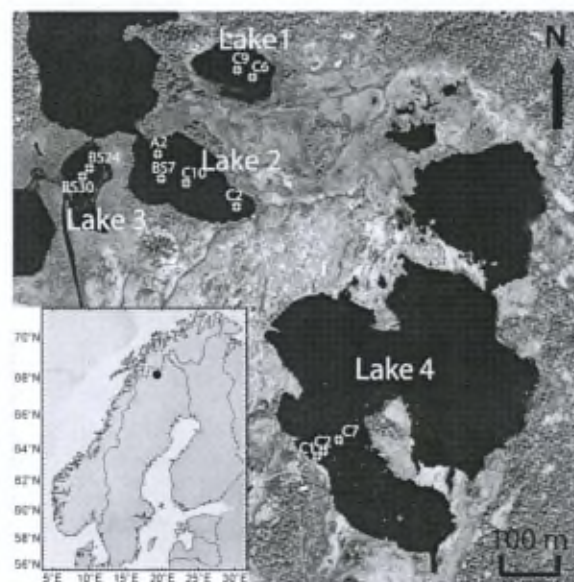


Figure 4.1 : Map showing the sampling locations and the numbering of different lakes as used in this paper. The crossed white circles show approximately the location of the cores and the associated codes allow to identify the samples listed in Table 4.1.

4.3 Methods

$\delta^{13}\text{-CH}_4$ and CH_4 mixing ratios were measured on 14 samples. These samples were carefully chosen in order to identify possible differences in isotopic signatures between the different lakes, the different types of bubbles and the various ice depths (see Figure 4.1 for sample locations). In this study, 4 types of bubbles described in Chapter 3 have been isolated and analysed; a) “cylindrical elongated bubbles” appearing typically in lake ice where the freezing front progressively encloses gases accumulating at the ice water interface; b) spherical and nut shaped bubbles common in lake ice where the freezing front is growing fast; c) “mixed ice” showing mixing between the various types of bubbles and; d) “large flat bubbles” resulting from direct sediment degassing. These 4 types of bubbles are illustrated in Figure 4.2 and the sample description and analytical results are shown in Table 4.1.

Ice core drilling was performed using a SIPRE-type ice auger (7.5 cm diameter) and the samples extracted were cut with a band-saw in a -20°C cold room.

The isotope analysis was performed using a dry extraction system following the principle described in Sapart *et al.* (2011). The ice samples were introduced in a 6 L stainless steel (SS) pot provided with a perforated cylinder and evacuated in a freezer at -30°C . Thereafter, following the dry extraction principle of Etheridge *et al.* (1988), the ice samples were grated to fine flakes in a shaking device in order to release the air trapped in the ice. The pot was then connected to the glass-line and the extracted air was cryopumped into 120 ml glass bottles filled with 40 ml of Haysep D, a powerful molecular adsorbent cooled to -196°C . The amount of CH_4 per sample was often larger than the calibrated range of the isotope ratio mass spectrometer; therefore, the samples were diluted in helium (He BIP 5.7, Air Products) to about 1000-5000 ppb of CH_4 . After dilution, the samples were connected to the low pressure inlet of the CH_4 isotope ratio mass spectrometry system for isotope analysis (Brass and Röckmann 2010; Sapart *et al.* 2011).

Isotope ratios are presented in $\delta^{13}\text{C}$ notation, which quantifies the relative deviation of the $^{13}\text{C}/^{12}\text{C}$ ratio in a sample from the same ratio in the international standard Vienna PeeDeeBelemnite (VPDB). CH_4 mixing ratios are reported as molar mixing ratios in $\text{ppm} = \mu\text{mole/mole} = 10^{-6}$.

4.4 Results

Figure 4.2 shows CH₄ mixing ratios and $\delta^{13}\text{C-CH}_4$ for the different bubble types. The general trend shows an inverse relationship between $\delta^{13}\text{C-CH}_4$ and CH₄ mixing ratio for the four bubble types studied. Elongated bubbles, which are formed in lake ice from gas exsolution during a relatively slow freezing front progress, show the largest variability for $\delta^{13}\text{C-CH}_4$ (from -68‰ to -33‰) and the highest isotopic values, but also the lowest CH₄ mixing ratios (lower than 325 ppm). Spherical and nut shaped bubbles are usually formed in lake ice where the freezing front progresses faster (Adams *et al.* 1998 and references therein). This type of bubbles contains CH₄ with lower isotopic values (from -71‰ to -53‰) and CH₄ mixing ratios from 74 to 1294 ppm. Only one sample of mixed ice, containing several types of bubbles (elongated bubbles, spherical and nut shaped bubbles and larger bubbles) was analysed. This sample had a $\delta^{13}\text{C-CH}_4$ value slightly lower than the previous type (-73‰) and a CH₄ mixing ratio barely higher (1379 ppm). The last bubble type, i.e. “large flat bubbles”, results directly from the ebullition process of sediments and shows the lowest values of $\delta^{13}\text{C-CH}_4$ (-78‰) and CH₄ mixing ratios between 278 and 1764 ppm.

Samples	Method	Bubble type	CH ₄ mixing ratio (ϕ_{CH_4}) (ppm)	$\delta^{13}\text{C-CH}_4$	1- σ	f^*	Oxidation fraction*
Lake 1 – C9	LP(1)	b	1294	-67.91	0.30	0.73	0.27
Lake 1 – C6	LP(2)	b	74	-53.19	0.04	0.04	0.96
Lake 2 – A2 ^a	CF	a	325	-57.58	0.18	0.18	0.82
Lake 2 – A2 ^b	CF	a	255	-50.51	0.18	0.14	0.86
Lake 2 – A2 ^c	CF	a	78	-67.45	0.18	0.04	0.96
Lake 2 – BS7	LP	d	1764	-75.31	0.50	1	0.00
Lake 2 – C2	LP	b	652	-65.66	0.04	0.37	0.63
Lake 2 – C10	LP	b	419	-71.39	1.18	0.24	0.76
Lake 3 – BS24	LP	d	602	-78.22	0.10	0.34	0.66
Lake 3 – BS30	LP	d	278	-75.06	0.37	0.16	0.84
Lake 4 – C1	LP	c	1379	-73.04	0.91	0.78	0.22
Lake 4 – C2	CF	a	221	-67.92	0.30	0.13	0.87
Lake 4 – C7 ^a	CF	a	3	-42.77	0.33	0	1.00
Lake 4 – C7 ^b	CF	a	9	-32.97	0.55	0.01	0.99

Table 4.1 : Sample description and analytical results

Note that all bubble types have been observed in all lakes except in Lake 3. This lake is specific because it is nearly devoid of bubbles in all observed cores, apart from scarce

occurrences of elongated bubbles, nut shaped bubbles and few isolated bubbles (see Chapter 3).

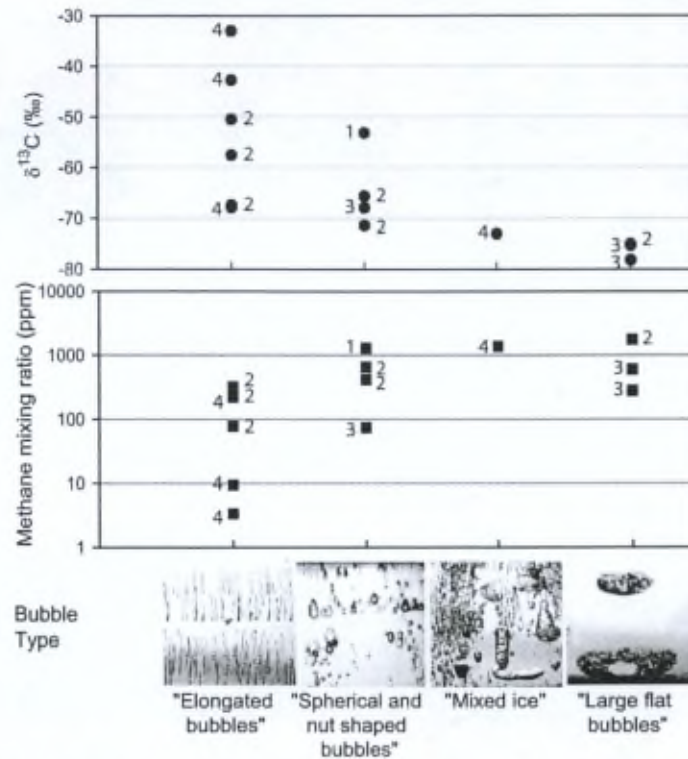


Figure 4.2 : $\delta^{13}\text{C}\text{-CH}_4$ and CH_4 mixing ratios for each of the bubble types. For illustration, representative photos of the different bubble types are shown below the x axis. Numbers indicate the lake origin (see Figure 4.1).

4.5 Discussion

Our study allows characterizing the different bubble types through their CH_4 isotopic composition. The $\delta^{13}\text{C}\text{-CH}_4$ values of large flat bubbles are around -75‰ , in agreement with values observed previously in lake sediments and ice kosHKas (Walter *et al.* 2008a). We consider this isotopic signature (identified from lakes 2 and 3) as the local source composition resulting from direct sediment degassing. In contrast, the elongated bubbles are strongly enriched in ^{13}C with values reaching $\delta^{13}\text{C}\text{-CH}_4 = -33\text{‰}$. Such high values have not been observed in bubbles from subarctic lakes (Walter *et al.* 2008a) but have already been observed for CH_4 dissolved in water (e.g. Grant and Whiticar 2002; Schubert *et al.* 2010) in association with an oxidation process. Spherical, nut shape bubbles and mixed ice types show intermediate values between -73 and -53‰ . This isotopic distribution, i.e. by bubble type,

does not seem to be influenced by the lake characteristics (Figure 4.2) and suggests the presence of an isotopic enrichment mechanism related to the process of bubble formation.

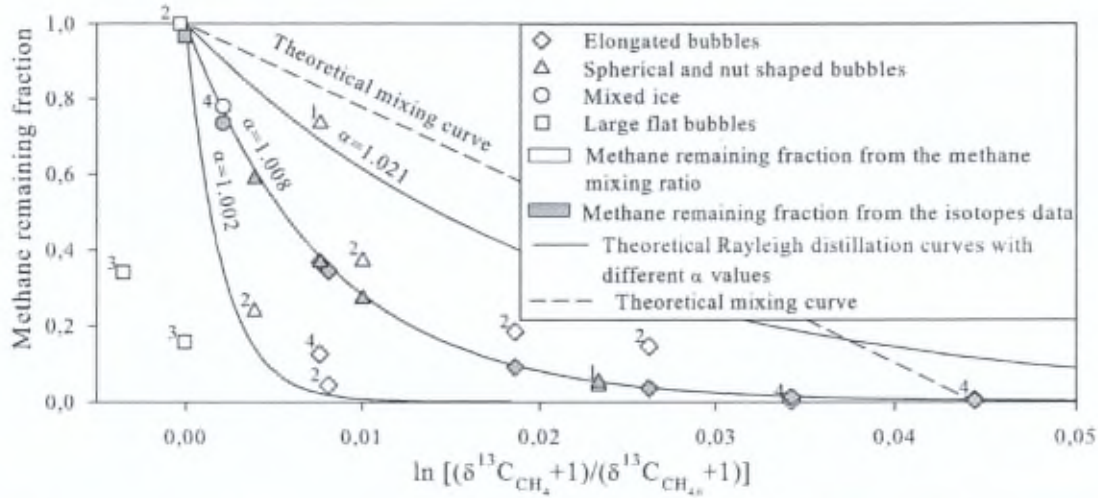


Figure 4.3 : Results from measurements and simple models for the correlation between the change in the isotopic composition ($\ln[(\delta^{13}\text{CH}_4 + 1)/(\delta^{13}\text{CH}_{4,0} + 1)]$) and the remaining fraction of CH_4 . White symbols show the methane remaining fraction calculated from the methane mixing ratio and grey symbols show the methane remaining fraction calculated from the isotope data with $\alpha = 1.008$. To model the removal of CH_4 by oxidation (solid lines), we start with the highest mixing ratio (top sample labelled 2) and calculate the evolution of isotopic composition for three α values of a Rayleigh distillation model. The dashed line shows a mixing curve between two reservoirs of plausible very high and very low CH_4 mixing ratio. Numbers indicate the lake of origin (see Figure 4.1) for the white symbols and the symbol shape refers to the bubble type (see Figure 4.2). See text for details.

CH_4 oxidation and mixing of several sources are two natural processes that can result in a wide range of isotopic signatures, as observed. Indeed, CH_4 oxidation to CO_2 , from bacterial activity in the water, favours consumption of $^{12}\text{CH}_4$ and therefore enriches the remaining reservoir in CH_4 heavy isotopes, increasing the $\delta^{13}\text{C}-\text{CH}_4$. In Figure 4.3, our results are compared to simple theoretical model calculations in order to identify the main controlling process for the CH_4 isotopic composition of lake ice bubbles. We used the Rayleigh distillation model (Equation 4.1) discussed in Mahieu *et al.* (2006) to describe the isotopic fractionation associated with CH_4 oxidation exclusively.

$$\ln \frac{\delta^{13}\text{CH}_4 + 1}{\delta^{13}\text{CH}_{4,0} + 1} = \left(\frac{1-\alpha}{\alpha} \right) * \ln f \quad (\text{Equation 4.1})$$

Where $\delta^{13}C_{CH_4,0}$ is the isotopic composition of the CH_4 source and the fractionation α is defined as $k^{12}CH_4/k^{13}CH_4$ where k is the removal rate coefficient for the two isotopologues. The sample Lake 2 – BS7 (Table 4.1) which shows the highest mixing ratio and one of the lowest $\delta^{13}C-CH_4$ values (-75.31‰) was taken as the starting point for the model $\delta^{13}C_{CH_4,0}$. In Figure 4.3, we show three different fractionation curves for $\alpha = 1.002$, $\alpha = 1.008$ and $\alpha = 1.021$. These values span the range of fractionation factors that have been observed in freshwater (Grant and Whiticar 2002). The methane remaining fraction (f) for each sample was calculated in two different ways. The white symbols show values calculated directly from the measured methane mixing ratio in the sample, assuming that the maximum value observed ($\phi_{CH_4,0}=1764$ ppm) was the initial mixing ratio for all samples, i.e., $f_i = \frac{\phi_{CH_4,i}}{\phi_{CH_4,0}}$, where $\phi_{CH_4,i}$ is the methane mixing ratio of sample i . The grey symbols show the methane remaining fraction calculated from the isotope data for $\alpha = 1.008$.

For the mixing hypothesis, we calculated the isotope signature resulting from a linear mixing between two reservoirs (Equation 4.2), where x is the CH_4 fraction of reservoir 1 and $\delta^{13}C_{source\ i}$ the isotopic signature of the reservoir $i=1$ or 2. Figure 4.3 shows the mixing curve where the sample with the highest δ value observed ($\delta^{13}C-CH_4=-32.97\text{‰}$) is mixed with the sample with the highest mixing ratio and $\delta^{13}C-CH_4=-75.31\text{‰}$ (the same sample that was also used as starting point for the distillation model).

$$\delta^{13}C_{CH_4} = x * \delta^{13}C_{source\ 1} + (1 - x) * \delta^{13}C_{source\ 2} \quad (\text{Equation 4.2})$$

In Figure 4.3, the three Rayleigh distillation curves are shown as black lines and the theoretical mixing curve as a dashed line. The symbols show the experimental results, where the numbers refer to the numbering of the lakes for the white symbols as in Figure 4.1 and the symbol shapes represent the bubble types. When f is calculated from the mixing ratios, there is not one single oxidation model line that fits all the data, whereas when f is calculated from the isotopes with a given α , the data are forced on this oxidation line. Both calculations assume that the original signature (mixing ratio of δ value) is the same for each bubble, but it is known that these two parameters can be variable. We suggest that the methane mixing ratio would be probably less stable than the isotopic composition, with regard to the amount of processes able to affect it. Although there are still uncertainties involved in the evaluation, Figure 4.3 shows that qualitatively the measurements are more in line with an oxidation process controlling the observed variability than with a mixing process. The general shape of

the dataset implies that a removal process (Rayleigh fractionation) is the main controller able to explain the observed variations depicted in Figure 4.3.

The large flat bubble from Lake 2 shows 0% of oxidation (remaining CH_4 fraction of 1) because it has been selected as starting point for the Rayleigh model. This bubble shows the highest CH_4 mixing ratio and a very low isotopic signature. On the other hand, the two other large flat bubbles from Lake 3 with very low isotopic values but intermediate CH_4 mixing ratios, are plotted to the left of the Rayleigh fractionation lines in Figure 4.3. This implies that the Rayleigh model is not applicable to these bubbles, and that other processes (e.g. different source signatures) must also contribute to the observed variability. Lake 3 is known (Chapter 3) to be influenced by open hydrological system conditions characterized by incoming water originating from a river (from South) and flowing into the lake to the northwest (see Figure 4.1). This water circulation results, *inter alia*, in the oxygenation of the water column and atmospheric O_2 mixing ratios have been measured in bubbles enclosed in that ice cover. These different properties of Lake 3 may also affect the CH_4 source substrate. The river, originating in a peat area, might bring in CH_4 or organic material with a lower isotopic signature, but further investigation of the source substrate was beyond the scope of this study.

The elongated bubbles clearly display an oxidation signature. The range of observed mixing ratios for the modelled Rayleigh curves indicates that oxidation can be very important, implying up to 99% of CH_4 depletion. Spherical and nut-shaped bubbles show a variable CH_4 oxidation ranging between 4 and 73%. This suggests that a significant fraction of the dissolved CH_4 in the lake water is oxidized by bacteria. In that context the elongated bubbles, characterized by a relatively slow freezing front, reflect this oxidation better than bubbles associated with a faster freezing front. In the latter case a shorter exchange time between CH_4 and the water or a potentially larger influence of small bubbles directly degassed from the sediment (as in the mixed ice type c)) could explain the greater variability of the observed isotopic signature.

This analysis suggests, as expected, that the CH_4 that originates from gas exsolution during lake ice formation and produces the elongated bubbles has been strongly oxidized in the liquid phase. Consequently, the ice cover enhance the CH_4 oxidation into carbon dioxide (which is 23 times less effective as a greenhouse gas) and therefore contributes to reducing the CH_4 emissions from lakes in permafrost areas.

Using these data we derived a rough estimate of the amount of CH₄ oxidized (O_{CH_4}) in the water of subarctic lakes before its entrapment as bubble in the lake ice cover (Equation 4.3).

$$O_{CH_4 i} = \phi_{CH_4 i} * \Gamma_i * \frac{M}{V_o} * \frac{1}{f} * O_{fraction i} * \rho_{ice} * V_{lake ice} * B_{ratio i} * \frac{1}{S_{lake}} * 10^6$$

(Equation 4.3)

Where: i = bubble type

$\phi_{CH_4 i}$ = methane mixing ratio

Γ_i = total gas content (ml g⁻¹_{ice})

M = methane molar mass (16.04 g)

V_o = gaseous molar volume under standard conditions (22.4146 l/mol)

$O_{fraction i}$ = $1-f$ = oxidized fraction by bubble type

ρ_{ice} = ice mass density (0.9168 kg l⁻¹)

$V_{lake ice}$ = total lake ice volume of the lakes studied (118 580 m³)

$B_{ratio i}$ = bubble type ratio (=proportion of ice bubble type “i” in the total ice volume)

S_{lake} = total surface of the lakes studied (150 000 m²)

The term $1/f$ allows reconstruction of the CH₄ amount available before oxidation for a given bubble type. The oxidized fraction by bubble type ($O_{fraction i}$) is the mean amount of methane removed by the oxidation process for each bubble type. It is calculated from the mean remaining CH₄ fraction of all samples available for a given bubble type, as referred to the surmised original sample mixing ratio. Table 4.2 summarizes the data used in the calculation (number of samples for each analysis, min – mean/med – max for total gas content, and CH₄ mixing ratios for each bubble type considered) and shows the amount of CH₄ (mg m⁻²) oxidized during the 3 months of ice cover existence, calculated for the elongated bubbles (type a), the spherical and nut-shaped bubbles (type b) and the mixed ice (type c). It should be noted that these are most probably lower limits because, as demonstrated in Chapter 3, the total gas content measurements are certainly underestimated. An unknown part of the gas content is indeed lost when cutting through bubbles during sampling. This error is most significant for the cylindrical elongated bubbles. On the other hand, the contribution from

large flat bubbles (type d) has not been included in our budget for two reasons: a) because we considered that the oxidation, for this bubble type, was negligible, b) because the ice sample size (7.5 cm diameter) is too small for the total gas volume in $\text{ml}_{\text{gas}} \text{g}^{-1}_{\text{ice}}$ to have a useful meaning, and c) because bubbles larger than the drill could not be sampled.

Bubble type	Bubble type ratio	Total gas content [†] (ml g^{-1}) mean or med* (min-max)	CH ₄ mixing ratios [†] (ppm) mean or med* (min-max)	Oxidized methane budget ($\text{mg CH}_4 \text{m}^{-2}$) mean or med* (min-max)
Samples	81	82	97	
Elongated bubbles	0.25	0.007 (0.003-0.019)	24.78* (3.22-16447.2)	0.24 ($5.46 \cdot 10^{-3}$ - $2.09 \cdot 10^4$)
Spherical and nut shaped bubbles	0.15	0.011* (0.002-0.078)	6551.37* (16.58-141727.25)	10.4 ($9.23 \cdot 10^{-4}$ - $1.93 \cdot 10^4$)
Mixed ice	0.22	0.011* (0.005-0.109)	393.08* (13.38-208895.37)	0.139 ($2.15 \cdot 10^{-3}$ - $730 \cdot 10^2$)
Total	0.62			10.8 ($8.52 \cdot 10^{-3}$ - $4.09 \cdot 10^4$)

Table 4.2 : Oxidized methane budget calculation ([†]from Chapter 3)

These first estimates of the amount of CH₄ that is oxidized during the 3 winter months in ice covered lakes could account for a significant fraction of the total CH₄ turnover, although the uncertainties at this point are still extremely large. The very large variability observed in Table 4.2 (up to 7 orders of magnitude) results from the cumulative variability of the individual components in the budget calculations. The minimum value about $8.52 \cdot 10^{-3} \text{ mg CH}_4 \text{m}^{-2}$ results from the combination of the minimum total gas content value with the minimum CH₄ mixing ratio and the minimum CH₄ oxidation fraction (similar for the maximum value of about $4.09 \cdot 10^4 \text{ mg CH}_4 \text{m}^{-2}$). This leads to the large range of calculated oxidation budget but these extreme values are certainly very unlikely. As a sensitivity test, Figure 4.4 shows 3 total oxidized CH₄ budget calculated from Equation 4.4 considering only the full range of values for one of the 3 parameters (i.e. total gas content, CH₄ mixing ratio or oxidation ratio) and using the mean/median value for the two other. This treatment considerably decreases the calculated range. Indeed, the total oxidation budget ranges are then between 2.07 to 76.1 $\text{mg CH}_4 \text{m}^{-2}$ with variable total gas content, 0.0624 to 459 $\text{mg CH}_4 \text{m}^{-2}$ with variable CH₄ mixing ratio and 2.24 to 137 $\text{mg CH}_4 \text{m}^{-2}$ with variable oxidation ratio. The exercise shows that the variations in the CH₄ mixing ratio cause the largest uncertainty.

However, the estimated mean value ($10.8 \text{ mg CH}_4 \text{ m}^{-2}$) is not negligible. If we divide this value by the number of days during which the ice cover was present, we can compare our results to total estimates of CH_4 emissions from other studies. We obtain an oxidation rate of $0.12 \text{ mg CH}_4 \text{ m}^{-2} \text{ d}^{-1}$. Several studies presented in Walter *et al.* (2010), in the same environment, calculated seasonal averages for total CH_4 emissions of around $10 \text{ mg CH}_4 \text{ m}^{-2} \text{ d}^{-1}$ while other studies can be higher by up to an order of magnitude. From the present first data set it is difficult to reliably scale the effect of oxidation to the total methane budget because the total production is not known. If the estimates of Walter *et al.* (2010) also hold for winter conditions and the lakes in our study area, then the oxidized fraction is only $\sim 1\%$ of the CH_4 that would otherwise be emitted. Further studies, including flux studies during the ice-free period are obviously required to assess this more quantitatively. Our estimate for CH_4 oxidation suggests that direct CH_4 emissions remain the dominant process, but CH_4 oxidation does still have a non negligible impact. Indeed, if we multiply the estimated mean value (Table 4.2) by an estimate of the total lake surface in the permafrost area ($396\,200 \text{ km}^2$), based on the Global Lake and Wetlands Database (GLWD) presented in Smith *et al.* (2007), we obtain an oxidation of 4290 tons of CH_4 . This contribution is probably underevaluated since the GLWD is known to underestimate lake numbers and areas and only takes into account lakes with sizes between 0.1 and 50 km^2 (Frey and Smith 2007). Walter *et al.* (2007b) suggested an error of the order of about 50%.

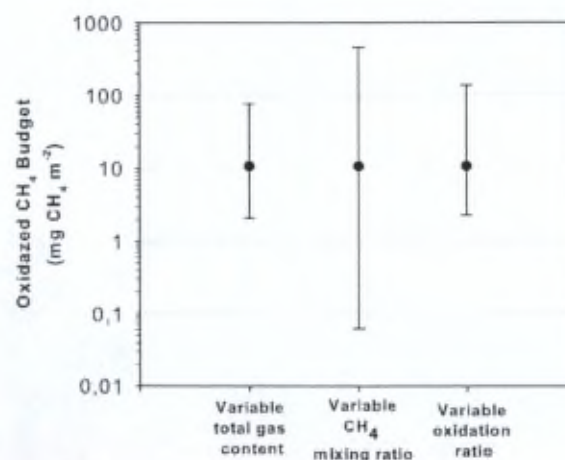


Figure 4.4 : Minimum, mean and maximum total oxidized CH_4 budget calculated from Equation 4.4 considering the full range of value for only one of the 3 parameters (i.e. total gas content, CH_4 mixing ratio and oxidation ratio) and using the mean value for the two other.

Our oxidation budget estimates focus on gases enclosed in the lake ice cover and do not take into account the methane that is still dissolved in the water under the ice which can be important. Kankaala *et al.* (2007) reported CH₄ oxidation rates between 0.01 and 14.4 mmol m⁻³ d⁻¹ in lake water before the autumnal turnover and these values are within the oxidation rates of other studies. Our estimation budget is equivalent to 0.0093 mmol m⁻³ d⁻¹ for the gas that is then trapped in the ice, i.e. at lower bound of the water values.

4.6 Conclusions

Analysis of the carbon isotopic composition of CH₄ in gas bubbles trapped in Arctic lake ice shows that different types of bubbles are characterized by specific $\delta^{13}\text{C}$ -CH₄ signature. This composition is mainly controlled by the CH₄ oxidation process during the period when lakes are ice covered. The process can be very important for bubbles resulting from gas exsolution (up to 99% of oxidized methane) during the ice formation.

Our oxidized CH₄ budget estimates reveal the impact of the winter-lake ice cover, on annual CH₄ fluxes from periglacial lakes and wetlands, potentially reducing global CH₄ emissions by about 4290 tons in comparison with emissions occurring during the ice-free period. This is equivalent to 0.12 mg CH₄ m⁻² d⁻¹ for the winter season, to be compared to the range of 0 to 25 000 mg CH₄ m⁻² d⁻¹ for CH₄ emissions from arctic lakes, as revised in Walter *et al.* (2010).

This amount of CH₄ is oxidized into carbon dioxide, which is 23 times less effective as greenhouse gas. Consequently, the ice cover reduces the contribution of Arctic lakes to climate change, all the more that the newly formed carbon dioxide will mainly contribute to the HCO₃⁻ pool in response to the carbonate equilibrium in freshwater (Zeebe and Wolf-Gladrow 2001).

Chapter 5. Conclusions

The contribution to the global carbon budget, of emissions of greenhouse gases such as carbon dioxide and methane from permafrost areas is difficult to estimate, since there are many pathways and processes responsible for their release to the atmosphere. This work has shed new light on the topic, using the original approach of measuring gas properties of ice wedges and winter lake ice from Siberia and Northern Sweden.

The study of ice wedges revealed that the future melting of this type of ice represents a minor contribution with regard to the other methane and carbon dioxide emitters (wetlands, lakes, oceans, estuaries, rivers, etc.). While measured concentrations of these gases were not negligible (from 860 to 110 000 ppm and from 0.5 to 72 ppm for CO₂ and CH₄ respectively), the total gas content, and subsequently the volume of the gas reservoir, was rather low (from 10 to 50 ml kg⁻¹ ice). Yet, ice wedges contribution is hard to quantify since it is still a challenge to build a reliable estimate of the total amount of this type of ice in soils, even though we know that present day polygonal nets are the most abundant feature of permafrost, which covers 24% of the land surface (French 2007).

Nonetheless, gas and crystallographic characteristics of the studied ice wedges enabled us to discuss the regional climatic conditions prevailing during the ice wedges formation, building additional support to the interpretation of the isotopic signal of the ice samples. Indeed the joint study of the crystal size, c-axes and total gas content revealed three contrasted environmental conditions for the genesis of the two studied ice wedges. The youngest (IW-26), embedded in a Pleistocene sedimentary unit but with a Holocene isotopic signature (with values around -25‰ and -180‰ for $\delta^{18}\text{O}$ and δD respectively), is characterized by relatively (in comparison to the other ice wedge (IW-28)) large crystals and a low total gas content

(around 30 ml air kg⁻¹ ice). This implies that the surrounding temperatures allowed growth and recrystallization of the crystals and a significant liquid water contribution. These conclusions suggested that this ice wedge had formed under relatively milder conditions in comparison with ice wedge IW-28. Two contrasted climatic conditions were identified during the growth of the latter, as deduced from the combined use of ice facies, total gas content, gas composition, crystal size, isotopic signature and d-excess values. Two sections were identified in this ice wedge, the outer one (i.e. the oldest one), called ice-sand wedge (ISW-28) is characterized by an important sediments content, medium crystal size, variable total gas content (between 11 to 42 ml air kg⁻¹ ice) and Pleistocene isotopic signature ($\delta^{18}\text{O}$ around -29.9‰ and δD around -237‰) whereas the central section (IW-28) is devoid of sediment, shows small crystals, a higher total gas content (around 45 ml air kg⁻¹ ice) and a slightly lower isotopic signature ($\delta^{18}\text{O}$ around -31‰ and δD around -240‰). These isotopic ranges point to a relatively mild period during the ice-sand wedge build-up and a colder period for the ice wedge genesis. The study of the gas composition further makes a case for the existence of biological processes such as respiration in the ice, and identifies methane production in the ice-sand wedge section.

Finally, the d-excess, which shows a strong contrast between the ice-sand wedge section (ISW-28) and the ice wedge section (IW-28), suggests that these two distinct units were formed under regional climatic conditions strongly affecting the d-excess. We used the data at hand to discuss the validity of our paleoclimatic interpretation (variation of sea ice cover extension, changes in atmospheric circulation) against possible local post-genetic isotopic fractionation under sublimation or evaporation processes.

Our lake ice investigations bring, in our opinion, an important contribution to the scarce existing knowledge on gas properties of bubbles in lake ice, and on the biogeochemical processes associated with the presence of the lake ice cover. We showed that the methane concentration depends on the type of bubbles, with strong contrasts existing between bubbles directly resulting from sediment degassing and those resulting from gas exsolution during ice formation, the latter showing lower methane concentrations. This contrast is confirmed by the $\delta^{13}\text{C}$ data which revealed the very important methane oxidation rate (up to 99%) for the bubbles formed by exsolution. This observation underlines the impact of the ice cover which reduces the methane budget by favouring oxidation from CH_4 to CO_2 , the latter being then mainly transferred to HCO_3^- , re-adjusting the carbonate equilibrium system.

The study of the ice cores at high resolution (5 cm) revealed depth-related mechanisms affecting both the gas composition and the bubble content. Indeed, the increase of the CO₂ mixing ratio in bubbles with depth (up to 46 600 ppm) is more important than the decrease in O₂, suggesting supplementary input of carbon dioxide into the water (from processes such as methane oxidation, sulfato-reduction, denitrification, acetate fermentation, a.s.o.).

The inter-lake comparison enabled us to detect two simultaneous bubbling events in the four studied lakes, being potentially synchronous with two fast atmospheric pressure drops thereby bringing support to previous work linking both processes. This inter comparison exercise also put forward the relationship between the hydrological characteristics of the lakes and the bubble content observed in the lake ice cover. We indeed observed that the lake affected by significant water circulation is almost depleted in bubbles (Lake 3) while the shallowest “closed-system” lakes showed record total gas contents. This part of our work suggested that not taking into account the geometrical and hydrological considerations might induce miscalculations in global GHG’s release estimates from permafrost areas.

The “minimal” methane budget that we proposed showed that the methane release from the melting lake ice cover is not negligible (between $6.52 \cdot 10^{-5}$ and $12.7 \text{ mg CH}_4 \text{ m}^{-2} \text{ d}^{-1}$) but is generally lower than the emissions measured during the other seasons. Yet, the oxidized methane budget calculation suggested an average oxidation rate of about $10.8 \text{ mg CH}_4 \text{ m}^{-2}$, equivalent to 4290 tons of oxidized methane if we apply the mean oxidation rate to the estimated total lake surface in the permafrost area of the Northern Hemisphere.

This work brings new, original, data sets on gas properties in permafrost ice (ice wedge and lake ice). It also enlightens biogeochemical processes at work in the water column under the lake ice cover. Clearly, a lot still needs to be done to further the outcome of this preliminary study. For example, technological improvements in order to measure the total gas content more accurately and to take the very large bubbles into account would seriously improve the budget calculations. Also, a dedicated study should focus on the impact of hydrological conditions on bubble inclusions in lake ice. Further, co-isotopic analyses ($\delta^{13}\text{C}$, $\delta^{18}\text{O}$, δD) on methane and carbon dioxide coupled with a study on dissolved gases in water would also be relevant to better identify sources and processes affecting the cycles of these two components.

These improvements are essential if we are to seriously take into account methane release from lakes in the global carbon budget and better constrain future climate modelling.

Annex A: Report: Gas properties of the EPICA Dronning Maud Land (EDML) basal refrozen water

Abstract

Gas composition and total gas content are studied and discussed for different samples of refrozen water retrieved from the bottom of the EPICA Dronning Maud Land (EDML) drilling site. At the end of this deep Antarctic drilling (2774.15 m), liquid water of subglacial origin swept and refroze into the bottom of the borehole, mixed with the drilling liquid and the densifier. This refrozen bottom water clearly differs from ice of meteoric origin and it is rather similar to clathrate ice. Total gas content measurements carried out using different methods reveal particularly high enclosed gas volume. The amount of gas collected (up to 4 liters per kilo of melted ice) could be explained by dissolution of air in water under high overburden pressure, which would be compatible with the local ice thickness. Analysis of the gas composition indicates the presence of a water/drilling fluid mixture, although atmospheric-type gases are present and their characteristics differ from standard atmospheric composition. Indeed, CO₂, CH₄ and O₂ mixing ratios are above the atmospheric composition and O₂ can reach values up to 50% which is difficult to understand. Potential explanations are discussed in relation with the local glaciological setting.

Introduction

EPICA Dronning Maud Land (EDML) project is one of the two deep ice core drilling of the multinational European project EPICA (European Project for Ice Coring in Antarctica). The drilling was performed at Kohnen station (75°00'S, 00°04'E, 2892 meters above sea level, Figure A.1) from 2003 to 2006.



Figure A.1: EDML drilling site location.

At the end of this deep drilling (2774.15 m), liquid water of subglacial origin swept and refroze into the bottom of the borehole, mixed with the drilling liquid (mixing of Foran and D40) and the densifier (HCFC-141b) which are used to maintain the hydrostatic equilibrium in the borehole. Figure A.2 describes the site configuration. The refrozen bottom water clearly differs visually from ice of meteoric origin and is rather similar to clathrate ice (Lambert *et al.* 2006): it presents a low density and appears very white and opaque (Figure A.3). X-ray and Raman spectrometry analyses show that this ice is made of 48% ($\pm 8\%$) of hexagonal ice, 48% ($\pm 8\%$) of hydrate type II and 4% ($\pm 4\%$) of n-pentane (preliminary results from analyses performed at the University of Goettingen). The n-pentane comes from the drilling fluid and is too big to produce hydrate type II (Davidson 1973; Miller 1973; Davidson *et al.* 1987). The main atmospheric gases (N_2 , O_2 , Ar, CO_2 and CH_4) can only produce hydrate type I. Consequently, some questions remain about the compounds forming the observed hydrate

type II. Also, the peculiarities of the total gas content and of the atmospheric gas mixing ratios still need to be discussed and understood.

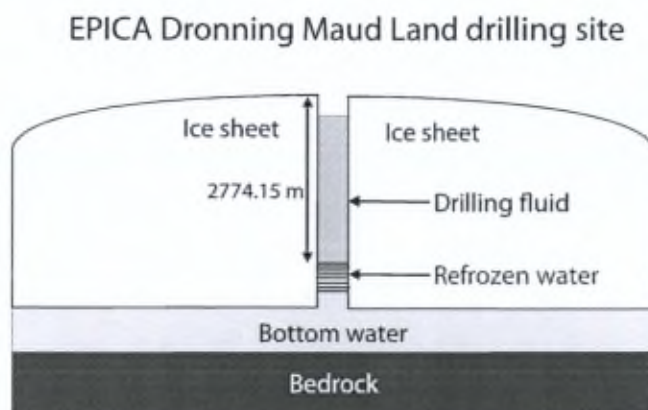


Figure A.2: Scheme of the site configuration.

In this work we have studied the total gas content and the gas composition using different methods since the ice contamination with the drilling liquids has forced us to adopt our traditional extraction and analytical procedure for the gases in ice.



Figure A.3: Ice sample from the refrozen bottom water of the EDML ice core.

Methods

Total gas volume

The Toepler pump method coupled with the melting-refreezing extraction technique described in Martinerie *et al.* (1994) to extract the gases appears to be inadequate for this study. Indeed, both the drilling liquid and the densifier are characterized by a high partial vapor pressure

(respectively 0.289 kPa and 79 kPa at 20°C; Wuhzou International Co.; Gerasimoff 2003). Consequently, the densifier continuously evaporates in the pre-evacuated line of the Toepler pump on sample connection and overwhelms the amount of atmospheric gases initially present in the sample in the collecting graduated burette. In order to get rid of this contamination, we have used a method inspired by a procedure already described by Langway (1958). This simple method consists in placing the ice sample under a reverted funnel connected to a burette filled with kerosene (Figure A.4). On melting, gases enclosed in the ice sample are collected and measured at the top of the burette.

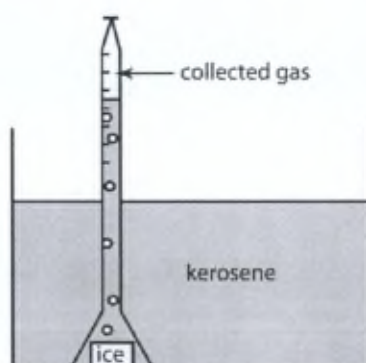


Figure A.4: Extraction system.

Preliminary analyses were performed in water rather than kerosene, therefore the drilling liquid and the densifier (both characterized by a lower density than water) accumulated between the gas and the water. "Bulk volumes" obtained using this first method were translate at 20°C and 1 atmosphere and the potential contributions of the vapor pressure of the other components have been removed, considering these gases were at saturation (water = 2.3%; densifier = 78%; drilling fluid = 0.29% of total volume). In such a way, the "new volumes" are minimum values for the total gas content, all the more because there are a few gases which are not collected in the burette (a few bubbles adhere to the funnel). This method therefore provides a first estimate of the total gas content but does not give any information on the potential undervaluation resulting from our corrections.

The use of a kerosene bath enables to separate the drilling liquid and the densifier from the gas phase, preventing gas-liquid equilibration (Henry's law) with a negligible risk of dissolution of atmospheric gases into the kerosene. Comparison of the three extraction methods (melting in water, melting in kerosene and dry-crushing, this latter being the usual method used to analyze gas composition) has been performed using gas chromatography on

the collected gas volumes. The FID chromatogram (Figure A.5) shows there is neither drilling liquid, nor densifier contamination with the “melting in kerosene” method: the characteristic peaks of these two components are indeed missing (red curve). A supplementary correction has however been applied to remove the potential contribution of the vapour pressure of kerosene (Zenstoves).

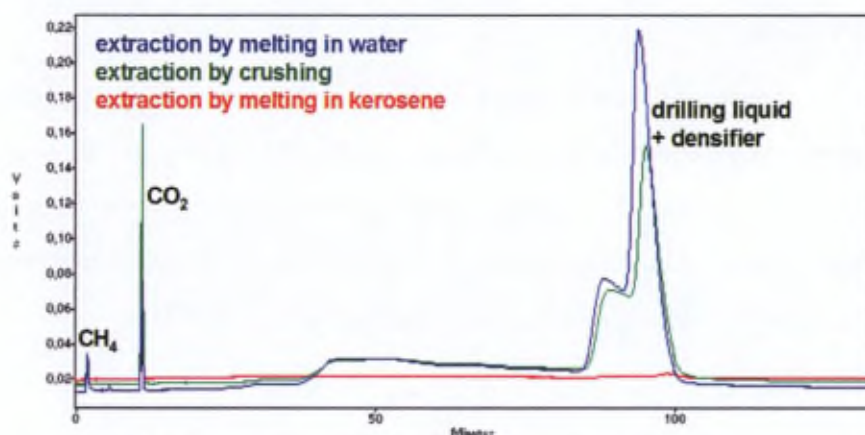


Figure A.5: FID detector chromatogram for the three total gas content extraction techniques.

To ensure that no contamination resulted from laboratory air entrapped within the ice porosity, this extraction method has been further modified in two different ways: either, the ice samples have been placed in the kerosene at low temperature (-15°C) during 20 minutes before being inserted below the funnel (we then consider that kerosene has filled up all the ice porosity), or, the samples have been enclosed in a sealed glass vessel at -80°C wherein the entrapped laboratory air has been extracted with a vacuum pump. Subsequently, the vessel has been opened into the kerosene and the sample inserted below the funnel.

Gas composition

Gas composition has been analyzed by gas chromatography. We used a chrompack CP 9001 chromatograph equipped with a FID detector for the carbon components and with a TCD detector for O_2+Ar and N_2 . A shincarbon micropacked column has been installed in order to adequately separate the light carbon components such as the drilling liquid and the densifier. A specific method has been set up (including a temperature ramp) to optimize the detection of the different gas components.

The gases have been extracted using both the traditional dry crushing method and the “melting in kerosene”. In the latter, the gases were sampled using a specific syringe inserted at the top of the funnel (through the rubber cap) and directly inject in the vacuum line feeding into the gas chromatograph.

Results

Total gas volume

Figure A.6 (note the logarithmic scale) shows total gas content results of 4 ice samples. For all samples, the method by extraction in the kerosene shows the maximum values of total gas. It suggests that the saturation of the drilling liquid and the densifier are not reached in the method by melting in water. Results vary from 0.4 to 4 ml air g⁻¹ ice which are clearly above the usual meteoric ice value of 0.09 ml air g⁻¹ ice (Martinerie *et al.* 1992).

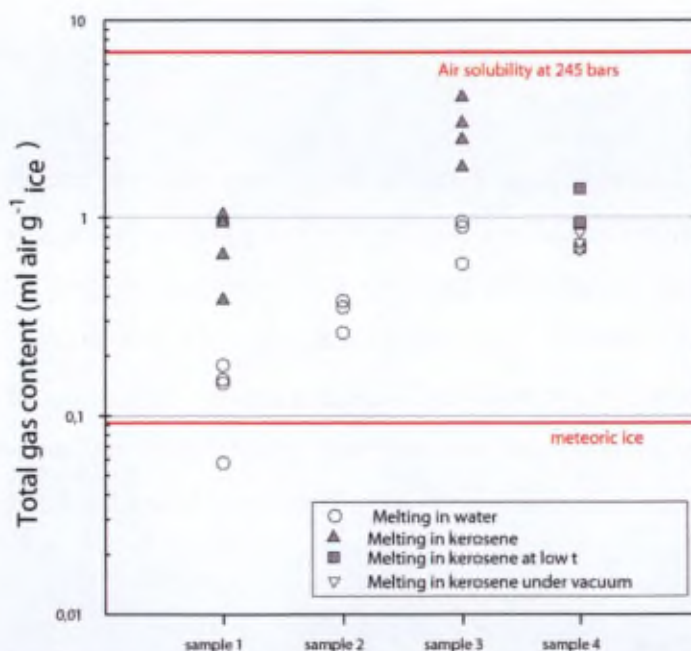


Figure A.6: Total gas content (in ml air g⁻¹ ice; seeping in kerosene, seeping in low temperature (-15°C) kerosene, dry pre-evacuation at -80°C).

The comparison of the extraction methods does not show significant difference, but, unfortunately, the 3 methods have not been tested on the same sample. Nevertheless the method by “melting in kerosene” with pre-evacuation shows slightly lower volumes than the extraction method in kerosene at low temperature. This observation should suggest that either

the vacuum process opens some cavities in the ice sample or that there are a few atmospheric gases remaining entrapped in the ice porosity using the melting in kerosene at low temperature method. The latter assumption is however not very likely because the observed gas composition is far away from the atmospheric composition (see below).

Gas composition

Gas composition analysis has been performed on 5 samples (Figure A.7), using the dry-crushing extraction method (white circles). Sample 1 and 3 have also been analyzed using the extraction method by melting in kerosene (grey circles). Comparing the 2 methods reveals that the one by melting in kerosene shows lower values for CO₂, CH₄, and O₂. In both cases, however, the CO₂ mixing ratio is clearly above the atmospheric value, showing a large variability between 1100 and 3600 ppm for the first method and a closer range (between 560 and 1024 ppm) for the second one. It is also true for CH₄ with mean values between 2.7 and 11 ppm and between 2.8 and 5.4 ppm for each method respectively. For O₂, the mixing ratios are above (up to twice) the atmospheric value for the method by dry crushing while they are between 16 and 27% with the method by melting in kerosene. N₂ mixing ratios present each time the balance with the other gases and O₂/N₂ ratios oscillate between 0.19 and 1.03.

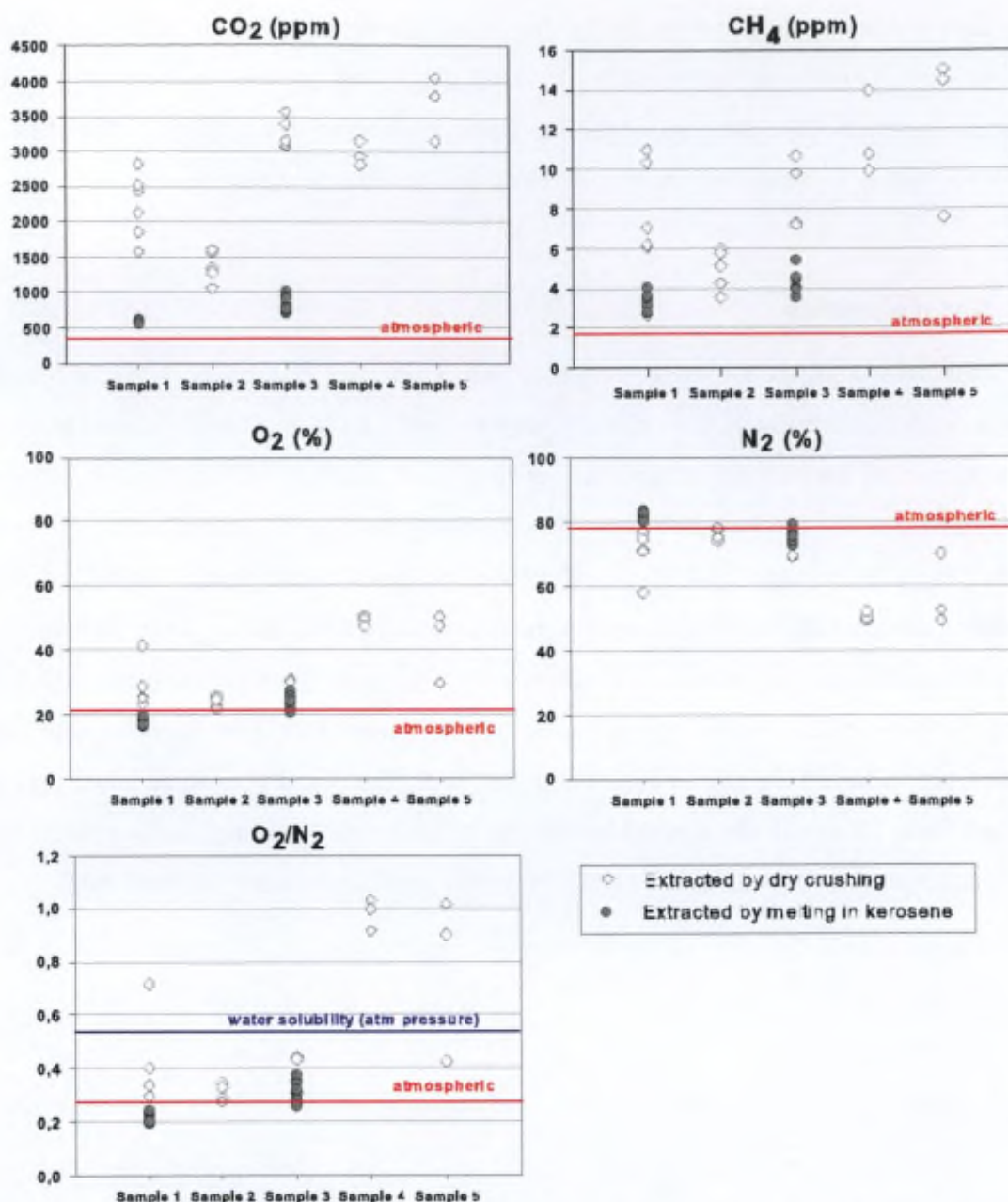


Figure A.7: Gas composition diagrams; white diamonds show results obtained from the traditional dry crushing extraction method, grey circles shows results obtained from the “melting in kerosene method”, the five samples correspond to five different ice blocks and each symbol is the result of a single analysis.

Discussion

Clathrate formation

X-ray and Raman Spectrometry showed that our samples are made of a mix of hexagonal ice, hydrate type II and n-pentane (Murshed *et al.* 2007). As explained in the introduction, the n-

pentane comes from the drilling fluid and is too big to produce hydrate type II. The atmospheric gases (N_2 , O_2 , Ar, CO_2 , CH_4 , etc.) can only produce hydrate type I (Davidson 1973; Miller 1973; Davidson *et al.* 1987). The only molecule being able to produce clathrate type II is CH_3CCl_2F . This molecule is the principal component of the densifier HCFC-141b used for the drilling. It is very similar to CH_3CClF_2 which is known to produce clathrate type II (Davidson 1973). Therefore, the clathrate formation should result from CH_3CClF_2 presence when the mixture water – densifier – drilling fluid is freezing into the borehole.

Total gas content

The observed total gas content shows anomalously high values for ice, by comparison with usual values in ice from deep ice core (around $0.09 \text{ ml air g}^{-1} \text{ ice}$). Such values can only be obtained if we consider that the gases are dissolved into water at high pressure. In our cases, the 2700 meters of ice thickness correspond to 245 bars, which might provide the necessary overburden pressure (about 6 liters of gas per kilo of water). But, even if we can physically explain the total gas content values in the refrozen water, we need to find a subglacial source for this amount of gases. In this work, different scenarios have been explored to explain the gas enrichment of the water.

Scenario I: steady-state ice sheet close to ice divide with underlying water body of constant volume

In this first scenario, we have considered a closed system in which the gas content dissolved in the subglacial water is provided by vertically advected ice downwards (i.e. with total gas content around 0.1 ml g^{-1}) (Figure A.8). In this case, the enrichment would result from melting ice in the water and refreezing of the same amount of water with full expulsion of the gases in the underlying water. The ice is then entrained side ways by flow and replaced by new unmodified glacier ice from above. Although this hypothesis is theoretically correct, it is not applicable for the EDML drilling site because it is not located at an ice divide.

EPICA Dronning Maud Land drilling site

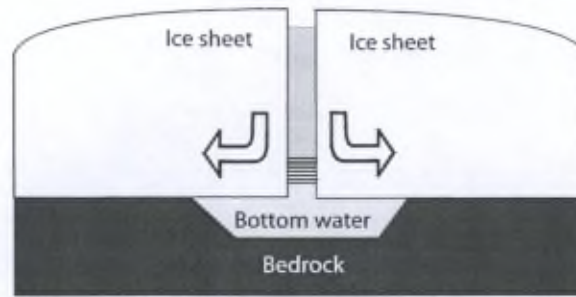


Figure A.8: Scheme of scenario I.

Scenario II: moving ice sheet with underlying water body of constant volume, no large scale melting-refreezing, recrystallization of deep ice

In scenario II, gas enrichment of the water reservoir would result from exchange with the horizontally advected deep meteoric ice layer via the intercrystalline sub-liquid layer during recrystallization close to the pressure melting point (Figure A.9).

EPICA Dronning Maud Land drilling site

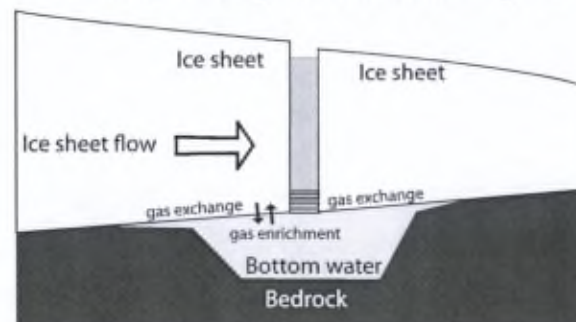


Figure A.9: Scheme of Scenario II.

This process has been identified under ice shelves (Souchez *et al.* 1995c), but only on decimetric scale. This process could participate to the gas enrichment, it would seem indeed that the basal ice of EDML drilling shows a lower conductivity and a lower gas content (Sepp Kipfstuhl, personal communication). To further argue in favour of this process, a detailed analysis of the EDML basal ice sequence would be needed.

Scenario III: moving ice sheet with underlying water body of constant volume and large-scale melting-refreezing (Vostok type)

In this case, the gas enrichment of the water reservoir would be related to both melting of meteoric ice and refreezing of lake ice in the context of an active lake water thermohaline circulation (Figure A.10). This process could produce a total gas enrichment well above meteoric ice values but no large water body has been detected at the EDML location.

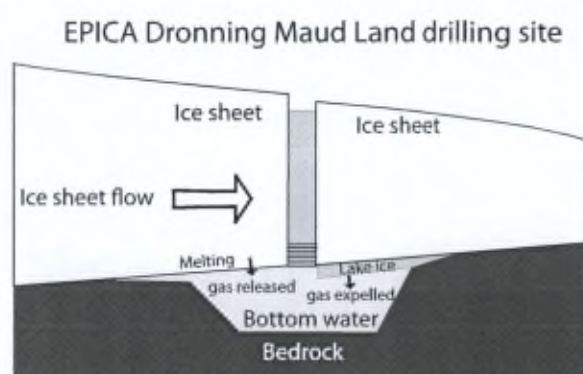


Figure A.10: Scheme of Scenario III.

Scenario IV: moving ice sheet, water layer and pressure-melting

Gas enrichment of the water reservoir is here provided by small-scale melting-refreezing as the ice passes bedrock bumps (Weertman process). Gases are expelled during refreezing, and the bottom water becomes cumulatively enriched by this process (Figure A.11). This assumption is plausible to explain the gas volume and composition (see below) observed at EDML where no large water body has been observed.

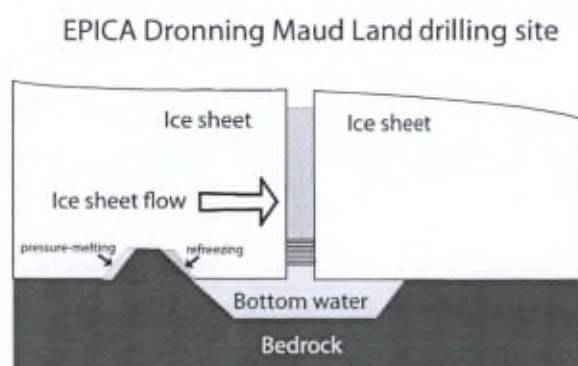


Figure A.11: Scheme of Scenario IV.

Other scenarios: water hosting biota or bedrock degassing

Long-term sustained microbial activity could alter the gas composition but difficultly explain such an increase in the total gas content of the water. We have no information on potential processes of the bedrock degassing. In both case, isotopic measurements on the gas phase would certainly help understanding its source(s).

Gas composition

Gas composition interpretation requires caution, first because the two methods used show noticeably different values (especially for O₂, CO₂ and CH₄) and secondly because of the large intra- and inter-samples variability (Figure A.7). There can be various ways of explaining the observed discrepancies between the two methods: melting in kerosene could be biased by air contamination during the syringe manipulation (pulling down the results of CO₂ and CH₄), or there could be interactions between the kerosene and the gaseous CO₂ and CH₄. On the other hand, it is plausible that the dry-crushing method would be biased by a CO₂ and CH₄ contamination from the gaseous interactions with the drilling liquid or the densifier, although the latter have been chosen to be inert. In all cases, we will discuss the results as a range of values, rather than specific values.

CO₂ and CH₄, both show values above the Holocene or Pleistocene atmospheric mixing ratios. The CO₂ enrichment is expected with a scenario in which sudden and rapid partial degassing of strongly pressurized basal water occurs when water infiltrates the drill hole, with a signature that reflects both relative solubility in water and bubbles degassing. It is also true for methane which is known to be more soluble at low temperature and high pressure (e. g. 0.14917 mol kg⁻¹ at 200 bar vs 0.00126 mol kg⁻¹ at 1 bar in pure water; Duan and Mao 2006). The CO₂ and CH₄ enrichment in water below an ice sheet would also be easily understandable if the basal ice was showing high mixing ratios as for the GRIP ice core (Souchez *et al.* 1995b) or Dye-3 core (Verbeke *et al.* 2002). Unfortunately such enrichment of the basal ice is not known for the EPICA DML ice core (EPICA Community Members 2006; Lüthi *et al.* 2008). Note that in both cases of basal ice sequences mentioned above, the high CO₂ and CH₄ levels were shown to result from biological processes that are clearly linked to the availability of organic matter in a debris-rich ice. No debris were described at the base of the EDML ice core.

O₂ and N₂ mixing ratios also show a large variability, although most of the range is between the atmospheric and solubility in water values (see the O₂/N₂ graph Figure A.7). The O₂ mixing ratio can show very high values up to 50%. These values certainly cannot be influenced by atmospheric infiltration during measurements, or by interactions with the drilling liquids, which have been chosen to be inert (Murshed *et al.* 2007). Basal ice in ice sheet is not known to be rich in oxygen (Souchez *et al.* 1995a), rather the opposite, and photosynthetic activity is of course precluded.

Conclusion

Refrozen ice from the bottom of the EPICA DML drill hole shows clear signs of drilling liquid and densifier (HCFC-141b) contamination, the latter being probably responsible of the clathrate type II formation. Total gas content suggests the existence of basal processes of gas enrichment in the subglacial hydrological system (up to 4 liters per kilo of melted ice). Gas composition revealed CO₂, CH₄ and O₂ enrichment by comparison with the atmospheric mixing ratio and the O₂ increase up to 50% remains difficult to explain.

Further investigations are now clearly needed to improve our understanding of the processes active at the base of the EDML drilling (total gas content and gas composition of deep ice layer, co-isotopic composition of deep ice layer, isotopes from gaseous phase in deep ice layer, detailed remote sensing of bedrock subglacial topography in drilling site area, etc.).

Bibliography

- Adams EE, Prisco JC, Fritsen CH, Smith SR, Brackman ST. 1998. Permanent ice covers of the McMurdo Dry Valleys lakes, Antarctica: bubble formation and metamorphism. In *Ecosystem Dynamics in a polar desert: the McMurdo Dry Valleys, Antarctica* (J. Priscu ed.), *Antarctic Research Series*, pp. 281–295, Washington, DC: American Geophysical Union.
- Åkerman HJ, Johansson M. 2008. Thawing permafrost and thicker active layers in sub-arctic Sweden. *Permafrost Periglac. Process.* **19**:279–292; doi:10.1002/ppp.626.
- Anderson B, Bartlett K, Frolking S, Hayhoe K, Jenkins J, Salas W. 2010. *Methane and nitrous oxide emissions from natural sources*. Report from the USA Office of Atmospheric Programs.
- Bäckstrand K, Crill PM, Jackowicz-Korczyński M, Mastepanov M, Christensen TR, Bastviken D. 2010. Annual carbon gas budget for a subarctic peatland, Northern Sweden. *Biogeosciences* **7**: 95–108.
- Bari SA, Hallett J. 1974. Nucleation and growth of bubbles at an ice-water interface. *Journal of Glaciology* **13**: 489–520.
- Barnola JM, Raynaud D, Neftel A, Oeschger H. 1983. Comparison of CO₂ measurements by two laboratories on air from bubbles in polar ice. *Nature* **303**:410–413; doi:10.1038/303410a0.
- Bastviken D, Cole J, Pace M, Tranvik L. 2004. Methane emissions from lakes: Dependence of lake characteristics, two regional assessments, and a global estimate. *Global Biogeochem. Cycles* **18**:12; doi:10.1029/2004GB002238.

- Berg TE, Black RF. 1966. Preliminary measurements of growth of nonsorted polygons, Victoria Land, Antarctica. In: *Antarctic Soils and Soil-Forming Processes, American Geophysical Union Antarctic Research Series* 61–108.
- Black RF. 1978. Fabrics of ice wedges in central Alaska. *Third International Conference on Permafrost* 247–253.
- Black RF. 1976. Features indicative of permafrost. *Annual Reviews Inc. Provided by the NASA Astrophysics Data System* 75–94.
- Black RF. 1963. Les coins de glace et le gel permanent dans le Nord de l'Alaska. *Annales de Géographie* 72: 257–271.
- Black RF. 1954. Permafrost - A review. *Bulletin of the Geological Society of America* 65: 839–856.
- Blunier T, Chappellaz JA, Schwander J, Barnola J-M, Despertis T, Stauffer B, *et al.* 1993. Atmospheric methane record from a Greenland ice core over the last 1000 years. *Geophysical Research Letters* 20: 2219–2222.
- Bobrov AA, Muller S, Chizhikova NA, Schirrmeister L, Andreev AA. 2009. Testate amoebae in late quaternary sediments of the Cape Mamontov Klyk (Yakutia). *Biol. Bull* 36: 363–372.
- Brass M, Röckmann T. 2010. Continuous-flow isotope ratio mass spectrometry method for carbon and hydrogen isotope measurements on atmospheric methane. *Atmospheric Measurement Techniques* 3: 1707–1721.
- Brouchkov A, Fukuda M. 2002. Preliminary Measurements on Methane Content in Permafrost, Central Yakutia, and some Experimental Data. *Permafrost and Periglacial Processes* 13: 187–197.
- Burton JA, Prim RC, Slichter WP. 1953. The Distribution of Solute in Crystals Grown from the Melt. Part I. Theoretical. *Journal of Chemical Physics* 21: 1987–1991. [Accessed 2012-06-04].
- Cardyn R, Clark ID, Lacelle D, Lauriol B, Zdanowicz C, Calmels F. 2007. Molar gas ratios of air entrapped in ice: A new tool to determine the origin of relict massive ground ice bodies in permafrost. *Quaternary Research* 68: 239–248.

- Carte AE. 1961. Air bubbles in ice. *Proceedings of the Physical Society* **77**:757–768; doi:10.1088/0370-1328/77/3/327.
- Casper P, Maberly SC, Hall GH, Finlay BJ. 2000. Fluxes of methane and carbon dioxide from a small productive lake to the atmosphere. *Biogeochemistry* **49**: 1–19.
- Clark I, Fritz P. 1997. *Environmental isotopes in hydrogeology*. CRC Press (Lewis Publishers).
- Corte AE. 1962. *Relationship between four ground patterns, structure of the active layer, and type and distribution of ice in the permafrost*. 79.
- Craig H. 1961. Isotopic variations in meteoric waters. *Science* **133**: 1702–1703.
- Dansgaard W. 1964. Stable isotopes in precipitation. *Tellus* **16**: 436–468.
- Davidson DW. 1973. *Clathrate hydrates*. In *Water: a comprehensive treatise*. Volume 5. London.
- Davidson DW, Gough SR, Handa YP, Ratcliffe CI, Ripmeester JA, Tse JS. 1987. Some Structural Studies of Clathrate Hydrates. *Journal De Physique* **48**: 537–542.
- Dereviagin AY, Meyer H, Chizhov AB, Hubberten H-W, Simonov EF. 2002. New data on the isotopic composition and evolution of modern ice wedges in the Laptev Sea region. *Polarforschung* **70**: 27–35.
- Duan Z, Mao S. 2006. A thermodynamic model for calculating methane solubility, density and gas phase composition of methane-bearing aqueous fluids from 273 to 523 K and from 1 to 2000 bar. *Geochimica et Cosmochimica Acta* **70**: 3369–3386.
- Etheridge DM, Pearman GI, de Silva F. 1988. Atmospheric trace-gas variations as revealed by air trapped in an ice core from Law Dome, Antarctica. *Annals of Glaciology* **10**: 28–33.
- Fenchel T, King GM, Blackburn TH. 1998. *Bacterial biogeochemistry: The Ecophysiology of mineral cycling - second edition*. Academic Press.
- French HM. 2007. *The Periglacial Environment, 3rd Edition*. Wiley.
- Frey KE, Smith LC. 2007. How well do we know northern land cover? Comparison of four global vegetation and wetland products with a new ground-truth database for West Siberia. *Global Biogeochem. Cycles* **21**:GB1016; doi:10.1029/2006GB002706.
- Gell WA. 1971. Ice Fabrics, Tuktoyaktuk, N.W.T.

- Gell WA. 1978. Ice-wedge ice, Mackenzie delta-Tuktoyaktuk peninsula area, N.W.T., Canada. *Journal of Glaciology* **20**: 555–562.
- Gell WA. 1976. Underground Ice in Permafrost, Mackenzie Delta-Tuktoaktuk, N.W.T.
- Gerasimoff M. 2003. *Drilling fluid observations and recommendations for U.S. polar program, Waiscores drilling project.*
- Gilichinsky DA, Nolte E, Basilyan AE, Beer J, Blinov AV, Lazarev VE, *et al.* 2007. Dating of syngenetic ice wedges in permafrost with ^{36}Cl . *Quaternary Science Reviews* **26**:1547–1556; doi:10.1016/j.quascirev.2007.04.004.
- Gow AJ, Langston D. 1977. Growth history of lake ice in relation to its stratigraphic, crystalline and mechanical structure. *USA CRREL Report (Cold Regions Research and Engineering Laboratory)* **77**: 24p.
- Grant NJ, Whiticar MJ. 2002. Stable carbon isotopic evidence for methane oxidation in plumes above Hydrate Ridge, Cascadia Oregon Margin. *Global Biogeochem. Cycles* **16**: 1124.
- Hinkel KM. 1983. Ice-cover growth rates at nearshore locations in the Great Lakes. *NOAA Tech. Memorandum ERL GLERL, Nat. Tech. Info. Serv, Springfield, VA* 22161.
- International Arctic Science Committee. 2004. *Arctic Climate Impact Assessment - Scientific Report.* Cambridge University Press.
- IPCC. 2007. *Climate change 2007: The physical Science Basis.* Cambridge University Press.
- Jacka TH. 1984. Laboratory studies on relationships between ice crystal size and flow rate. *Cold Regions Science and Technology* **10**: 31–42.
- Johansson M, Christensen TR, Akerman HJ, Callaghan TV. 2006a. What Determines the Current Presence or Absence of Permafrost in the Torneträsk Region, a Sub-arctic Landscape in Northern Sweden? *Ambio* **35**: 190–197.
- Johansson T, Malmer N, Crill PM, Friborg T, Åkerman JH, Mastepanov M, *et al.* 2006b. Decadal vegetation changes in a northern peatland, greenhouse gas fluxes and net radiative forcing. *Global Change Biology* **12**:2352–2369; doi:10.1111/j.1365-2486.2006.01267.x.
- Johnsen SJ, Dansgaard W, White JWC. 1989. The origin of Arctic precipitation under present and glacial conditions. *Tellus* **41B**: 452–468.

- Jonsson A, Åberg J, Jansson M. 2007. Variations in pCO₂ during summer in the surface water of an unproductive lake in northern Sweden. *Tellus B* **59**:797–803; doi:10.1111/j.1600-0889.2007.00307.x.
- Jouzel J, Masson-Delmotte V, Stievenard M, Landais A, Vimeux F, Johnsen SJ, *et al.* 2005a. Rapid deuterium-excess changes in Greenland ice cores: a link between the ocean and the atmosphere. *Comptes Rendus Geoscience* **337**:957–969; doi:10.1016/j.crte.2005.05.011.
- Jouzel J, Merlivat L. 1984. Deuterium and oxygen 18 in precipitation: modeling of the isotopic effects during snow formation. *Journal of Geophysical Research* **89**: 11749–11757.
- Jouzel J, Merlivat L, Lorius C. 1982. Deuterium excess in an East Antarctic ice core suggests higher relative humidity at the oceanic surface during the last glacial maximum. *Nature* **299**: 688–691.
- Jouzel J, Stievenard M, Johnsen SJ, Landais A, Masson-Delmotte V, Sveinbjornsdottir A, *et al.* 2005b. The GRIP deuterium-excess record. *Quaternary Science Reviews* **26**: 1–17.
- Kankaala P, Taipale S, Nykänen H, Jones RI. 2007. Oxidation, efflux, and isotopic fractionation of methane during autumnal turnover in a polyhumic, boreal lake. *J. Geophys. Res.* **112**:G02033; doi:10.1029/2006JG000336.
- Katayama T, Tanaka M, Moriizumi J, Nakamura T, Brouchkov A, Douglas TA, *et al.* 2007. Phylogenetic analysis of bacteria preserved in a permafrost ice wedge for 25,000 years. *Appl. Environ. Microbiol.* **73**: 2360–2363.
- Killawee JA, Fairchild IJ, Tison J-L, Janssens L, Lorrain R. 1998. Segregation of solutes and gases in experimental freezing of dilute solutions: Implications for natural glacial systems. *Geochimica et Cosmochimica Acta* **62**: 3637–3655.
- Kling G, Kipphut G, Miller M. 1992. The flux of CO₂ and CH₄ from lakes and rivers in arctic Alaska. *Hydrobiologia* **240**: 23–36.
- Kokfelt U, Rosén P, Schoning K, Christensen TR, Förster J, Karlsson J, *et al.* 2009. Ecosystem responses to increased precipitation and permafrost decay in subarctic Sweden inferred from peat and lake sediments. *Global Change Biology* **15**:1652–1663; doi:10.1111/j.1365-2486.2009.01880.x.

- Koven CD, Ringeval B, Friedlingstein P, Ciais P, Cadule P, Khvorostyanov D, *et al.* 2011. Permafrost carbon-climate feedbacks accelerate global warming. *PNAS* **108**:14769–14774; doi:10.1073/pnas.1103910108.
- Kuznetsova LP. 1998. Atmospheric moisture content and transfer over the territory of the former USSR. In *Second International Workshop on Energy and Water Cycle in GAMESiberia, 1997, OhataT, HiyamaT (eds). Research Report of IHAS. Institute for Hydrospheric-Atmospheric Sciences, Nagoya University: Nagoya, Japan*; 145–151.
- Lacelle D, Radtke K, Clark ID, Fisher D, Lauriol B, Utting N, *et al.* 2011. Geomicrobiology and occluded O₂–CO₂–Ar gas analyses provide evidence of microbial respiration in ancient terrestrial ground ice. *Earth and Planetary Science Letters* **306**:46–54; doi:10.1016/j.epsl.2011.03.023.
- Lachenbruch AH. 1962. Mechanics of thermal contraction cracks and ice wedge polygons in permafrost. *Geological Society of America Special Papers* **70**: 1–69.
- Langway CCJ. 1958. Ice fabrics and the universal stage. *SIPRE Technical Report* **62**.
- Lauriol B, Duchesne C, Clark ID. 1995. Systématique du remplissage en Eau des Fentes de Gel: les Résultats d'une étude Oxygène-18 et Deutérium. *Permafrost and Periglacial Processes* **6**: 47–55.
- Lorrain R, Sleewaegen S, Fitzsimons S, Stievenard M. 2002. Ice formation in an Antarctic glacier-dammed lake and implications for glacier lake interactions. *Arct. Antarct. Alp. Res.* **34**(2): 150–158.
- Lorrain RD, Fitzsimons SJ, Vandergoes MJ, Stievenard M. 1999. Ice composition evidence for the formation of basal ice from lake water beneath a cold-based Antarctic glacier. *Ann. Glaciol.* **28**: 277–281.
- Lüthi D, Le Floch M, Bereiter B, Blunier T, Barnola J-M, Siegenthaler U, *et al.* 2008. High-resolution carbon dioxide concentration record 650,000–800,000 years before present. *Nature* **453**; doi:10.1038/nature06949.
- Mackay JR. 1974. Ice-Wedge Cracks, Garry Island, Northwest Territories. *Can. J. Earth Sci.* **11**:1366–1383; doi:10.1139/e74-133.
- Mahieu K, Visscher AD, Vanrolleghem PA, Cleemput OV. 2006. Carbon and hydrogen isotope fractionation by microbial methane oxidation: Improved determination. *Waste Management* **26**:389–398; doi:doi: 10.1016/j.wasman.2005.11.006.

- Martinerie P, Lipenkov VY, Raynaud D, Chappellaz J, Barkov NI, Lorius C. 1994. Air content paleo record in the Vostok ice core (Antarctica): A mixed record of climatic and glaciological parameters. *J. Geophys. Res.* **99**: 10565–10576.
- Martinerie P, Lipenkov VY, Raynaud D. 1990. Correction of air-content measurements in polar ice for the effect of cut bubbles at the surface of the sample. *Journal of Glaciology* **36**: 299–233.
- Martinerie P, Raynaud D, Etheridge DM, Barnola JM, Mazaudier D. 1992. Physical and climatic parameters which influence the air content in polar ice. *Earth Planet. Sci. Lett.* **112**: 1–13.
- Masson-Delmotte V, Jouzel J, Landais A, Stievenard M, Johnsen SJ, White JWC, *et al.* 2005. GRIP Deuterium Excess Reveals Rapid and Orbital-Scale Changes in Greenland Moisture Origin. *Science* **309**: 118–121.
- Mattson MD, Likens GE. 1990. Air pressure and methane fluxes. *Nature* **347**: 718–719.
- Merlivat L, Jouzel J. 1979. Global climatic interpretation of the deuterium-oxygen 18 relationship for precipitation. *Journal of Geophysical Research* **84**: 5029–5033.
- Meyer H, Dereviagin A, Siegert C, Schirrmeister L, Hubberten H-W. 2002a. Palaeoclimate Reconstruction on Big Lyakhovsky Island, North Siberia—Hydrogen and Oxygen Isotopes in Ice Wedges. *Permafrost and Periglacial Processes* **13**: 91–105.
- Meyer H, Dereviagin AY, Siegert C, Hubberten H-W. 2002b. Paleoclimate studies on Bykovsky Peninsula, North Siberia - hydrogen and oxygen isotopes in ground ice. *Polarforschung* **70**: 37–51.
- Meyer H, Schirrmeister L, Andreev A, Wagner D, Hubberten H-W, Yoshikawa K, *et al.* 2010a. Lateglacial and Holocene isotopic and environmental history of northern coastal Alaska - Results from a buried ice-wedge system at Barrow. *Quaternary Science Reviews* **29**: 3720–3735; doi:doi: 10.1016/j.quascirev.2010.08.005.
- Meyer H, Schirrmeister L, Yoshikawa K, Opel T, Wetterich S, Hubberten H-W, *et al.* 2010b. Permafrost evidence for severe winter cooling during the Younger Dryas in northern Alaska. *Geophys. Res. Lett.* **37**: L03501; doi:10.1029/2009GL041013.
- Meyer H, Schönicke L, Wand U, Hubberten H-W, Friedrichsen H. 2000. Isotope studies of hydrogen and oxygen in ground ice—Experiences with the equilibration technique. *Isotopes in environmental and health studies* **36**: 133–149.

- Michel FA. 1982. *Isotope investigations of permafrost waters in northern Canada*. University of Waterloo, Ontario, Canada, Dept. of Earth Sciences.
- Michmerhuizen CM, Striegl RG, McDonald ME. 1996. Potential Methane Emission from North-Temperate Lakes Following Ice Melt. *Limnology and Oceanography* **41**: 985–991.
- Miller SL. 1973. The Clathrate Hydrates - Their Nature and Occurrence. *Physics and Chemistry of Ice*. Royal Society of Canada 42–50.
- Moser H, Stichler W. 1980. Environmental isotopes in ice and snow. In *Handbook of Environmental Isotope Geochemistry, the terrestrial environment, 1A* (P. Fritz and J. Fonteseds.), pp. 141–178, Amsterdam: Elsevier.
- Müller S, Bobrov AA, Schirrmeister L, Andreev AA, Tarasov PE. 2009. Testate amoebae record from the Laptev Sea coast and its implication for the reconstruction of Late Pleistocene and Holocene environments in the Arctic Siberia. *Palaeogeography, Palaeoclimatology, Palaeoecology* **271**:301–315; doi:10.1016/j.palaeo.2008.11.003.
- Murshed MM, Faria SH, Kuhs WF, Kipfstuhl S, Wilhelms F. 2007. The role of hydrochlorofluorocarbon densifiers in the formation of clathrate hydrates in deep boreholes and subglacial environments. *Annals of Glaciology* **47**:109–114; doi:doi:10.3189/172756407786857659.
- Nedell SS, Anderson DW, Squyres SW, Love FG. 1987. Sedimentation in ice-covered Lake Hoare, Antarctica. *Sedimentology* **34**: 1093–1106.
- Opel T, Dereviagin AY, Meyer H, Schirrmeister L, Wetterich S. 2011. Palaeoclimatic information from stable water isotopes of Holocene ice wedges on the Dmitrii Laptev Strait, northeast Siberia, Russia. *Permafrost Periglac. Process.* **22**:84–100; doi:10.1002/ppp.667.
- Petrenko VF, Whitworth W. 1999. *Physics of Ice*. Oxford University Press.
- Phelps AR, Peterson KM, Jeffries MO. 1998. Methane efflux from high-latitude lakes during spring ice melt. *J. Geophys. Res.* **103**: 29029–29036.
- Pickering FB. 1976. *The basis of Quantificative Metallography*. Metals and Metallurgy Trust.
- Popp S, Diekmann B, Meyer H, Siegert C, Syromyatnikov I, Hubberten H-W. 2006. Palaeoclimate Signals as Inferred from Stable-isotope Composition of Ground Ice in the

- Verkhoyansk Foreland, Central Yakutia. *Permafrost and Periglacial Processes* **17**: 119–132.
- Raffi R, Stenni B, Flora O, Polesello S, Camusso M. 2004. Growth processes of an inland Antarctic ice wedge, Mesa Range, northern Victoria Land. *Annals of Glaciology* **39**:379–385; doi:10.3189/172756404781814195.
- Raynaud D, Chapellaz J, Barnola JM, Korotkevich Y, Lorius C. 1988. Climatic and CH₄ cycle implications of glacial-interglacial CH₄ change in the Vostok ice core. *Nature* **333**: 655–657.
- Raynaud D, Delmas D, Ascencio JM, Legrand M. 1982. Gas extraction from polar ice cores: a critical issue for studying the evolution of atmospheric CO₂ and ice-sheet surface elevation. *Annals of Glaciology* **3**: 265–268.
- Repo ME, Huttunen JT, Naumov AV, Chichulin AV, Lapshina ED, Bleuten W, *et al.* 2007. Release of CO₂ and CH₄ from small wetland lakes in western Siberia. *Tellus B* **59**:788–796; doi:10.1111/j.1600-0889.2007.00301.x.
- Rinke A, Dethloff K, Spekat A, Enke W, Hesselbjerg Christensen J. 1999. High resolution climate simulations over the Arctic. *Polar Research; Vol 18, No 2 (1999): Special issue: Proceedings of the International Symposium on Polar Aspects of Global Change*. Available from: <http://www.polarresearch.net/index.php/polar/article/view/6567>.
- Robbins LL, Hansen ME, Kleypas JA, meylan SC. 2010. *CO₂calc: A User-Friendly Seawater Carbon Calculator for Windows, Mac OS X, and iOS (iPhone)*. Available from: <http://pubs.usgs.gov/of/2010/1280/>. [Accessed 2012-01-12].
- Romanosky NN. 1976. The scheme of correlation of polygonal wedge structures. *Biuletyn Peryglacjalny* 287–294.
- Rudd JM., Harris R, Kelly CA. 1993. Are hydroelectric reservoirs significant sources of greenhouse gases? *Ambio* **22**: 246–248.
- Sander R. 1999. *Compilation of Henry's Law Constants for Inorganic and Organic Species of Potential Importance in Environmental Chemistry*.
- Sapart C, Van de Veen C, Vigano I, Brass M, van de Wal RSW, Bock M, *et al.* 2011. Simultaneous stable isotope analysis of methane and nitrous oxide on ice core samples. *Atmos. Meas. Tech.* **4**: 2607–2618.

- Schirrmeister L, Grosse G, Kunitsky V, Magens D, Meyer H, Dereviagin A, *et al.* 2008. Periglacial landscape evolution and environmental changes of Arctic lowland areas for the last 60,000 years (Western Laptev Sea coast, Cape Mamontov Klyk). *Polar Research* **27**: 249–272.
- Schirrmeister L, Siegert C, Kuznetsova T, Kuzmina S, Andreev A, Kienast F, *et al.* 2002. Paleoenvironmental and paleoclimatic records from permafrost deposits in the Arctic region of Northern Siberia. *Quaternary International* **89**: 97–118.
- Schubert C, Lucas F, Durisch-Kaiser E, Stierli R, Diem T, Scheidegger O, *et al.* 2010. Oxidation and emission of methane in a monomictic lake (Rotsee, Switzerland). *Aquatic Sciences - Research Across Boundaries* **72**: 455–466.
- Schwamborn G, Meyer H, Fedorov G, Schirrmeister L, Hubberten H-W. 2006. Ground ice and slope sediments archiving late Quaternary paleoenvironment and paleoclimate signals at the margins of El'gygytgyn Impact Crater, NE Siberia. *Quaternary Research* **66**: 259–272; doi:10.1016/j.yqres.2006.06.007.
- Semiletov IP. 1999. Aquatic Sources and Sinks of CO₂ and CH₄ in the Polar Regions. *Journal of the Atmospheric Sciences* **56**: 286–306.
- Shumskii PA. 1964. *Principles of structural glaciology - The petrography of fresh-water ice as a method of glaciological investigation*. Dover Publications, Inc., New York.
- Smith LC, Sheng Y, MacDonald GM. 2007. A first pan-Arctic assessment of the influence of glaciation, permafrost, topography and peatlands on northern hemisphere lake distribution. *Permafrost Periglac. Process.* **18**: 201–208; doi:10.1002/ppp.581.
- Sonesson M, Jonsson S, Rosswall T, Rydén BE. 1980. The Swedish IBP/PT Tundra Biome Project Objectives-Planning-Site. *Ecological Bulletins* 7–25.
- Souchez R, Janssens L, Lemmens M, Stauffer B. 1995a. Very low oxygen concentration in basal ice from Summit, Central Greenland. *Geophysical Research Letters* **22**: 2001–2004.
- Souchez R, Jouzel J, Landais A, Chapellaz J, Lorrain R, Tison J-L. 2006. Gas isotopes in ice reveal a vegetated central Greenland during ice sheet invasion. *Geophysical Research Letters* **33**: L24503; doi:10.1029/2006GL028424.
- Souchez R, Lemmens M, Chapellaz J. 1995b. Flow-induced mixing in the GRIP basal ice deduced from the CO₂ and CH₄ records. *Geophysical Research Letters* **22**: 41–44.

- Souchez R, Lemmens M, Tison J-L, Lorrain R, Janssens L. 1993. Reconstruction of basal boundary conditions at the Greenland Ice Sheet margin from gas composition in the ice. *Earth and Planetary Science Letters* **118**: 327–333.
- Souchez R, Lorrain R. 1991. *Ice Composition and Glacier Dynamics*. Springer-Verlag.
- Souchez R, Tison J-L, Lorrain R, Fléhoc C, Stiévenard M, Jouzel J, *et al.* 1995c. Investigating processes of marine ice formation in a floating ice tongue by a high resolution isotopic study. *J. Geophys. Res.* **100**: 7019–7025.
- Squyres SW, Anderson SW, Nedell SS, Wharton RA. 1991. Lake Hoare, Antarctica: sedimentation through a thick perennial ice cover. *Sedimentology* **38**: 363–379.
- Stenni B, Jouzel J, Masson-Delmotte V, Röthlisberger R, Castellano E, Cattani O, *et al.* 2004. A late-glacial high-resolution site and source temperature record derived from the EPICA Dome C isotope records (East Antarctica). *Earth and Planetary Science Letters* **217**: 183–195.
- Stenni B, Masson-Delmotte V, Johnsen S, Jouzel J, Longinelli A, Monnin E, *et al.* 2001. An Oceanic Cold Reversal During the Last Deglaciation. *Science* **293**: 2074–2077.
- Steven B, Pollard WH, Greer CW, Whyte LG. 2008. Microbial diversity and activity through a permafrost/ground ice core profile from the Canadian high Arctic. *Environmental Microbiology* **10**:3388–3403; doi:10.1111/j.1462-2920.2008.01746.x.
- St-Jean M, Lauriol B, Clark ID, Lacelle D, Zdanowicz C. 2011. Investigation of ice-wedge infilling processes using stable oxygen and hydrogen isotopes, crystallography and occluded gases (O₂, N₂, Ar). *Permafrost Periglac. Process.* **22**:49–64; doi:10.1002/ppp.680.
- Stumm W, Morgan JJ. 1996. *Aquatic Chemistry: Chemical Equilibria and Rates in Natural Waters, 3rd Edition*. Wiley-Interscience.
- Svensson BH, Christensen TR, Johansson E, Å–quist M. 1999. Interdecadal Changes in CO₂ and CH₄ Fluxes of a Subarctic Mire: Stordalen Revisited after 20 Years. *Oikos* **85**: 22–30.
- Tison JL. 1994. Diamond wire-saw cutting technique for investigating textures and fabrics of debris-laden ice and brittle ice. *Journal of Glaciology* **40**: 410–414.

- Tison J-L, Souchez R, Wolff EW, Moore JC, Legrand MR, de Angelis M. 1998. Is a periglacial biota responsible for enhanced dielectric response in basal ice from the Greenland Ice Core Project ice core. *Journal of Geophysical Research*, 1998 **103**: 18885–18894.
- Vaikmäe R. 1989. *Oxygen isotopes in permafrost and ground ice - a new tool for paleoclimatic investigations*. 543–553.
- Vasil'chuk YK, Vasil'chuk AC. 1998. Oxygen-isotope and C14 data associated with Late Pleistocene syngenetic ice-wedges in mountains of Magadan region, Siberia. *Permafrost and Periglacial Processes* **9**: 177–183.
- Verbeke V, Lorrain R, Johnsen SJ, Tison J-L. 2002. A multiple-step deformation history of basal ice from the Dye3 (Greenland) core: new insights from the CO₂ and CH₄ content. *Annals of Glaciology* **35**: 231–236.
- Vimeux F, Cuffey K, Jouzel J. 2002. New insights into Southern Hemisphere temperature changes from Vostok ice cores using deuterium excess correction over the Last 420,000 Years. *Earth and Planetary Science Letters* **203**: 829–843.
- Vimeux F, Masson-Delmotte V, Jouzel J, Stiévenard M, Petit JR. 1999. Glacial-interglacial changes in ocean surface conditions in the southern Hemisphere. *Nature* **398**: 410–413.
- Wagner D, Liebner S. 2009. Global warming and carbon dynamics in permafrost soils: Methane production and oxidation. In *Permafrost Soils* (R. Margesined.), pp. 219–236, Springer Berlin Heidelberg.
- Walter Anthony KM, Anthony P, Grosse G, Chanton J. 2012. Geologic methane seeps along boundaries of Arctic permafrost thaw and melting glaciers. *Nature Geosci* advance online publication; doi:10.1038/ngeo1480. Available from: <http://dx.doi.org/10.1038/ngeo1480>.
- Walter KM, Chanton JP, Chapin FS, Schuur EAG, Zimov SA. 2008a. Methane production and bubble emissions from arctic lakes: Isotopic implications for source pathways and ages. *J. Geophys. Res.* **113**:16; doi:10.1029/2007JG000569.
- Walter KM, Edwards ME, Grosse G, Zimov SA, Chapin FS. 2007a. Thermokarst Lakes as a Source of Atmospheric CH₄ During the Last Deglaciation. *Science* **318**: 633 –636.
- Walter KM, Engram M, Duguay CR, Jeffries MO, Chapin FS. 2008b. The Potential Use of Synthetic Aperture Radar for Estimating Methane Ebullition From Arctic Lakes1.

JAWRA *Journal of the American Water Resources Association* **44**:305–315; doi:10.1111/j.1752-1688.2007.00163.x.

Walter KM, Smith LC, Stuart Chapin F. 2007b. Methane bubbling from northern lakes: present and future contributions to the global methane budget. *Philosophical Transactions of the Royal Society A: Mathematical, Physical and Engineering Sciences* **365**: 1657–1676.

Walter KM, Vas DA, Brosius L, Chapin III FS, Zimov SA, Zhuang Q. 2010. Estimating methane emissions from northern lakes using ice-bubble surveys. *Limnology and Oceanography: Methods* **8**: 592–609. [Accessed 2011-04-12].

Walter KM, Zimov SA, Chanton JP, Verbyla D, Chapin FS. 2006. Methane bubbling from Siberian thaw lakes as a positive feedback to climate warming. *Nature* **443**:71–75; doi:10.1038/nature05040.

Weeks WF, Wettlaufer JS. 1996. Crystal orientations in floating ice sheets. *The Johannes Weertman Symposium* 337–350.

Wetterich S, Kuzmina S, Andreev AA, Kienast F, Meyer H, Schirrmeister L, *et al.* 2008. Palaeoenvironmental dynamics inferred from late Quaternary permafrost deposits on Kurungnakh Island, Lena Delta, Northeast Siberia, Russia. *Quaternary Science Reviews* **27**: 1523–1540.

Wetterich S, Rudaya N, Tumskey V, Andreev AA, Opel T, Schirrmeister L, *et al.* 2011. Last Glacial Maximum records in permafrost of the East Siberian Arctic. *Quaternary Science Reviews* **30**:3139–3151; doi:10.1016/j.quascirev.2011.07.020.

Wharton RA, McKay CP, Clow GD, Andersen DT. 1993. Perennial ice covers and their influence on Antarctic lake systems. In *Physical and biogeochemical processes in Antarctic lakes* (W.J.G. a. E.I. Friedmaned.), *Antarctic Research Series*, pp. 53–70, Washington, DC: American Geophysical Union.

Wuhzou International Co. Ltd catalogue: <http://www.wuzhouchem.com>.

Yershov ED. 1989. *Geokryologija SSSR (Geocryology of the USSR)*. Nedra, Moscow.

Yurtsever Y, Gat JR. 1981. Atmospheric waters. In *Stable Isotope Hydrology: Deuterium and Oxygen in Water Cycle* (T. Rep.ed.), pp. 103–145, IAEA, Vienna.

Zeebe RE, Wolf-Gladrow D. 2001. *CO₂ in Seawater: Equilibrium, Kinetics, Isotopes*, 65. Elsevier.

Zenstoves. *Technical report published on <http://zenstoves.net>.*

Zimov SA, Voropaev YV, Davidov SP, Zimova GM, Davidova AI, Chapin III FS, *et al.* 2001. Flux of methane from North Siberian aquatic systems: Influence on atmospheric methane. In *Permafrost response on economic development, environmental security and natural resources*, pp. 511–524, R. Paepe and V. Melnikov.

Publications

- Boereboom T., Depoorter M., Coppens S. and Tison J-L., Gases properties of winter lake ice in Northern Sweden: implication for carbon gas release. *Biogeosciences*, 9, 827-838, 2012.
- Boereboom T., Samyn D., Meyer H. and Tison J-L., Stable isotope and gas properties of two ice wedges from Cape Mamontov Klyk, Laptev Sea, Northern Siberia, *The Cryosphere*, under review, 2012.
- Boereboom T., Sapart C., Röckmann T. and Tison J-L. Methane isotopic signature of gas bubbles permafrost winter lake ice: a tool for quantifying variable oxidation levels, *JGR-Biogeosciences*, under review, 2012.

Acknowledgements

First of all I would like to express my sincere gratitude to my supervisor for his unfailing support during my PhD. Thank you really Jean-Louis for your rigour, your enthusiasm in pushing the borders in the analysis of the data and for having taken all the time required to supervise my work.

Furthermore I also would like to express my thankfulness to all the members of the “Laboratoire de Glaciologie” with whom I shared some good time and hearty emotions during the six years we spent together in the D.C.4 corridor. Special thanks also to Saïda for the technical help, to Claire for all the management issues, to Frank for the unforgettable moments such as the “poêlée forestière”, to Marie for the “belette” moments and to Charlotte for her motivation and her support in writing this PhD as for all the rest.

Mathieu and Sarah, I want to thank you for the unvaluable work that you performed in the framework of your Master thesis, both in the field and during the lab work as well as for the discussions on the data sets, all significantly contributing to the completion of this work.

To Célia, thank you for your efficiency regarding the isotopic analyses. Our active collaboration started only a few months ago, but it has been salutary to bring this work to a safe end.

To the Professor Thomas Röckmann from the Institute for Marine and Atmospheric Research in Utrecht (IMAU), thank you for the supervision of the isotopic analyses and fruitful discussions.

I also wish to thank all the participants to the Russian-German expedition “Lena-Anabar 2003”, a part of the Russian-German cooperative scientific project “System Laptev Sea”, for allowing access to the ice wedge samples, and I also would like to thank Antje

Eulenburg, Eileen Nebel, Ute Bastian and Lutz Schönicke for the samples treatment and their analytical work in the AWI Potsdam laboratories.

All my gratitude also goes to the Abisko Scientific Research Station (ANS) in Sweden for providing the grant and the weather data, to the "Fonds de Service pour la Recherche Glaciologique Polaire de l'Université Libre de Bruxelles" and the "Crédits pour Brefs Séjours à l'étranger" of the FNRS for the financial support to the Sweden expedition.

The isotope measurements on lake ice bubbles were supported by the Dutch Science Foundation (NWO, grant number 851.30.020 and 865.07.001).

The work on gas properties of EPICA Dronning Maud Land (EDML) basal refrozen water has been funded under the EPICA-MIS EU contract #003868 (GOCE) and the ASPI Belgian Science policy Office program #SD/CA/02A.

I also thank the "Fonds David et Alice Van Buuren" for their financial support.

My gratitude also goes out to my family which has never doubted about the completion of this PhD, with special thanks to Nuno who made chapters 4 and 5 more understandable in English.

And last, but not least, thank you so much Caroline for your unwavering support.

